RCA REVIEW

a technical journal

RADIO AND ELECTRONICS
RESEARCH • ENGINEERING

VOLUME XVII JUNE 1956 NO. 2

PRINTED IN U.S.A.

RCA REVIEW, published quarterly in March, June, September, and December by RCA Laboratories, Radio Corporation of America, Princeton, New Jersey. Entered as second class matter July 3, 1950 at the Post Office at Princeton, New Jersey, under the act of March 3, 1879. Subscription price in the United States and Canada; one year $2.00, two years $3.50 three years $4.50; in other countries: one year $2.40, two years $4.30, three years $5.70. Single copies in the United States, $.75; in other countries, $.85.

RCA REVIEW

a technical journal

RADIO AND ELECTRONICS
RESEARCH • ENGINEERING

Published quarterly by
RCA LABORATORIES
in cooperation with all subsidiaries and divisions of
RADIO CORPORATION OF AMERICA

VOLUME XVII | JUNE, 1956 | NUMBER 2

CONTENTS

RCA REVIEW is regularly abstracted and indexed by *Industrial Arts Index Science Abstracts* (I.E.E.-Brit.), *Electronic Engineering Master Index, Chemical Abstracts, Proc. I.R.E., and Wireless Engineer.*

RCA REVIEW

BOARD OF EDITORS

RECENT IMPROVEMENTS IN THE 21AXP22 COLOR KINESCOPE

By

R. B. Janes, L. B. Headrick, and J. Evans

RCA Tube Division,
Lancaster, Pa.

Summary—The quality of the 21AXP22 color kinescope has been steadily improved since the tube was first announced in September 1954. As a result of experience gained in the manufacture of thousands of tubes and changes in tube construction and processing, nearly perfect color purity and white uniformity have been achieved. A large proportion of the improvements obtained are the result of changes in the "lighthouse" on which the phosphor screens are exposed. After a brief review of the principles of the tube and data on its operation, there is a discussion of the changes which have been made in the tube and in the lighthouses used to produce the tubes. Equipment used to obtain data for the changes is also described.

Introduction

THE 21AXP22[1], shown in Figure 1, is a shadow-mask color kinescope employing a formed mask. A simplified internal view of the tube is shown in Figure 2. The front section, or "top cap," of the two-piece metal envelope contains the spherical faceplate and formed aperture mask. The mask has a radius of curvature slightly smaller than that of the faceplate and is welded to a light metal frame which is supported from the side walls or panel section of the top cap by a unique three-point stud and spring arrangement, as shown in Figure 3. Excellent mask replaceability is achieved with this arrangement. The phosphor-dot pattern is placed directly on the inner surface of the faceplate, and consists of 357,000 dot trios, one for each of the apertures in the formed mask. Each trio is composed of equal-sized dots of red-, green-, and blue-emitting phosphor. The glass funnel-neck section sealed to the small end of the conical metal shell contains three complete electron guns arranged in a delta pattern. This gun structure, shown in Figure 4, employs electrostatic focusing, and a combination of mechanical and magnetic methods for obtaining convergence of the three beams.

The electrostatic focusing lenses are formed by the No. 3 and No. 4 grids of the guns. Corresponding lens elements are connected in

[1] H. R. Seelen, H. C. Moodey, D. D. VanOrmer, and A. M. Morrell, "Development of a 21-Inch Metal-Envelope Color Kinescope," *RCA Review*, Vol. XVI, pp. 122-139, March, 1955.

Fig. 1—Photograph of 21AXP22 color kinescope.

parallel, so that only a single focusing adjustment is used. Approximate static convergence is obtained by mechanical tilt of the three guns toward the tube axis. Precise static convergence is obtained by means of the three sets of beam-converging pole pieces located at the top of the gun structure, and the single set of blue-positioning pole pieces. The beam-converging and blue-positioning pole pieces can be coupled to the fields of external magnets and permit, respectively, radial positioning of the three beams with respect to the tube axis, and tangential positioning of the blue beam. The external purifying mag-

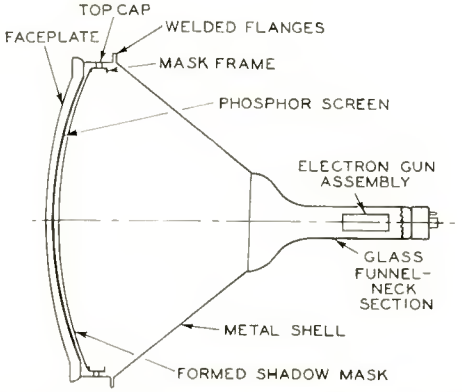

Fig. 2—Schematic diagram of 21AXP22 color kinescope.

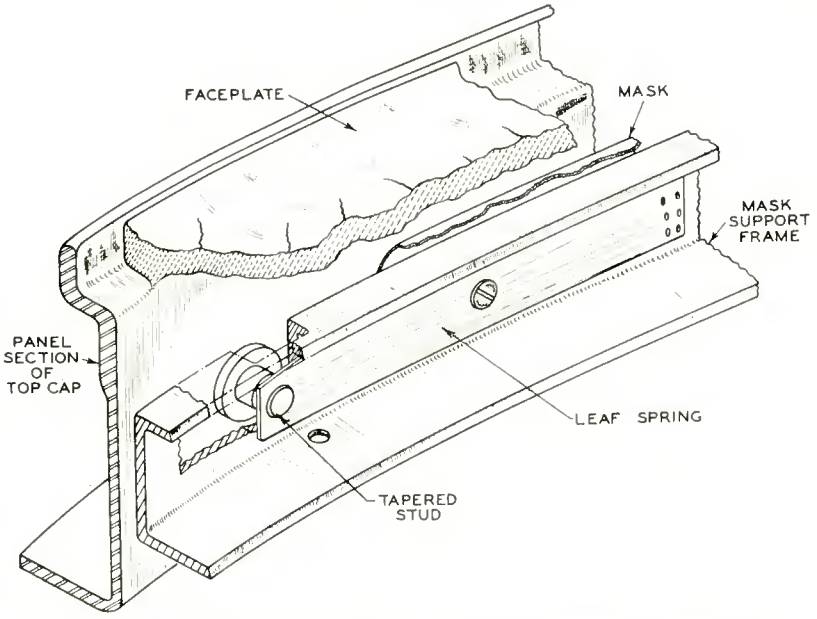

Fig. 3—Detail of spring mounting for shadow-mask support frame.

net is installed on the tube neck, and provides a transverse magnetic field which is used to correct for misalignment between the gun assembly and top cap and for the effects of the earth's magnetic field.

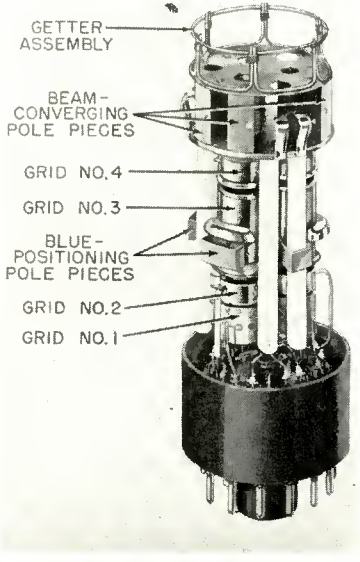

Fig. 4—Photograph of electron-gun assembly.

Principle of Operation

The operating principles of the 21AXP22 are basically the same as those of the planar-mask color kinescope described by H. B. Law.[2] Each of the three electron beams is used to produce one of the primary colors. As shown in Figure 5, the three beams are converged at the shadow mask, and after passing through a common aperture, strike the appropriate phosphor dots of a color trio lying behind the aperture.

The spacing, D, between phosphor dots of the same color, or between the centers of adjacent color trios, is a magnification of the spacing, a, between mask apertures. That is,

$$\frac{D}{p+q} = \frac{a}{p},$$

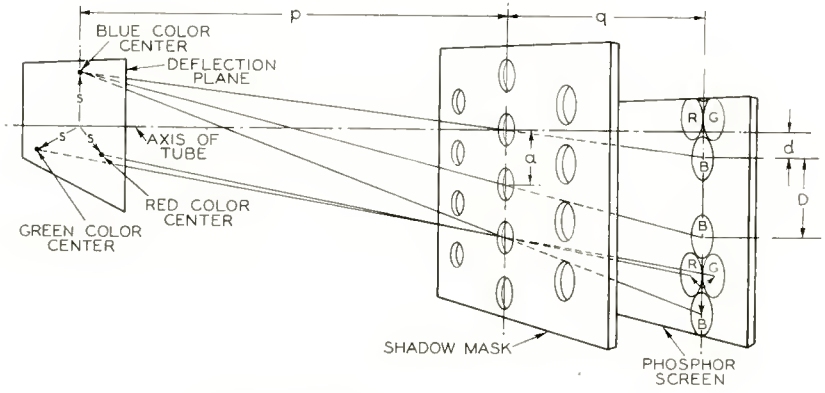

Fig. 5—Geometry of planar-mask system.

where p is the spacing between deflection plane and mask, and q is the spacing between mask and screen.

The spacing, d, of a phosphor dot from the center of its trio is proportional to the spacing, s, between the corresponding deflection center or color center and the tube axis in the deflection plane. That is,

$$\frac{s}{p} = \frac{d}{q}.$$

In a planar-mask tube the spacing between phosphor dots of one color or between adjacent phosphor-dot trios, is a constant magnification of the mask-aperture spacing, regardless of the deflection angle,

[2] H. B. Law, "A Three-Gun Shadow-Mask Color Kinescope," *Proc. I.R.E.*, Vol. 39, pp. 1186-1194, October, 1951.

and the spacing of the phosphor dots within a color trio is a constant demagnification of the deflection-center or color-center spacing in the deflection plane. These constant magnification and demagnification properties permit the screen of a planar-mask tube to be covered completely with tangent phosphor dots.

It is desirable that the formed-mask tube also have constant magnification and demagnification properties in order to obtain optimum utilization of the phosphor screen. However, as explained by Seelen,[1] and shown in Figure 6, precisely constant magnification cannot be obtained when both the aperture mask and the phosphor screen are curved. If the faceplate or screen has a radius of curvature R_f, a mask having a slightly smaller radius of curvature R_m and its center of curvature at point D will give constant magnification for a single electron source located at point 0. When three electron sources equi-

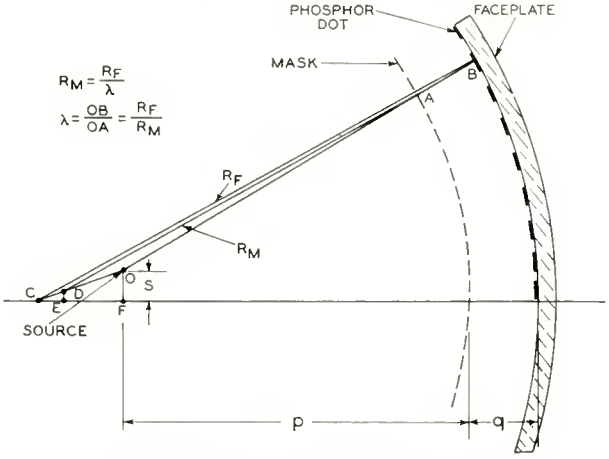

Fig. 6—Geometry of spherical system.

distant from the tube axis and spaced 120 degrees apart are employed, the center of curvature of the mask must be located on the tube axis at point E. This change of center causes a slight deviation from constant magnification. The consequences of this deviation will be discussed later.

Phosphor-Screen Fabrication Technique

Positioning and formation of the phosphor dots on the faceplate of the 21AXP22 are accomplished photographically in a special optical device called a "lighthouse." This device, shown in Figure 7, contains a small high-intensity light source placed in the same geometrical position with respect to the mask and screen as one of the deflection

centers, or color centers, of the tube. This light source can be rotated about the central axis of the system in steps of 120 degrees so as to place it successively in the positions of the three effective deflection centers. At each of these positions light from the source passes through the mask apertures and strikes the screen at points which would be struck by an electron beam passing through the corresponding deflection center and traveling in straight lines.

In phosphor-screen processing, the inside of the cap is first covered with a thin, uniform, layer of a mixture containing one color phosphor

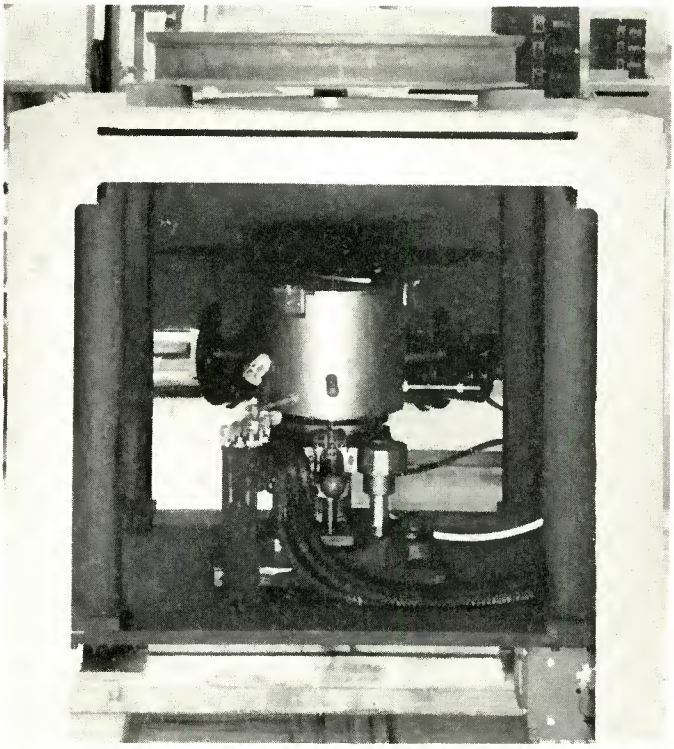

Fig. 7—Optical lighthouse used for phosphor-screen production.

and a photoresistive material. The formed mask is then installed in the top cap and the entire cap assembly placed on the lighthouse. Proper positioning of the cap with respect to the light source is assured by three dimples in the top cap flange which fit into grooves in the lighthouse table.

The phosphor-photoresist mixture is then exposed by allowing the light from the high-intensity source to pass through the mask aper-

tures. The screen is then developed to produce a pattern of phosphor dots of one color.

These steps are repeated for the second and third color phosphors. Between exposures the light source is rotated about the axis of the system in 120-degree steps so that it falls in the proper position for each color field.

Factors Affecting Tube Quality

The screen of an ideal shadow-mask tube would be completely covered with tangent phosphor dots of uniform diameter. In addition, each electron beam of such a tube would have perfect "landing"—that is, it would be in perfect register with all phosphor dots of a particular color—and the resulting electron spots at the screen would have the same uniform diameter as the phosphor dots. An ideal shadow-mask tube would therefore be capable of producing three separate color fields, each having perfect color purity and uniform brightness. If these three fields were produced simultaneously in the proper relative brightness,* the result would be a uniform white field. This last consideration is extremely important, since in the present (compatible) system color tubes must be capable of producing high quality black-and-white pictures.

The following effects must be taken into consideration in making color tubes capable of displaying pure color fields and good black-and-white pictures:

1. Effects of the earth's magnetic field.
2. Mechanical deformation of faceplate and shadow-mask.
3. Change of deflection center of yoke with deflection angle.
4. Asymmetrical spreading ("degrouping") of the electron-spot trios when dynamic convergence is applied.
5. Asymmetrical compression ("grouping") of phosphor-dot trios resulting from nonuniform magnification.
6. Variation in phosphor-dot size due to nonuniformities in the optical lighthouse.

A typical register pattern for one beam of an early formed-mask tube is shown in Figure 8. The scale of the figure is distorted to emphasize the amounts by which the beam-landing spots are displaced from the phosphor dots in many regions of the screen. The numerical values shown at the misregister points represent mils, or thousandths of an inch. Perfect register at the center of the screen was obtained

* Obtained at the following ratios of individual beam currents to total ultor current: red, 51 per cent; blue, 19 per cent; green, 30 per cent.

by positioning the electron beam in the deflection plane of the yoke so that the effective deflection center for the beam, or color center, had the same geometrical location as the light source used to produce the phosphor dots. The beam is positioned at the center of the screen by adjustment of the purifying magnet referred to previously.

A change in the position of the deflection yoke will cause a radial change in register. In this instance the yoke was positioned so that there was no radial misregister at the left-hand end of the horizontal line.

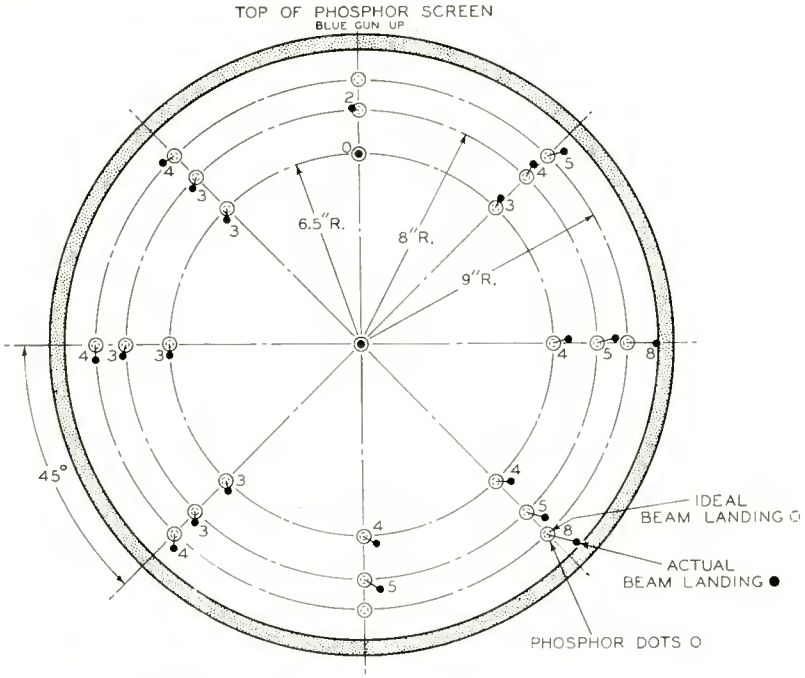

Fig. 8—Typical register pattern on an early tube.

Effect of Earth's Magnetic Field

The greatest difficulty encountered in evaluating the various factors responsible for misregister was distinguishing individual effects. The earth's magnetic field, for example, is always present, and can cause appreciable misregister despite its weakness and the high velocity with which the electron beams travel from the cathodes to the phosphor screen. Figure 9 shows the misregister caused by the earth's magnetic field on a 21AXP22 at Lancaster, Pennsylvania, facing north.

In setting up a shadow-mask kinescope in a test set or receiver,

the effects of the earth's magnetic field on the undeflected beams are minimized by adjustment of the purifying magnet on the tube neck. The earth's field is not uniform over the limited region occupied by the kinescope because of the effect of the metal envelope. Misregister produced at the screen during scanning is corrected by means of a ring-shaped "magnetic-field equalizer" installed at the periphery of the screen. The eight-pole equalizer described by Seelen[1] has since been replaced by the six-pole type shown in Figure 10.

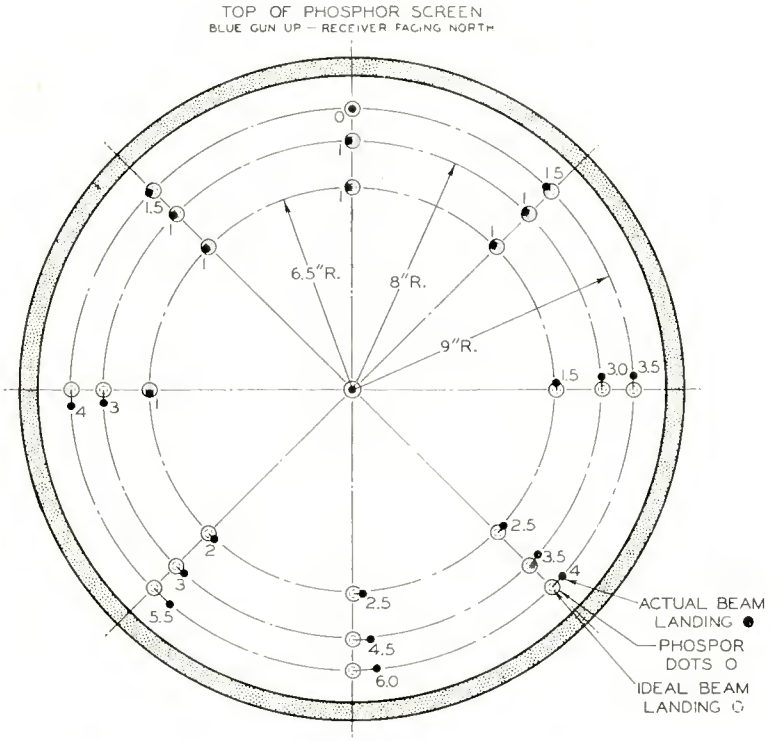

Fig. 9—Misregister caused by earth's magnetic field on the 21AXP22 located at Lancaster, Pa.

The most satisfactory method for evaluating the effects of the earth's magnetic field is to simulate it by means of the six-coil arrangement shown in Figure 11. With such an arrangement (called a Helmholtz-Coil Field Simulator), the magnitude and direction of the earth's magnetic field at any location can be simulated by applying the proper currents to the coils. No attempt is made either to shield out or to cancel the earth's field in these measurements. Instead, the simulated field is added to the field already present.

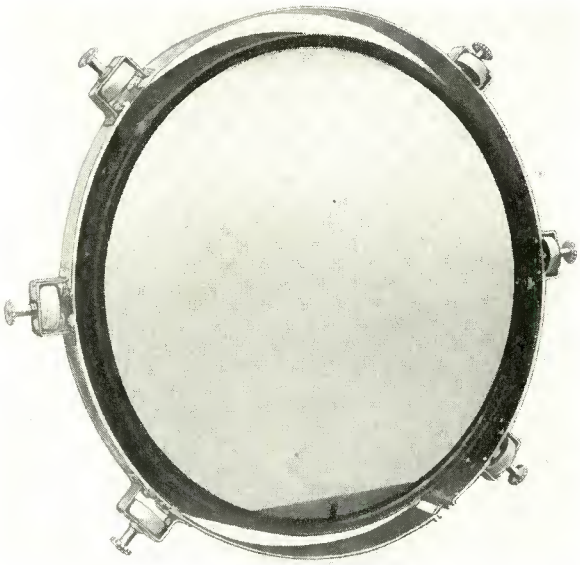

Fig. 10—Six-pole magnetic field equalizer.

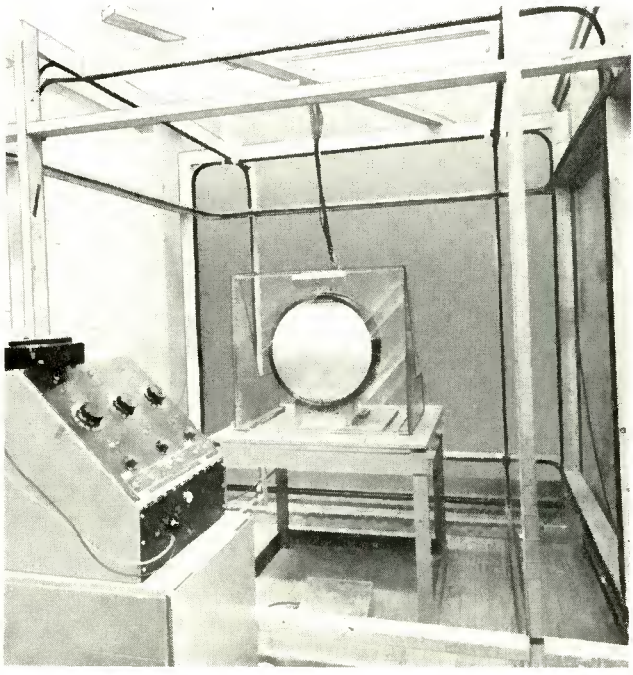

Fig. 11—Coils used to simulate the earth's magnetic field.

For analysis the earth's field may be separated into its horizontal and vertical components. The horizontal component varies in both magnitude and direction with the geographical location and orientation of the tube. Because the vertical component is always perpendicular, misregister caused by this component is always in the same direction (to the left in the northern hemisphere) when looking into the tube face and varies only in magnitude with geographical location.

In the United States, the average strength of the horizontal component is 0.21 gauss, and that of the vertical component 0.54 gauss. Since the vertical component is by far the predominant factor, the amount of correction required for resulting misregister can be minimized by offsetting the entire top-cap assembly to the right of the lighthouse axis. Tests conducted in the Helmholtz-coil setup under a variety of conditions have made it possible to predict the amount of misregister which will be caused by the earth's magnetic field at any geographical location or with any orientation of the kinescope in the normal (horizontal) operating plane. As a result of these tests, an offset of the top-cap is now being used in the lighthouse. This offset is based on the average magnitude of the vertical component in the United States, weighted for population density.

In order to eliminate the effects of the earth's magnetic field and other magnetic fields in the evaluation of the various factors responsible for misregister, the magnetically shielded room shown in Figure 12 was constructed. This room is constructed of Allegheny 4750 metal 3/32 inch thick and is eight feet square and eight feet high. The earth's magnetic field within the room is less than 0.01 gauss.

Mechanical Deformation

Because the phosphor screen of each 21AXP22 is a photographic image of its own aperture mask, it is not necessary that masks or screens from various tubes be interchangeable. To assure tubes of uniformly good quality, however, it is necessary that the contours of all aperture masks and faceplates be as close as possible to the design values. Originally, these contours were measured by means of dial-gauge and jig-borer arrangements. This method, however, is cumbersome and time consuming and these contours are now measured by means of Moore air gauges. In this method, the part to be measured is positioned over a number of preset measuring heads, as shown in Figure 13. Each of these heads contains a small valve through which air is allowed to escape. Deviations from the design dimensions cause changes in the valve apertures and the resulting changes in back pressure on the individual air lines are used to indicate the amounts

of deviation. Displacements as small as 0.003 inch can be measured by this method.

During processing, the faceplate and aperture mask are subjected to mechanical stresses which can change the geometry of the system sufficiently to cause misregister. Extensive tests on the 21AXP22 have indicated that the most serious deformations occur during the exhaust operation.

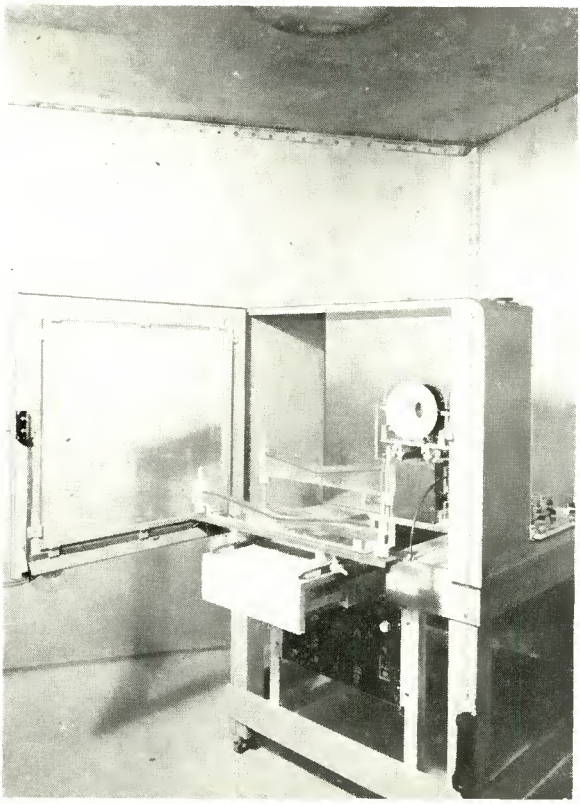

Fig. 12—Magnetically shielded room used for yoke tests.

The movements and deformations of the faceplate and aperture mask during exhaust were measured by means of dial gauges and depth-measuring microscopes. Figure 14 illustrates the changes observed in a typical top-cap assembly. There is a minute flattening of the faceplate, and the aperture mask moves closer to the faceplate but is not appreciably changed in shape. These changes all have radial symmetry about the tube axis, and are responsible for an outward

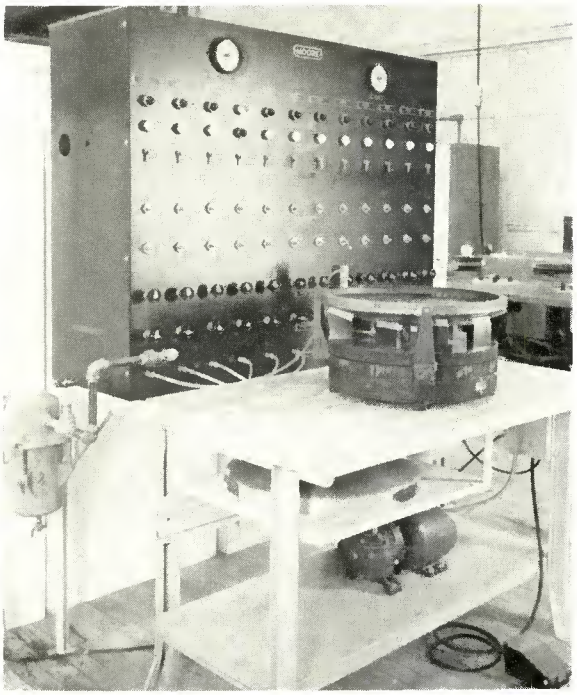

Fig. 13—Moore air gauge used for measuring face-plate and mask contours.

radial misregister of 0.0010 inch to 0.0015 inch at the edge of the screen.

Change in Deflection Center

The effective deflection center in a magnetic deflection yoke moves forward as the angle of deflection is increased. This effect occurs

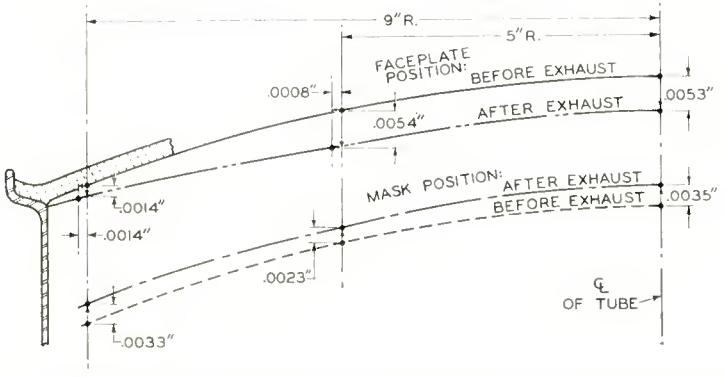

Fig. 14—Face-plate and aperture-mask deformation during tube exhaust.

whether the yoke field is an ideal one having uniform length and strength, or a practical one in which fringing is present. The reason for this change in the apparent origin of the electron beam is shown in Figure 15. During scanning, the beam travels through the yoke field along a curved path. After leaving the field the beam travels in a straight line tangent to its previous curved path at the point of exit. When the strength of the yoke field is increased to obtain greater deflection the radius of the curved path is decreased, and the beam remains longer within the yoke field. If the resulting exit tangents are extended back to the tube axis it can be seen that the effective deflection center moves forward with each increase in deflection angle. For very small deflection angles the beam apparently originates at the

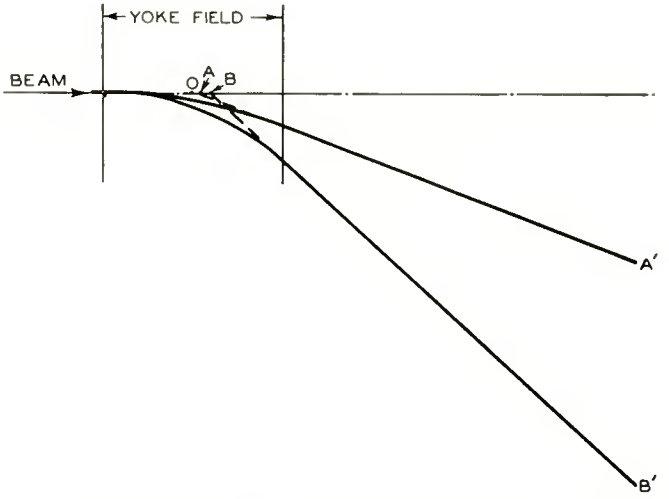

Fig. 15—Sketch illustrating motion of deflection centers.

center of the yoke (point 0 in Figure 15). For successively larger deflection angles the source of the beam apparently moves forward to A and then B. The effective distance between electron source and mask therefore decreases with increased deflection angle. However, the light-source-to-mask distance p used to produce the phosphor screen is constant for all deflections.

These differences between the values of p obtained in operation and the value of p used in the lighthouse can cause radial misregister between the beam spots and their corresponding phosphor dots. This effect is shown in Figure 16. The scale of this figure has been distorted for clarity. It can be seen that as the deflection center moves forward an amount Δp an outward misregister Δr results. This misregister is

not easily distinguished in an operating tube, from that caused by mechanical deformation described above.

A large number of tubes were checked for register in the magnetically shielded room. Only one beam, or color field, was used in these tests in order that any misregister observed would be solely the result of changes in the deflection center of the yoke and the mechanical deformations described above. Each amount of misregister observed during these tests was broken down into its radial and tangential components. The average tangential was found to be small in magnitude and random in direction. The average radial component, however, proved to be large and to have constant magnitude and direction. Figure 17 shows plots of this radial misregister versus distance from

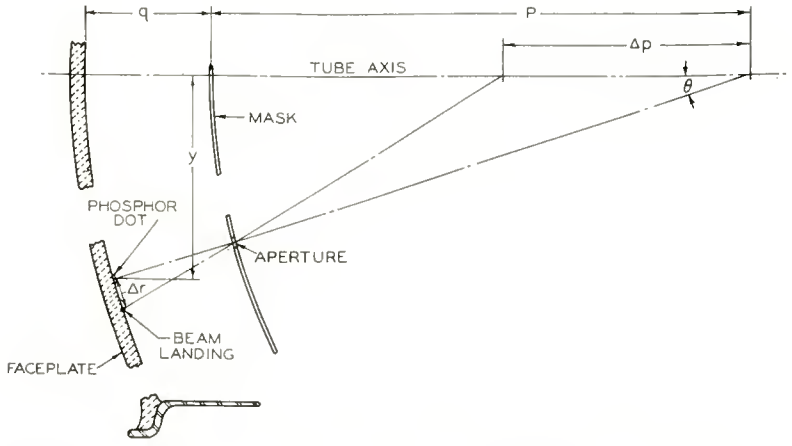

Fig. 16—Radial register change Δr versus deflection-center motion Δp.

the tube axis for an average tube. The three curves show the results obtained with the deflection yoke in different positions on the tube neck. With the yoke in the design position (curve 1), there is an outward radial misregister of 0.005 inch at the 9 inch radius. If the yoke is pulled back on the neck, curves such as 2 and 3 result. It is apparent that the yoke can be positioned so as to correct for radial misregister at any given radius on the tube face, but not so as to correct for misregister at all radii.

Noncoincidence of Horizontal and Vertical Deflection Centers

It was also found that the deflection centers of the horizontal and vertical deflection fields of a yoke are not always coincident. This lack

of coincidence is responsible for a difference in maximum radial misregister in the horizontal and vertical directions. With some commercial yokes this difference was greater than .002 inch.

Radial Correction Lens

The discovery that the radial misregister caused by a change in the effective deflection center of the yoke was constant from tube to tube suggested that it could be corrected by means of a lens in the optical lighthouse. A suitable correction lens[3] was, therefore, designed

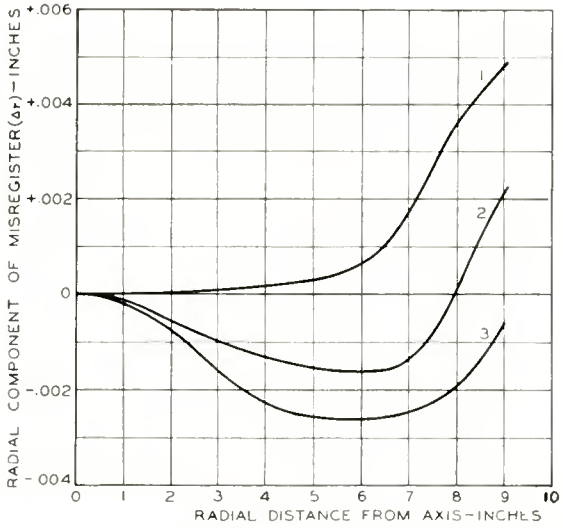

Fig. 17—Radial component of misregister as a function of distance from tube axis.

and constructed. This lens almost completely eliminated the uniform radial misregister, and such lenses are now used in all factory lighthouses.

The correction lens is placed between the light source and the top cap containing the phosphor screen to be exposed. Its action is shown in Figure 18. Without the lens (Figure 18) a ray of light originating at 0 and traveling at an angle θ with respect to the deflection axis will pass through a mask aperture at point A, and strike the phosphor screen at point E. During the exposure of the screen a phosphor dot

[3] D. W. Epstein, P. Kaus, and D. D. VanOrmer, "Improvements in Color Kinescopes Through Optical Analogy," *RCA Review*, Vol. XVI, December, 1955.

will be located at this point. When the completed tube is operated with a conventional yoke, the apparent source of the electron beam for a deflection angle θ will be point B, and the resulting beam path will be BAF. The beam landing spot F, therefore, will be displaced radially outward from its corresponding phosphor dot by an amount Δr.

When a correction lens having the proper curvature is placed between the light source and the phosphor screen to be exposed, as shown in Figure 18, some ray of light OC will be refracted so that on leaving the lens it travels along the path DAF. Since this path is coincident with the path BAF in Figure 18, the phosphor dot created by this ray during the screen exposure will lie at the same point F at which the electron beam will land in an operating tube. In order to provide the

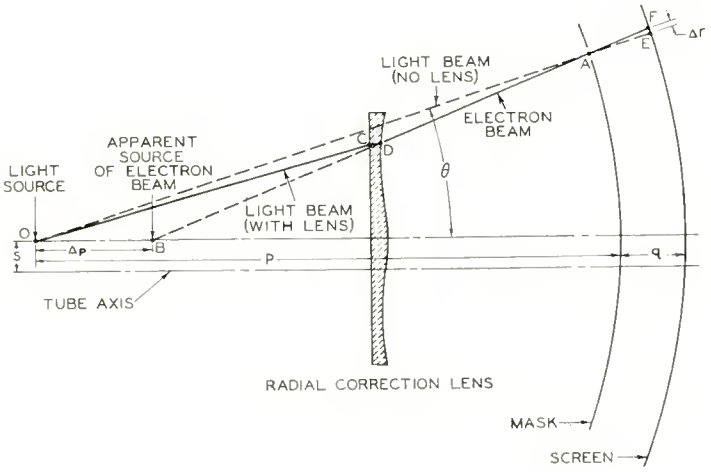

Fig. 18—Action of radial correction lens.

proper amount of correction at each point on the screen the lens curvature must vary from center to edge in such a manner that the spacing between the actual light source O and the virtual light source B increases with deflection angle in the same manner as Δp increases in an operating tube.

Since the deflection point B for each beam lies a distance S from the tube axis, the center of the correction lens must also lie off the axis by this amount. When the light source is rotated to put it in position for the production of the second and third sets of phosphor dots, the lens is rotated with it. In order to eliminate adverse effects which might result from tilting, i.e., improper alignment of the lens in the lighthouse structure, the lens was made as large as possible. The large

size of the lens also simplified the coating procedure (described later in the paper).

Figures 19 and 20 show the lens installed in the lighthouse.

Improved Coincidence of Horizontal and Vertical Deflection Centers

Improvements have also been made in the yoke to reduce the spacing between horizontal and vertical deflection centers.[4]

Investigation showed that differences in the positions of the hori-

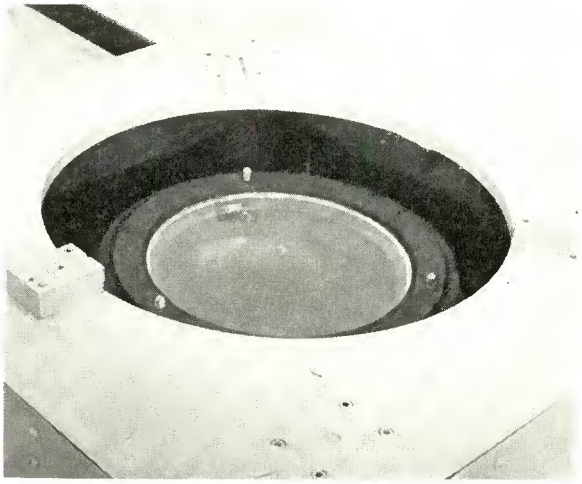

Fig. 19—Mounting of radial correction lens.

zontal and vertical deflection centers of yokes could be minimized by changing the shielding materials used to prevent yoke fields from affecting convergence. In early commercial color yokes, ferrite washers were used as shielding for the low-frequency vertical-deflection field and copper discs as shielding for the high-frequency horizontal-deflection field. With these materials, the difference in maximum horizontal and vertical misregister for a typical yoke was 0.0013 inch.

Substitution of a four-ply silicon-steel washer for the ferrite washer and of an aluminum disc for the copper disc reduced this difference to 0.0003 inch in the standard 230FD1 yoke. This difference is considered negligible, and was obtained without undesirable changes in the other characteristics of the yoke.

---

[4] M. J. Obert, "Deflection and Convergence of the 21AXP22 Color Kinescope," *RCA Review*, Vol. XVI, pp. 140-169, March, 1955.

Dynamic Degrouping

As a result of the mechanical tilt of the three electron guns and the action of the beam-converging pole pieces, the undeflected beams converge on the tube axis at the plane of the aperture mask. During scanning the beams converge at a highly curved surface concave toward the deflection center. Because of the relative "flatness" of the aperture mask, at the larger deflection angles the beams converge before reaching the mask. This undesirable condition is corrected by the application of a "dynamic convergence" current derived from, and in synchronism with, the horizontal and vertical scanning waveforms and

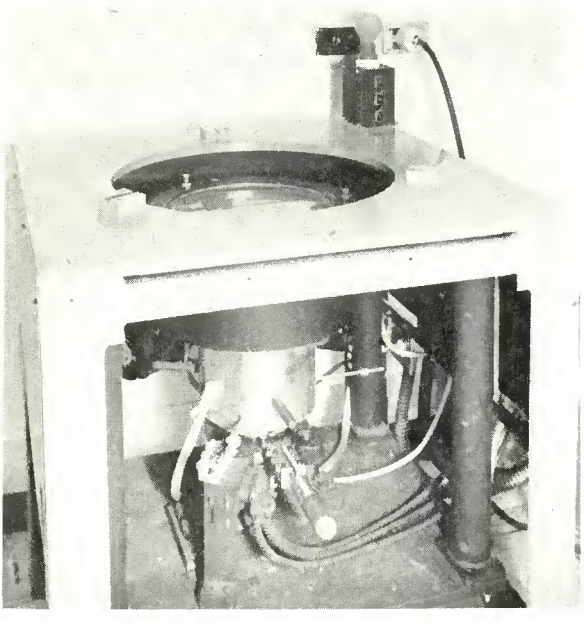

Fig. 20—Optical lighthouse with radial correction lens.

applied to the windings of the external convergence magnets. The effects of this current are shown in Figure 21. For simplicity only two of the three beams are shown.

In the absence of scanning, the beams pass through the deflection plane at points A and B, at equal distances S from the tube axis, and converge at the plane of the mask. The dynamic-convergence fields developed during scanning shift the beams away from the axis, so that at maximum deflection they pass through the deflection plane at points A' and B'. Since the spacing between beam spots at the screen is a

constant demagnification of the spacing between beams in the deflection plane, the increase in beam spacing during scanning results in spreading or "degrouping" of the electron spots with respect to the phosphor dots. This "dynamic degrouping" increases with deflection angle in the manner shown in the inserts at the right of Figure 21. In early 21AXP22 tubes the average dynamic degrouping at the edge of the screen was 0.0023 inch—that is, the distance from the center of a beam landing spot to the center of the beam spot trio was 0.0023 inch greater than the distance from the center of a phosphor dot to the center of the phosphor dot trio.

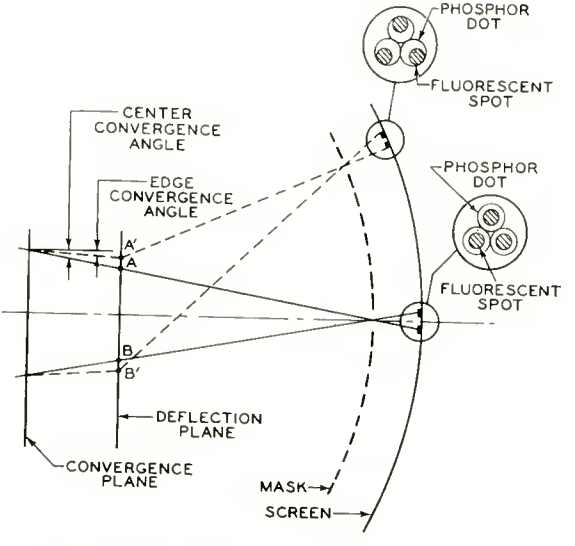

Fig. 21—Sketch illustrating effect of dynamic convergence.

Correction for Dynamic Degrouping

Various schemes for correcting this dynamic degrouping have been considered. The most practical solution developed to date has been the use of a compromise value of s in the optical lighthouse. The results of this modification are shown in Figure 22.

In the modified lighthouse, the light source is placed at point C, an increased distance s' from the tube axis. This change caused a corresponding degrouping of the phosphor dots at the screen, as shown at $B'B'$ and $B''B''$, so that it was necessary to decrease the spacing q between mask and screen in order to maintain the desired spacing within the dot trios. Since the original value of s is used in the gun

assembly, the "dynamic degrouping" effects are redistributed in an operating tube. At zero deflection angle the electron beams again pass through the deflection plane at points *AA*, but, because of the reduced spacing *q*, are "grouped" at the screen—that is, they strike the screen at points which are slightly closer to the center of the phosphor dot trios than the centers of the individual phosphor dots. At large deflection angles the beam spots are still degrouped, but by much smaller amounts than in the original design. Perfect register between beam spots and phosphor dots is obtained at points approximately midway between the center and edge of the screen. The compromise value of *s* used on the lighthouse is 0.327 inch, as compared with the value of 0.276 inch used in the original lighthouse design and in the electron

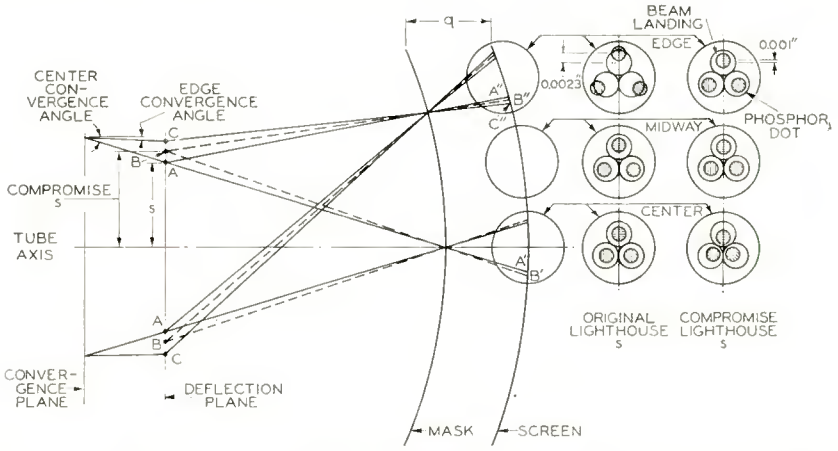

Fig. 22—Sketch illustrating effect of dynamic convergence on a tube with a compromise S valve.

gun assembly. The mask-to-screen spacing, *q*, has been decreased from 0.535 to 0.451 inch. As a result of these changes dynamic degrouping at the edge of the screen has been reduced from 0.0023 to less than 0.001 inch.

Phosphor-Trio Asymmetry

In a planar-type shadow-mask tube the phosphor-dot trios form perfect equilateral triangles over the entire surface of the screen. In a formed-mask tube, however, the curvature of the mask and screen causes a radial compression of these trios which increases with deflection angle. This radial compression or "grouping" amounts to more than 0.001 inch at the edges and is particularly undesirable because it is in opposition to the dynamic *degrouping* of the beam spots.

Correction for Phosphor-Trio Asymmetry

This radial grouping of the phosphor dots can be minimized by shifting the center of the correction lens off the center line of the light source. Such a shift increases the refraction on one side of the center line and decreases it on the other, and thus redistributes the dot grouping in the same manner as the use of a compromise value of s redistributes the degrouping of the beams. A substantial reduction in phosphor trio grouping has been obtained by offsetting the center of the lens 0.075 inch beyond the center line of the light source. Figure 23 shows the present arrangement, using the compromise offset

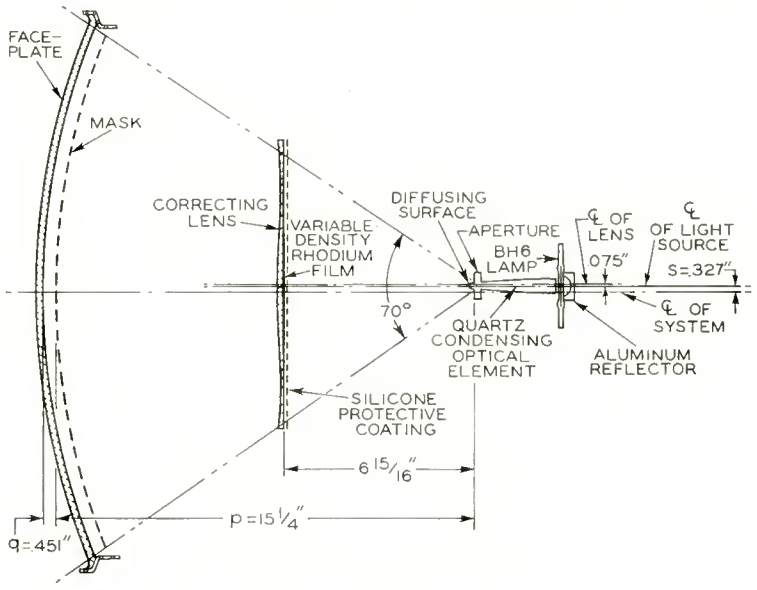

Fig. 23—Complete lighthouse geometry.

of 0.327 inch for the light source and an additional offset of 0.075 inch for the lens.

Light Source Nonuniformity

The phosphor dots produced on the screen during the lighthouse exposure are, in the ideal case, demagnified images of the light source used to produce them. However, the characteristics of the photoresist are such that the sizes of the phosphor dots vary considerably with light intensity and exposure time. The optical system used in early lighthouses was designed to pick up radiation throughout a wide-angle cone, and to pass the condensed radiation through a circular aperture

of about 0.160 inch diameter to a hemispherical diffusing surface. In these lighthouses, the variation in light intensity from center to edge was approximately 35 per cent, and resulted in a corresponding variation in phosphor dot size, the smallest dots occurring at the edge of the screen. Consequently when tubes produced on these lighthouses were operated, even small amounts of misregister caused the beams to miss the phosphor dots at the edge of the screen. As a result, there was considerable variation in light output and color purity in these regions. It was possible to obtain more nearly uniform dot size over the screen by increasing the exposure time so that the edge received adequate exposure. When this was done, however, the center portion

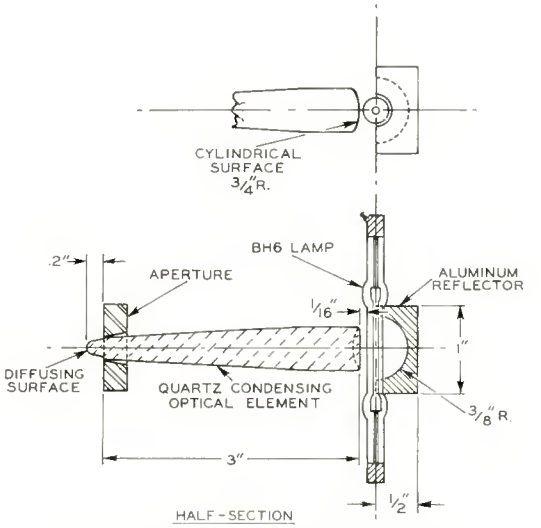

Fig. 24—Improved lighthouse optics.

of the screen, where the radiation intensity was highest, was overexposed.

Improved Lighthouse Optics

The optics of the new and more efficient lighthouse assembly mentioned by Seelen[1] are shown in Figure 24. The light source is a 1-kilowatt high-pressure capillary mercury-arc lamp, selected as the brightest source of ultraviolet and blue radiation in the region 3,400 to 5,000 angstroms commercially available, and for its good stability and life. The reflector is a spherical mirror having a highly polished aluminum surface.

The light-collecting end of the quartz condensing optic has been

made cylindrical, with a radius of curvature of about 0.75 inch. This configuration provides maximum light collection in the direction perpendicular to the axis of the lamp when the optic is mounted with the axis of its cylindrical end parallel to the lamp axis.

The optimum shape for the diffusing surface was found to be parabolic rather than hemispherical, the optimum diameter 0.220 inch, and the optimum extension beyond the defining aperture 0.200 inch (see Figure 25). These changes reduced the maximum variation in light intensity across the screen from 35 to 25 per cent. However, with proper exposure at the center of the screen there was still considerable variation in dot size across the screen.

Analysis of the radiation intensity over the screen surface showed that the equal-intensity contours were approximately elliptical, with their long axes parallel to the axis of the lamp. It was determined that the variation in radiation intensity over the screen could be reduced

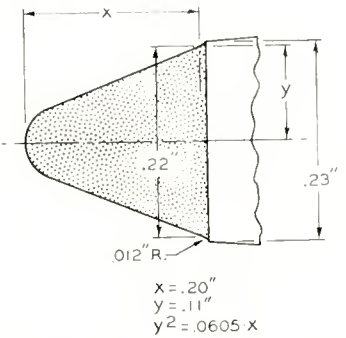

Fig. 25—Optimum lightsource diffusing surface.

to about 15 per cent by the application of a metal film of varying density to the flat surface of the lens. Rhodium was selected as a suitable material for this film because of its stability in air and relative ease of evaporation. The rhodium was evaporated from a plated tungsten filament, shaped and positioned so as to produce a film having an essentially elliptical density distribution and gradients equivalent to those of the radiation intensity. The thickness of the film was controlled so as to obtain white-light transmission of approximately 75 per cent at the center, and of almost 100 per cent at the two edge points perpendicular to the axis of the lamp.

These new features have made it possible to achieve a uniformity of dot size within 0.002 inch over the entire screen area, and have permitted a 40 per cent reduction in exposure time over the older system. Work is being directed toward even further improvement.

ACKNOWLEDGMENT

The authors would like to acknowledge the contributions of many people to this program. Especial thanks are due to D. D. VanOrmer, Miss H. C. Moodey, P. Kaus, and M. J. Obert.

EFFECT OF MAGNETIC DEFLECTION ON ELECTRON BEAM CONVERGENCE

By

Peter E. Kaus

RCA Laboratories,
Princeton, N. J.

Summary—*The image curvatures of deflection yokes are calculated and minimized using third-order perturbation theory. It is found that the mean image curvature is too large to dispense with dynamic convergence when a point focus is needed. Proper field shaping, however, can produce a good line focus over the whole screen without dynamic convergence.*

Introduction

THE quality of deflection yokes has become increasingly important, particularly for color kinescopes using three beams. Misconvergence of the three beams caused by the yoke is proportional to both the deflection angle and the convergence angle of the beams. In consequence, it has been necessary to introduce dynamic convergence as a means of keeping the three beams converged over the whole surface of the screen. Since dynamic convergence introduces a misregister effect known as "degrouping," it is desirable to minimize or eliminate the need of dynamic convergence by minimizing or eliminating those aberrations of the deflection yoke which are responsible for misconvergence.

This paper investigates the aberrations of a deflection coil, using its symmetry properties, by a perturbation treatment developed by W. Glaser and G. Wendt.[1,2] It will be shown that significant improvement over present yokes is possible for line-screen kinescopes and that the length of the yoke field is the most important parameter.

Description of the Magnetic Field

Magnetic deflection fields as they are used in television tubes have as a common property the symmetry group to which they belong. If we take as the z axis the axis of the tube and the x and y axes as the horizontal and vertical axes, then the symmetry property of the field of a *vertical-deflection* yoke coil (Figure 1) is given by

---

[1] W. Glaser, "Über die Ablenkfehler von electrischen und magnetischen Ablenksystemen," *Zeitschrift für Physik*, Vol. 111, 1938.

[2] G. Wendt, "Über die Abbildungsfehler magnetischer Ablenkfelder," *Telefunkenröhre*, April, 1939.

$$H_x(x,y,z) = H_x(-x,y,z) = H_x(x,-y,z),$$
$$H_y(x,y,z) = -H_y(-x,y,z) = -H_y(x,-y,z), \tag{1}$$
$$H_z(x,y,z) = -H_z(-x,y,z) = H_z(x,-y,z).$$

In the region of deflection, the field must obey Maxwell's equations for a region free of charge, current, or electric field:

$$\text{curl } \vec{H} = 0,$$
$$\text{div } \vec{H} = 0. \tag{2}$$

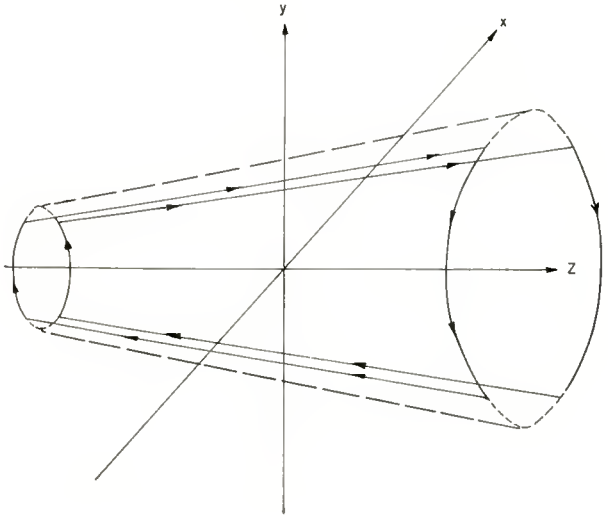

Fig. 1—Symmetry of a vertical-deflection coil.

Equations (1) and (2) limit considerably the possibilities of choices for deflection fields. In a power-series expansion of the field one obtains

$$H_x = H_1(z) - [H_2(z) + H''_1(z)/2]\, x^2 + H_2(z)\, y^2 + \text{fourth-order terms},$$
$$H_y = 2H_2(z)\, xy + \text{fourth-order terms}, \tag{3}$$
$$H_z = H'_1(z)\, x + H'_2(z)\, xy^2 - \frac{1}{6}[H''_1(z) + 2H'_2(z)]\, x^3 + \text{fourth-order terms},$$

where $H'(z) = dH(z)/dz$.

The meaning of Equations (3) is that for sufficiently small x and y, the curves for $H_x =$ constant are ellipses or hyperbolas in a plane $z =$ constant. The curves $H_y =$ constant are hyperbolas. The curves $H_z =$ constant are slightly more complicated, but for very small x and y they are straight lines parallel to the y axis.

Figure 2 gives a plot of H_x, H_y, and H_z as it was measured in a typical deflection yoke at some arbitrary $z =$ constant. Of course, Equations (3) need no experimental verification, being a simple consequence of the symmetry properties of the yoke coils and Maxwell's equation. The figures do indicate, however, for what ranges of x and y a third-order expansion of the field will give good approximation.

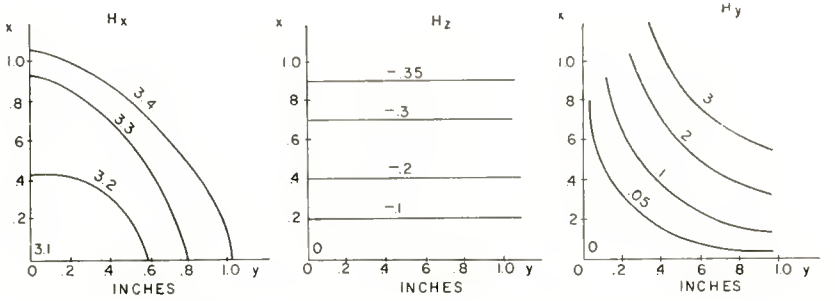

Fig. 2—Lines of constant field strength; $z =$ constant.

Equations (3) also show that the whole field in the region where third-order theory is good, is given by two arbitrary functions, $H_1(z)$ and $H_2(z)$. Therefore, in order to know the field, it is only necessary to obtain these functions. This is easily done by measuring the total field along two lines parallel to the z axis: (a) The z axis itself ($x = 0$, $y = 0$,) and (b). Some line of constant y and $x = 0$ ($x = 0$, $y = y_c$). The first will give $H_1(z)$ directly as can be seen by an inspection of Equations (3). The second will give $H_1(z) + H_2(z)y^2{}_c$.

This means that simply measuring the total field at say ten points on line (a) and line (b) makes it possible to pass tenth-order polynomials through $H_1(z)$ and $H_2(z)$, which in turn specify the whole field in the regions of interest.

The third-order expansion should be good for deflection angles of up to 25 degrees. This is perfectly adequate for questions of convergence, since certain boundary conditions about the surfaces of best

convergence will then make it possible to extrapolate to larger deflection angles, as will be demonstrated later.

Now introduce a vector potential $\vec{A}$, such that

$$\vec{H} = \text{curl } \vec{A}.$$

One particular choice of $\vec{A}$ is the following:

$$\begin{aligned} A_x &= 0 + \text{fourth-order terms}, \\ A_y &= (1/2) H'_1(z) x^2 + \text{fourth-order terms}, \\ A_z &= H_1(z) y + (1/3) H_2(z) y^3 - H_2(z) x^2 y \\ &\quad + \text{fifth-order terms}. \end{aligned} \tag{4}$$

Perturbation Method

Lagrangian and Equations of Motion

The integration of the path by the perturbation method has been derived in detail for magnetic deflection fields.[1,2] Only as much of the argument will be repeated here as is necessary for an understanding of the conclusions.

The lagrangian for an electron trajectory can be written

$$W = \int_{P_0}^{P_1} F dz$$

in close analogy to Fermat's principle in light optics, where

$$F = \eta ds/dz.$$

In electron optics, the index of refraction becomes

$$\begin{aligned} \eta &= (\zeta)^{1/2} - (e/2m)^{1/2} [A_x(dx/ds) \\ &\quad + A_y(dy/ds) + A_z(dz/ds)], \\ F &= (\zeta)^{1/2} (1 + x'^2 + y'^2)^{1/2} \\ &\quad - (e/2m)^{1/2} (A_x x' + A_y y' + A_z). \end{aligned} \tag{5}$$

The function ζ is simply the electric potential taken with respect to a particle at rest, and in the case of a purely magnetic field it is

It is seen from Equations (13) that for $z = L$, where the screen is located,

$$x = 0, \qquad y = D(L), \tag{14}$$

and $D(z)$ is strictly proportional to $H_1(z)$. This situation is also referred to as "perfect gaussian deflection." The whole cone, regardless of convergence angle or deflection angle, comes to a point of convergence at $y = D(L)$, and $D(L)$ depends linearly on $H_1(z)$. Any deviation from Equations (14) will be called a "deflection error."

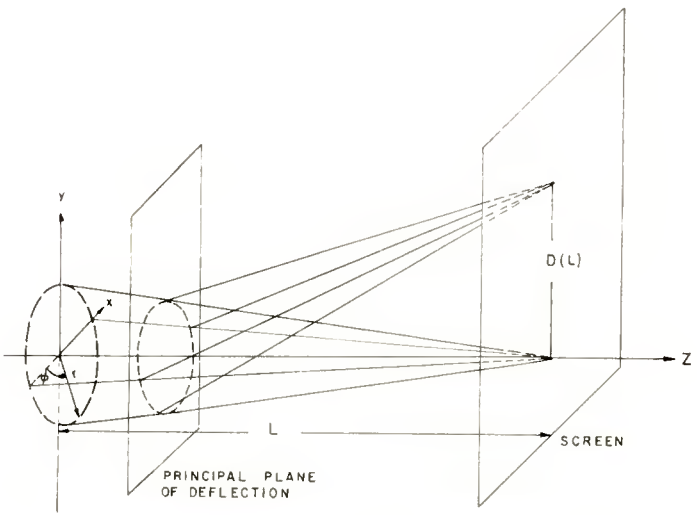

Fig. 3—Ideal deflection of a conical bundle.

Third-Order Calculation

The solution for the first-order calculation is

$$\begin{aligned} x &= (z - L)\ \alpha \cos \phi, \\ y &= (z - L)\ \alpha \sin \phi + D(z), \\ x' &= \alpha \cos \phi, \\ y' &= \alpha \sin \phi + D'(z), \end{aligned} \tag{15}$$

where: $$D'(z) = -\mu \int_0^z H_1(w)\, dw.$$

Substituting these values into Equations (9) for the higher powers of

x, y, x', and y', the equations can be easily integrated. Then, neglecting terms of the order of α^2,

$$x(L) = I_P \alpha \cos \phi,$$
$$y(L) = I_T \alpha \sin \phi + D(L) + I_D. \tag{16}$$

Here, I_P, I_T, and I_D are integrals of the field quantities, which will be given later. They will be given the following names:

$$I_P = \text{perpendicular astigmatism},$$
$$I_T = \text{tangential astigmatism},$$
$$I_D = \text{distortion}.$$

Figures 4, 5, and 6, will give these "errors" meaning. Figure 4 is a picture in the $x = 0$ plane of the central ray ($r = 0$) and two rays whose original coordinates are given by $\cos \phi = 0$, $\sin \phi = \pm 1$. From Equations (16), in that case

$$x(L) = 0,$$
$$y(L) = \pm I_T \alpha + I_D + D(L).$$

For the central ray $\alpha = 0$, and it will simply be displaced from the "perfect" position $D(L)$ by an amount I_D. The rays coming from $\sin \phi = \pm 1$, will be displaced by an amount $\pm I_T \alpha + I_D$. If I_T is positive (as it usually is), then the three rays will cross at a position $z = z_T$. The curve which is generated by these crossings will be called the "tangential image curvature" and its radius of curvature (constant in third-order theory) is R_T.

Similarly, a projection of the rays characterized by initial position $\sin \phi = 0$, $\cos \phi = \pm 1$ are given in a plane $y =$ constant (Figure 5a) and $x =$ constant (Figure 5b). Here, the only distortion arises from the term I_P and the two rays will cross at a position $z = z_p$. The curve which is generated by these crossings will be called the "perpendicular image curvature" and its radius of curvature (constant in third-order theory) is R_P.

Finally, there is a curve along which the whole bundle of rays form the smallest circle. It is along this curve that best over-all convergence is obtained. This curve is called "mean image curvature" and its radius of curvature R is given by

$$(1/R) = (1/2)\,[(1/R_P) + (1/R_T)]. \tag{17}$$

Figure 6 gives a diagram of the total situation, showing the three image curvatures. In order to obtain good convergence, it is, therefore, desirable to maximize these radii of curvature in order to make them correspond to the curvature of a screen that is not too severely curved towards the gun system. That the mean radius of convergence has definite upper limits will make up the main part of the rest of this paper.

Let it also be mentioned, with respect to Equations (16), that it thus appears that the ring of rays starting from $z = 0$, $x^2 + y^2 = r^2$, will, on a flat screen, at $z = L$, appear as an ellipse, whose center is at $x = 0$, $y = D(L) + I_D$ and whose axes are $I_P\alpha$ in the horizontal and $I_T\alpha$ in the vertical directions.

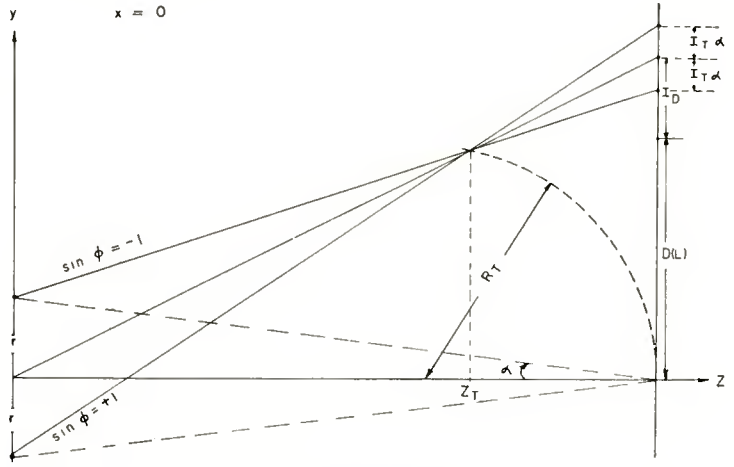

Fig. 4—Vertical deflection of tangential rays (sin $\phi = \pm 1$).

The Surfaces of Convergence

In order to obtain the tangential, perpendicular, and mean image curvatures, i.e., R_T, R_P, and R, use is made of the fact that in third-order theory these radii are constant. That means that without loss of generality the radii for infinitesimally small deviations can be calculated and they will hold for the whole region in which third-order theory holds (up to deflection angles of about 25 degrees). Later, it will be shown how these can be extrapolated to higher angles.

For very small deviations, D can be considered as an infinitesimal quantity and quantities of the order of D^2 can be neglected. The calculation is made with reference to Figure 7. Two relations hold exactly in that figure:

$$R_T^2 = m^2 + [R_T - (L - z_T)]^2 \tag{18}$$

and

$$I_T\alpha/r = (L - z_T)/z_T. \tag{19}$$

Consistent with the small angle of deviation, let

$$m^2 = D^2$$

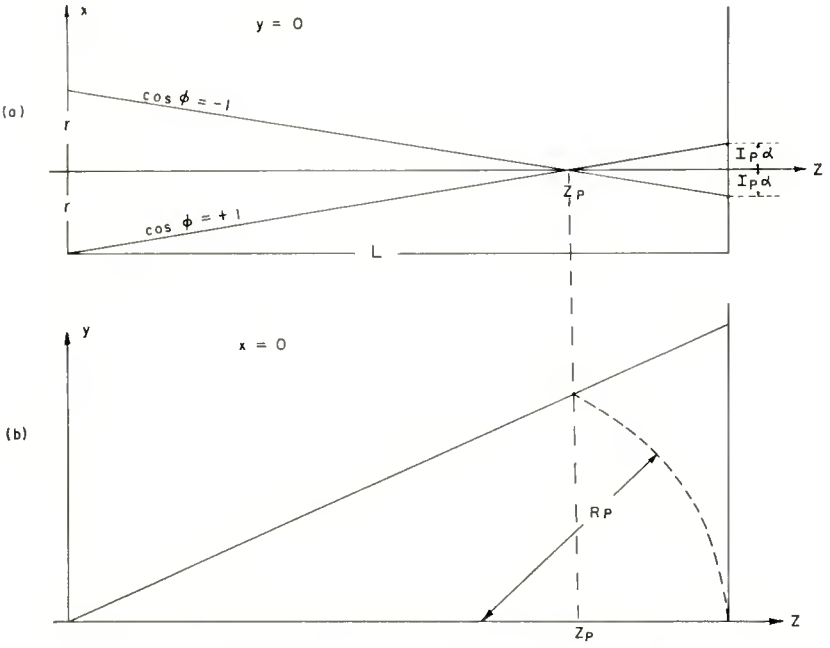

Fig. 5—Vertical deflection of perpendicular rays (cos $\phi = \pm 1$).

and neglect $(L - z_T)^2$ compared to $(L - z_T)$. When these approximations are used consistently, Equation (18) gives

$$R_T = D^2/2\ (L - z_T)\ ;$$

and from Equation (19), letting $\alpha z_T/r = z_T/L \approx 1$,

$$R_T = D^2/2I_T. \tag{20}$$

Similarly,

$$R_P = D^2/2I_P; \tag{21}$$

and from Equation (17),

$$1/R = (I_T + I_P)/D^2. \tag{22}$$

Actually, the quantities I_T/D^2 and I_P/D^2 turn out to be independent of D^2, and it appears useful to define

$$J_T = I_T/D^2,$$
$$J_P = I_P/D^2. \tag{23}$$

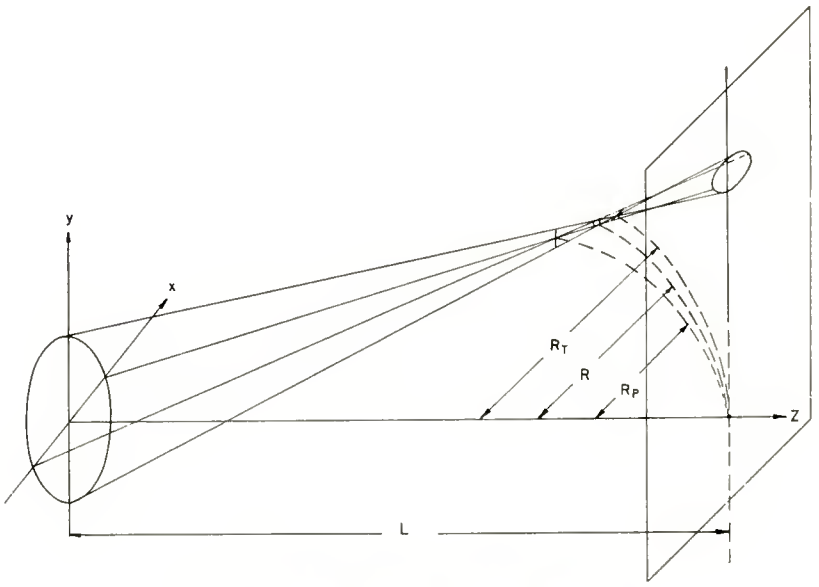

Fig. 6—The composition of astigmatism.

Then

$$1/R_T = 2J_T,$$
$$1/R_P = 2J_P, \tag{24}$$
$$1/R = J_T + J_P.$$

Now give attention to the form of J_T and J_P and note their dependence on the field distribution $H_1(z)$ and $H_2(z)$. Assume that a conical bundle of rays enters the deflection field at $z = 0$. The deflection field is different from zero up to $z = l$. The original bundle was convergent on the z axis at $z = L$. The aberrations J_T and J_P are then given by

$$J_T = (3/2)\ S_1 + 2S_2\,,$$

$$J_P = -(1/2)\ S_1 - 2S_2 + S_3\,, \tag{25}$$

where

$$S_1 = [1/D(L)\,]^2 \int_0^L [\,D'(z)\,]^2\, dz,$$

$$S_2 = \mu\,[1/D(L)\,]^2 \int_0^l H_2(z)\ D(z)\ (z-L)^2\, dz, \tag{26}$$

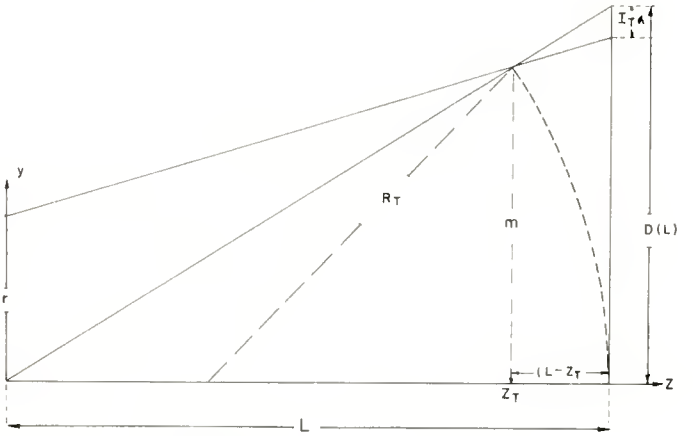

Fig. 7—Calculation of R_T.

$$S_3 = \mu^2\,[1/D(L)\,]^2 \int_0^l H_1^2(z)\ (z-L)^2\, dz.$$

It will be remembered from Equations (14) and (15) that

$$D(z) = -\mu \int_0^z dw \int_0^w H_1(v)\, dv,$$

$$D'(z) = -\mu \int_0^z H_1(w)\, dw.$$

It follows that

$$D(L) = -\mu \int_0^l dz \int_0^z H_1(v)\, dv + (L-l)\ D'(l). \tag{27}$$

Substituting Equations (25), (26), and (27) into Equations (24),

$$1/R = \frac{\int_0^L [D'(z)]^2\, dz + \mu^2 \int_0^l H_1^2(z)\ (z-L)^2\, dz}{D^2(L)}. \quad (28)$$

The first important result is that Equation (28) does not depend on $H_2(z)$ at all. This means that even though R_T and R_P depend very sensitively on $H_2(z)$, *the radius of best over-all convergence depends only on the field along the axis*, $H_1(z)$. Secondly, it is obvious from Equation (28) that $1/R$, and therefore R, is always positive. This means that *the surface of best convergence must always bend towards the source of the electrons.*

It now remains to minimize the expression for $1/R$, Equation (28), which will maximize R and, therefore, yield the best possible field distribution.

In order to make Equation (28) more amenable to mathematical treatment, the following function is introduced:

$$K(z) = \left[\int_0^z H_1(w)\, dw\right] \left[\int_0^l H_1(w)\, dw\right]^{-1}. \quad (29)$$

In that case the reciprocal radius of image curvature becomes

$$1/R = \left[\int_0^l K^2\, dz + \int_0^l K'^2 (z-L)^2\, dz + (L-l)\right] \left[\int_0^l K dz + (L-l)\right]^{-2} \quad (30)$$

The boundary conditions on $K(z)$ are

$$K(0) = 0, \qquad K(l) = 1, \qquad K'(z) = 0, \quad (31)$$

for $z < 0$ and $z > l$. The derivative of $K(z)$ with respect to z, $K'(z)$, is $H_1(z) \left[\int_0^l H_1(z)\, dz\right]^{-1}$. The $K(z)$ simply represents a normalized potential. Figure 8 shows the relationship between $K(z)$ and $H_1(z)$.

The next step is to minimize Equation (30), which means finding that distribution of $K(z)$ which will give a minimum $1/R$. The results of this calculation are given in the next section.

Results

The Uniform Field

The solution of the equation

$$\delta(1/R) = 0,$$

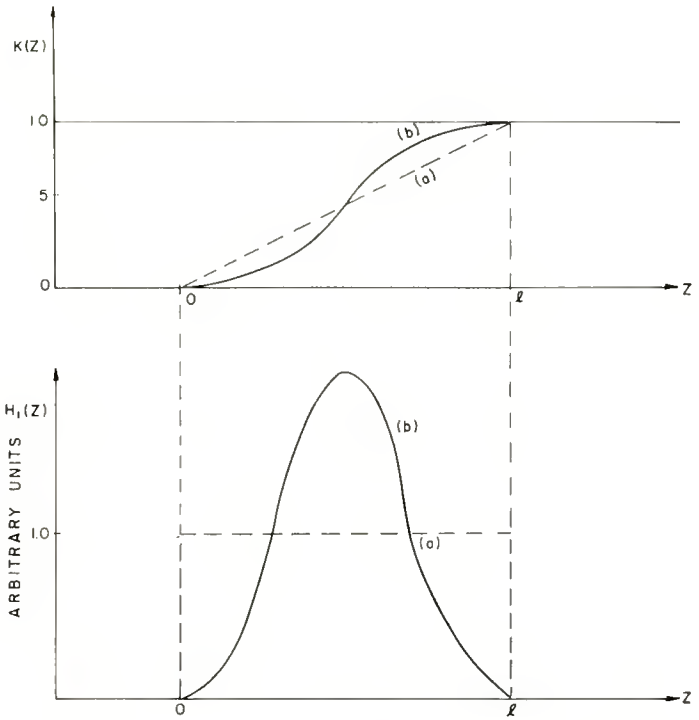

Fig. 8—Relationship between $K(z)$ and $H_1(z)$.

where $(1/R)$ is given by Equation (30), has proved to be too difficult in closed form. It was, therefore, desirable to use polynomials of a certain degree n, such as Legendre polynomials, for $K(z)$, and minimize for each case. The first-order case corresponds to a uniform field. This case is of particular interest because it has been discussed by several authors in the past, mostly incorrectly, due to a disregard of Maxwell's equation. The first correct treatment and experimental

verification of the uniform field case was given by Marschall and Schroder.[3]

For the uniform field, $K(z)$ takes the following form:

$$\begin{aligned} K(z) &= 0, & z &\leq 0, \\ K(z) &= z/l, & 0 &\leq z \leq l, \\ K(z) &= 1, & l &\leq z, \end{aligned} \tag{32}$$

(see Figure 8).

Substituting Equation (32) into Equation (30),

$$(R/L) = (l/L)\,[1 - (l/L) + (1/4)\,(l/L)^2]\,[1 - (1/3)\,(l/L)^2]^{-1} \tag{33}$$

To render this result dimensionless, we define new quantities:

$$\rho = R/L, \qquad \lambda = l/L.$$

Obviously, λ can vary from 0 to 1.

In terms of the parameters ρ and λ, Equation (33) becomes

$$\rho = \lambda\,[1 - \lambda + (1/4)\,\lambda^2]\,[1 - (1/3)\,\lambda^2]. \tag{34}$$

The solid line in Figure 9 gives a plot of Equation (34). The main feature of this result is that for short fields ($l \ll L$ and, therefore, $\lambda \ll 1$) ρ is equal to λ, and consequently

$$R \approx l. \tag{35}$$

This means that for short yokes the image curvature is not related to the yoke to screen distance (L), as is widely believed, but is simply the length of the yoke field (l). As the length of the yoke field increases, i.e., as λ approaches 1, the image curvature approaches

$$R \approx (3/8)L. \tag{36}$$

This result is in perfect agreement with Marschall and Schroder[3] and has been verified experimentally by them.

---

[3] H. Marschall and W. Schröder, "Die Bestimmung der mittleren Bildwölbung doppelsymmetrischer Ablenkspulen für Kathodenstrahlröhren," *Zeitschrift für technische Physik*, Vol. 23, 1942.

Higher-Order Solution

The analysis of the uniform field still leaves the question open as to whether more general field distributions can yield a larger radius of curvature R, than is given by Equation (33). For this purpose, higher-order polynomials were used for $K(z)$, and $1/R$ was minimized with respect to the parameters of the expansion. Of course, $K(z)$ must obey its boundary conditions at $z = 0$ and $z = l$.

The expansion of $K(z)$ was done in terms of Legendre polynomials. In order to change the interval 0 to l of z, into an interval -1 to $+1$,

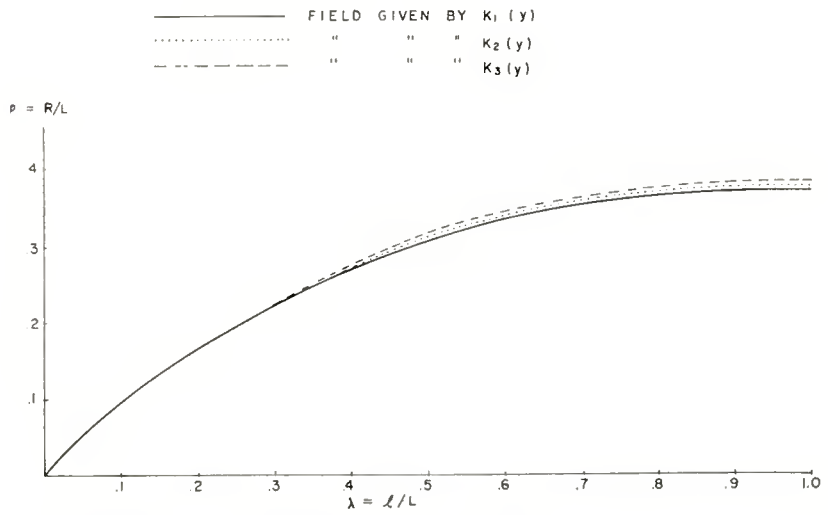

Fig. 9—Maximum radius of curvature for a polynomial expansion of the field.

change variables from z to y, where y is given by

$$y = (2z/l) - 1. \tag{37}$$

Now more general expressions for $K(z)$ can be given:

First-order

$$K_1(y) = (1/2)P_0(y) + (1/2)P_1(y) \quad \text{(uniform field)},$$

Second-order

$$K_2(y) = a_0P_0(y) + (1/2)P_1(y) + (1/2 - a_0)P_2(y),$$

Third-order

$$K_3(y) = a_0P_0(y) + a_1P_1(y) + (1/2 - a_0)\,P_2(y) + (1/2 - a_1)\,P_3(y).$$

The minimum radii of curvature for each case are given in Figure 9, in terms of $\rho = R/L$ and $\lambda = l/L$.

The main conclusion of this investigation is that the improvement that can be achieved by using a more general field distribution than the uniform field is completely insignificant. For example, always using the best choice of a_0 and a_1 in $K_3(y)$,

$$\rho = \frac{\lambda\ (1 - \lambda + .13\lambda^2 + .06\lambda^3 + .01\lambda^4)}{(1 - .52\lambda^2 - .01\lambda^3 + .04\lambda^4)}. \tag{38}$$

Quantitative comparison of Equations (38) and (34), as shown in Figure 9, demonstrates how insignificant the improvement of the more general third-order field is over the uniform field.

Equivalent Uniform Field

For a practical application of the results in the preceding section, one point needs further clarification. Actual fields are not precisely confined to a region from 0 to l. In order to give the formulas meaning, therefore, we must define a length which will be associated with an actual field distribution which ranges from plus to minus infinity. This is possible, particularly when one recognizes from Equations (34) or (38) that R is sensitive to the length of the field only for short fields. Therefore, the formula for the equivalent length should be very good for short fields, $l < L/3$, and qualitatively correct for larger fields.

An analysis of Equation (30) in connection with Equations (29) and (34) gives, for the effective l,

$$l_e = \left[\int_{-\infty}^{\infty} H_1(w)\ dw\right]^2 \left[\int_{-\infty}^{\infty} H_1^2(w)\ dw\right]^{-1}, \tag{39}$$

where w represents an arbitrary coordinate system. In order to place the origin of the z coordinate system, the principal plane of deflection must be known. This is given by

$$w_p = \left[\int_{-\infty}^{\infty} wH_1(w)\ dw\right] \left[\int_{-\infty}^{\infty} H_1(w)\ dw\right]^{-1}. \tag{40}$$

The z-coordinate system is now defined by

$$z = w - w_p + l_e/2. \tag{41}$$

The image curvature can be predicted by measuring $H_1(w)$, deter-

mining l_c from Equation (39), w_P from Equation (40) and the z-coordinate system from Equation (41). This gives L. To get the image curvature, Equation (34) is used, substituting l_e/L for λ.

Therefore, in order to predict the image curvature, it is necessary to know only $H_1(w)$, the field distribution along the axis.

$H_2(z)$ Contributions

Even though the surface of least confusion, that is, the mean image curvature, is independent of $H_2(z)$ in Equations (3), nearly all other properties of the yoke are extremely sensitive to that function. It is, therefore, important to adjust $H_2(z)$ carefully to obtain desired results.

$H_2(z)$ can be used to give anastigmatic yokes, or purposely astigmatic yokes to fulfill special purposes such as line focus, etc. These possibilities will now be taken up in turn. Since for every special purpose $H_2(z)$ will depend very sensitively on $H_1(z)$, it shall be assumed in what follows that $H_1(z)$ is a uniform field of length l, where $l \ll L/3$. Similar calculations, of course, can be made for any particular $H_1(z)$ distribution.

Anastigmatic Deflection. An examination of Figure 6 will show that if it is desired for the beam, converged on the surface of least confusion, to be a point, then $R_T = R_P = R$. In Equations (25) this means that $J_T = J_P$. Substituting the assumed constant H_1 gives, neglecting terms of the order $(l/L)^2$,

$$H_2 \approx -H_1(3/2l^2). \tag{42}$$

Recalling Equations (3) and the fact that for the assumed uniform $H_1(z)$ field the derivatives are zero, gives for the deflection field,

$$\begin{aligned} H_x &= H_1\,[1 + (3/2)\ (x^2/l^2) - (3/2)\ (y^2/l^2)\,], \\ H_y &= -3H_1(xy/l^2), \\ H_z &= 0. \end{aligned} \tag{43}$$

Figure 10 shows the field distribution for an anastigmatic coil with a length l of about 5 inches.

Horizontal Line Convergence. In the case of a line screen, it may be only necessary to converge to a horizontal or vertical line, rather than a round spot. Figure 6 shows that in that case $R_T = \infty$ or $J_T = 0$. Applying this condition to Equations (25), and assuming a uniform H_1 as before,

$$H_2 \approx H_1\ (9/2lL). \tag{44}$$

Substituting into Equations (3), gives, for the field distribution,

$$\begin{aligned} H_x &= H_1 \left[1 - (9/2)\ (x^2/lL) + (9/2)\ (y^2/lL)\right], \\ H_y &= 9H_1\ (xy/lL), \\ H_z &= 0. \end{aligned} \tag{45}$$

Such a magnetic field would produce a spot converged on a horizontal line. Figure 11 gives such a field distribution for a yoke screen distance $L = 20$ and a yoke length $l = 5$.

Vertical Line Convergence. If it is desired to bring about convergence on a vertical line, then Figure 6 shows that $R_P = \infty$, or $J_P = 0$. (Since all the calculations are for vertical-deflection coils, it is obvious that if it is desired to have both vertical- and horizontal-deflection

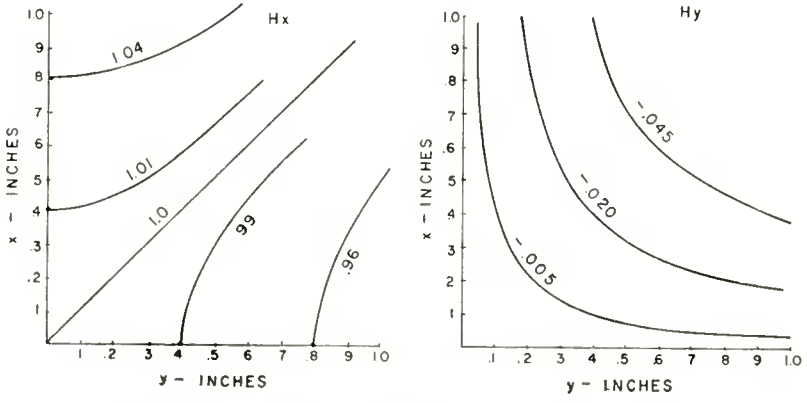

Fig. 10—Example of a non-astigmatic field distribution ($l = 5$).

coils produce horizontal line convergence, it is only necessary to rotate the field here calculated through ninety degrees and use it as a horizonal-deflection coil).

The condition $J_P = 0$, when applied to Equations (25) with uniform short $H_1(z)$, gives for H_2,

$$H_2 = -H_1\ (3/l^2). \tag{46}$$

Substituting into Equations (3) gives, for the field distribution,

$$\begin{aligned} H_x &= H_1 \left[1 + 3\,(x^2/l^2) - 3\,(y^2/l^2)\right], \\ H_y &= -6H_1\,(xy/l^2), \\ H_z &= 0. \end{aligned} \tag{47}$$

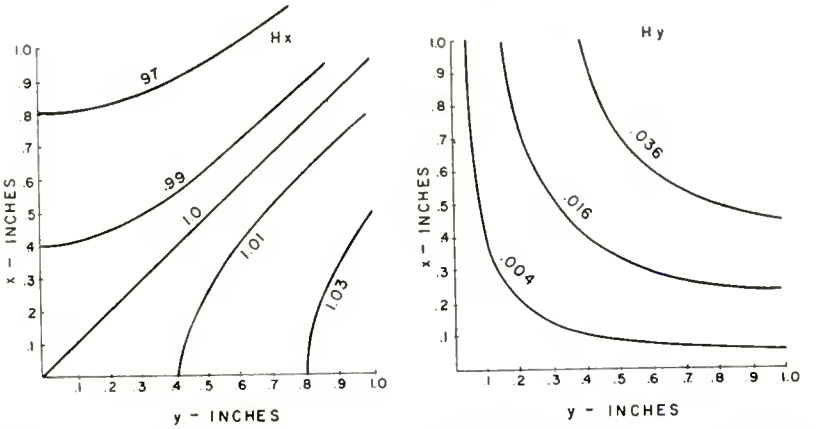

Fig. 11—Vertical-deflection field with a horizontal line convergence length l, of 5 inches and a field-screen distance, L, of 20 inches.

Figure 12 shows such a field distribution for a yoke length $l = 5$.

Extrapolation to Higher Angles

The radius of image curvature, R, implies that the surface of least confusion in the y–z plane is given by

$$y^2 + 2wR + w^2 = 0, \tag{48}$$

where w is given by $(z - L)$. This equation must hold for small angles. On the other hand, for larger angles, the fact that the surface has to pass through $y = 0$, $w = -L$ can be used. This can be achieved by modifying the w^2 term. This gives, for the complete surface,

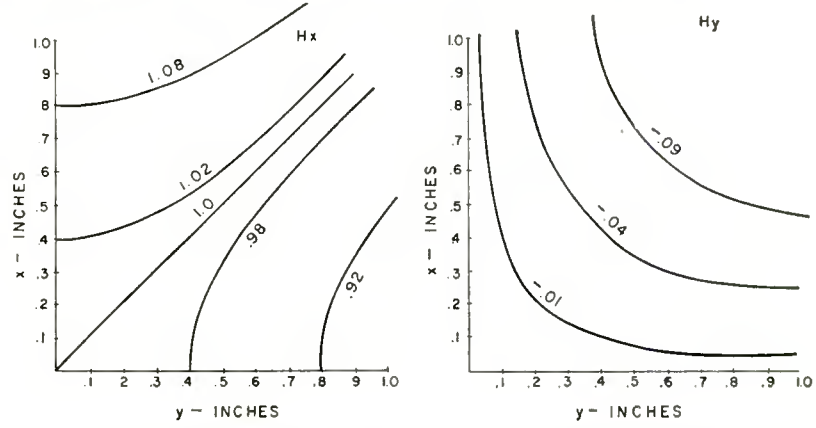

Fig. 12—Vertical-deflection field with a vertical line convergence length, l, of 5 inches.

$$y^2 + 2Rw + (2R/L)\, w^2 = 0. \tag{49}$$

Or, in the z-coordinate system,

$$y^2 - 2Rz + (2R/L)\, z^2 = 0. \tag{50}$$

Equation (50) is easily recognized as an ellipse with the center at $y = 0$, $z = L/2$, with a semi-major axis in the z direction of magnitude $L/2$, and a semi-minor axis in the y direction of magnitude $(RL/2)^{1/2}$. Figure 13 gives such surfaces of best convergence for various values of $l/L = \lambda$.

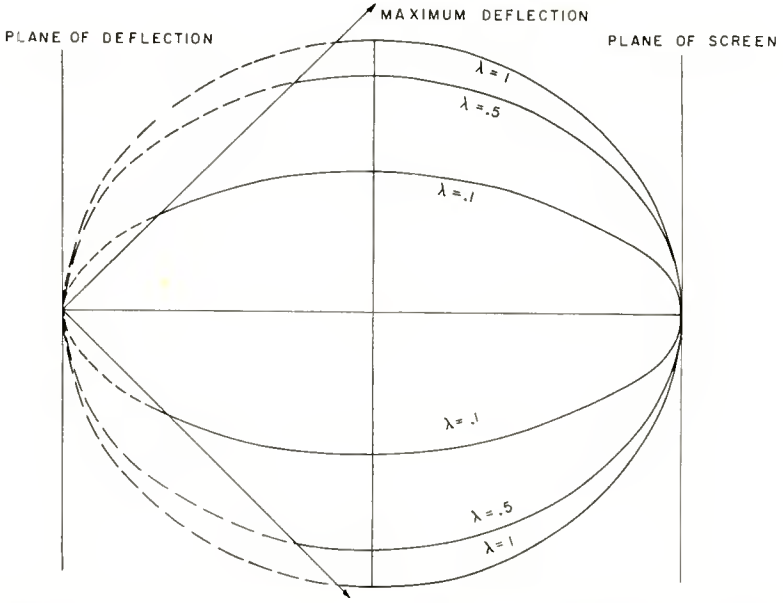

Fig. 13—Surfaces of best convergence for various field lengths ($\lambda = l/L$).

Spot Size

From Equations (16) and (33), the shape of the spot on a flat screen can be evaluated. The spot must be an ellipse with semi-axes given by a and b such that

$$a + b \approx L(1 + L/l)\, \alpha \tan^2 \gamma, \tag{51}$$

where α is the aperture angle (r/L) (see Figure 4) and γ is the deflection angle.

The significance of the $H_2(z)$ function is that a and b can be changed at will, as long as the sum $a + b$ remains constant. This result is in essential agreement with E. Gundert.[4]

Conclusions

The following conclusions can be drawn from this investigation:

(a) The main features of a deflection field can be obtained by relatively few measurements of the magnetic flux. Due to the symmetry properties of a deflection coil and Maxwell's equations, measurements on the central axis and along one line parallel to the central axis give the field anywhere reasonably close to the axis.

(b) The surface of best convergence bends rather sharply towards the source of electrons. Under the best circumstances, it would have a radius of curvature approximately equal to 0.4 of the distance from gun to screen. Since such a curvature is impractical for a screen, it is necessary to use dynamic focusing. Therefore, it is to be concluded that the effect known as degrouping in shadow mask tubes cannot be eliminated by shaping the magnetic yoke field such that dynamic focusing becomes unnecessary, but must be corrected by other means.

(c) However, in the case of a line screen where it is only necessary to form a vertically converged spot, it is theoretically possible to design a yoke which would give the desired result without the use of dynamic convergence.

(d) Relaxation of the conventional symmetry properties of yokes would make these conclusions invalid. It may be possible to eliminate image curvature for asymmetric yokes. Significant improvements may result from an investigation of this possibility.

---

[4] E. Gundert, "Dimensionierung von Kathodenstrahlröhren," *Telefunkenröhre*, 1953.

ELECTROLYTIC TRANSPORT PHENOMENA IN THE OXIDE CATHODE*

By

R. H. Plumlee

RCA Laboratories,
Princeton, N. J.

Summary—*An experiment is described in which some of the chemical changes produced in a BaO cathode by the process of drawing electron emission were detected. The experimental results include the measurement of field-dependent evaporation of H_2, H_2O, O_2, CO, and CO_2 from the cathode. The evaporation of these gases was found to be dependent also upon cathode temperature, state of activity of the cathode, time, and previous duty period. Correlations between residual gas partial pressures and cathode activity were also found.*

These experimental results are interpreted as evidence that the oxide cathode coating contains impurity species incorporated as anions which are in labile equilibrium with their molecular dissociation fragments present in the vacuum space at small partial pressures. This conclusion is shown to be crystallographically and thermodynamically feasible.

Introduction

That the emission of electrons from an oxide cathode is accompanied by chemical change was shown by Becker.[1] Becker found oxygen evolution from oxide-coated filaments when the electron emission was temperature limited but not when the emission was space-charge limited. The oxygen evolution increased with current and with anode voltage. He also found that oxygen evolution occurred at a temperature considerably lower than that at which barium evaporation occurred. An electrolytic transport of ions was postulated by Sproull[2] to account for the decay of pulse emission. He derived empirically an equation which described the emission decay.

The fundamental importance of the Sproull equation was apparent when Nergaard[3] later showed that it can be expressed as a simple

---

* A preliminary description of these results is contained in *Report on Fourteenth Annual Conference on Physical Electronics*, Massachusetts Institute of Technology, Cambridge, Mass., pp. 29-37, March, 1954.

[1] J. A. Becker, "Phenomena in Oxide Coated Filaments I," *Phys. Rev.*, Vol. 34, pp. 1323-1351, November, 1929.

[2] R. L. Sproull, "An Investigation of Short-Time Thermionic Emission from Oxide-Coated Cathodes," *Phys. Rev.*, Vol. 67, pp. 166-178, March 1 and 15, 1945.

[3] L. S. Nergaard, unpublished results.

exponential decay formula if the t variable is first converted into a q or total electronic-charge-passed variable by the relationship

$$q = \int idt.$$

In differentiated form, the Sproull pulse-emission decay formula thus became

$$\frac{\partial i}{\partial q} = -k\left(\frac{i - i_\infty}{i_\infty}\right),$$

$$\frac{d\ln(i - i_\infty)}{dq} = -\frac{k}{i_\infty}.$$

In this form it resembles the equation describing the rate of first-order chemical reaction processes but with current substituted for concentration and charge passed substituted for time.

The fact that the instantaneous pulse current depends on the previous history of charge passed thus appears to be related to Becker's observations[1] that the amount of oxygen or barium liberated by passing electrons through the coating was proportional to the electronic charge passed.

Previous preliminary experiments[4] with oxide-cathode samples in the mass spectrometer supported Becker's observations on oxygen evolution and showed in addition that anionic impurities[5] such as Cl^- are eliminated from the cathode in a fashion that is field dependent and temperature dependent.

Further similar experiments with the cathode sample contained in a more favorable geometric arrangement appeared valuable as a means of determining in more detail the internal chemistry of the cathode.

Some of the questions which such experiments seem likely to answer are the following:

1. Under what conditions of activity, field, temperature, and residual gas pressures is oxygen eliminated from the cathode?

---

[4] R. H. Plumlee and L. P. Smith, "Mass Spectrometric Study of Solids I. Preliminary Study of Sublimation Characteristics of Oxide Cathode Materials," *Jour. Appl. Phys.*, Vol. 21, pp. 811-819, August, 1950.

[5] R. H. Plumlee, "Preliminary Mass Spectrometric Study of the Sublimation Characteristics of Solids Subjected to Electron Bombardment and Elevated Temperatures," Dissertation, Ohio State University, 1951.

2. Beyond what concentration does the remaining stoichiometric excess of barium evaporate?
3. What are the chemical and physical properties of such excess barium?
4. Is this excess of barium relieved by evaporation or by incorporation of anionic impurities to balance the oxygen lost?

The experimental results answered some of these questions but raised many more. One of the most tantalizing of the questions raised is "Will an oxide cathode function in a vacuum?"

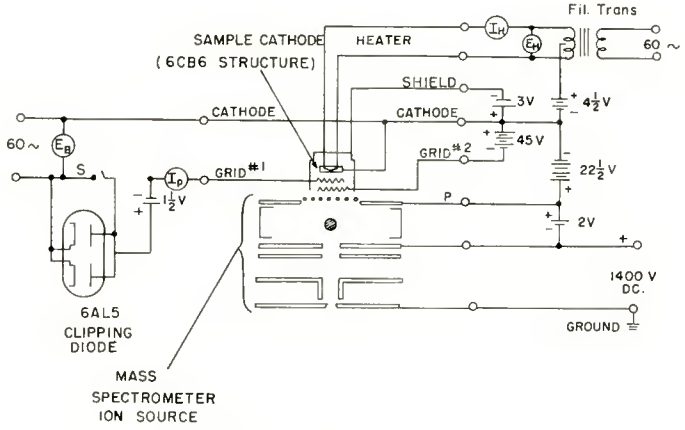

Fig. 1—Circuit schematic.

Experimental Procedure

The apparatus consisted of a sample diode structure mounted in the ion source of a 60° mass spectrometer as shown in Figure 1. The test diode was comprised of parts of a 6CB6 receiving tube. These included the mica supports, shield, and first two grids. The cathode had the same dimensions as that of the commercial tube but was made from a pure $BaCO_3$ spray on "pure" nickel rather than from the commercial mixed carbonates and nickel alloy. The grids were spiral wound from .002 inch diameter molybdenum wire, with turns spaced .005 inch. The spacing from first grid to coating was .005 inch. The coated cathode area was about 0.25 square centimeter. The estimated maximum "anode" area was about 0.4 square centimeter.

Bias voltages were used between various electrodes to prevent the electrons and ions formed in the test diode from entering the ionizing chamber of the spectrometer ion source. With this arrangement the spectrometer measured only the ions formed by its own ionizing elec-

tron beam from neutral gas molecules in its usual ionizing chamber.

A 60-cycle anode voltage was applied to draw emission from the cathode. Neutral materials which evaporated flowed through the grid structure into the path of the spectrometer's ionizing beam. There they became ionized, then analyzed and recorded as part of the mass spectrum. The high perveance of the diode structure (1.7×10^{-2} amp.cm.$^{-2}$ $v^{-3/2}$) allowed the use of low anode voltages (less than 13 volts) for drawing electron emission. This kept average grid power dissipation low (less than 0.1 watt per square centimeter) and produced very little gas ionization.

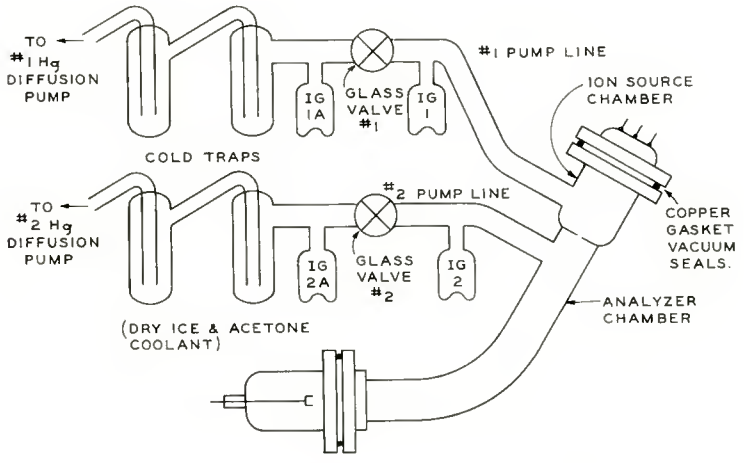

Fig. 2—Vacuum-system schematic.

A 6AL5 diode was connected in the anode circuit so that, if desired, the positive half of the voltage cycle could be clipped, thereby preventing application of a positive anode voltage to the test diode. This was occasionally done to determine whether mica electrolysis contributed a field-dependent component to the peak height increments observed. None was found, and it was concluded that only the application of positive anode voltages produced the observed enhancement of the various spectrum peaks.

Figure 2, shows the schematic diagram of the pumping system. Processing of the assembled vacuum system consisted of a bakeout (350°C, 4 hours), a degassing of the cathode (a nominal 6.3-volt heater variety) by applying heater voltages up to 10 volts. After the initial processing, the residual gas pressure normally remained at about 5×10^{-8} millimeter. Measurements were made intermittently,

and the cathode was operated with more than 6.3 volts heater voltage for a total of about 200 hours (during about six months in high vacuum) before the experiment was terminated by failure of the spectrometer filament. Neither the residual gas composition nor the cathode behavior changed appreciably in this period. Between measurements, cathode and ion source were usually kept at room temperature.

After the source and sample had been warmed from room temperature to operating temperature, an equilibration time of about one hour was needed to stabilize the composition of the residual gas sufficiently to permit sensible measurements. However, neither the cathode nor the system could be said to have stabilized completely at any time during the course of the experiments.

The partial pressures of the gases H_2, H_2O, CO, O_2, and CO_2 evolving from the heated cathode (1035°K) were found to be substantially greater than those contributed by the remainder of the system

Table I

Gas Species	Approximate Partial Pressures (millimeters of mercury)	
	$E_H = 7$ volts (1035°K)	$E_H = 0$ volts
H_2	1.6×10^{-8}	3.2×10^{-9}
H_2O	5.4×10^{-8}	1.5×10^{-8}
$CO + N_2$	2.4×10^{-8}	8×10^{-9}
O_2	1.9×10^{-9}	1.1×10^{-9}
CO_2	1.8×10^{-9}	1.1×10^{-9}

even after the cathode had been continuously heated to 1035°K or higher for 48 hours. Table I gives such partial pressure data.

After the residual gas spectrum had "stabilized" for a particular cathode temperature at which emission could be drawn, the spectrometer was adjusted so that a selected peak of the spectrum could be measured. By biasing out most of the signal at the input of the electrometer amplifier, one could record directly, with any desired amplifier gain, the increment produced in the peak height by the anode voltage applied to the test diode. As will be seen, these increments ranged from less than 1 per cent of the background peak to values as high as 90 per cent of the background peak.

General Results of Measurements of Cathode Reactions

O_2 Evolution

The first measurements were made on the molecular oxygen peak,

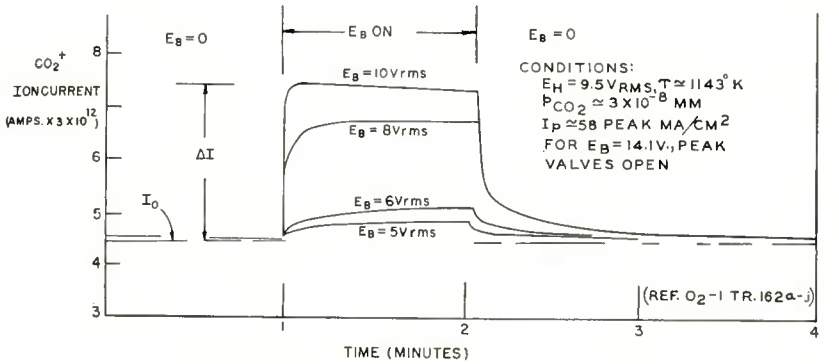

Fig. 3—CO_2 evolution from BaO cathode.

O_2^+, as a function of applied anode voltage. (All the oxygen evaporation which was detected occurred as molecular O_2.) The increment in the O_2^+ peak is time dependent in a manner similar to that shown for CO_2 in Figure 3. The asymptotic (equilibrium) values of the O_2^+ increments produced are plotted in Figure 4. The O_2 evolution is proportional to anode voltage up to $E_p \simeq 12$ volts (peak). Above this it becomes erratic and appears to saturate. The lines with the various slopes were taken for slightly different degrees of cathode activity. Though the measurements are not conclusive, the indication is that the less the slope of the line, the higher the state of activity, suggesting a lower rate of O_2 elimination. The maximum ratio of increment, ΔI, to background, I_0, measured for O_2 was

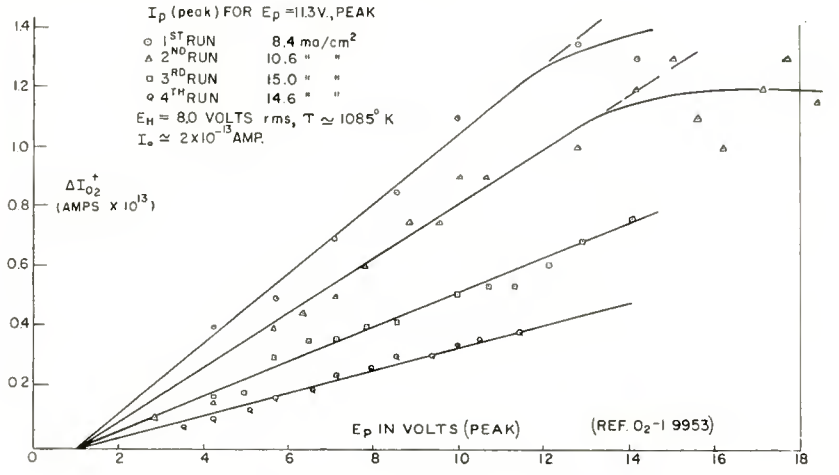

Fig. 4—O_2 evolution from BaO cathode.

$$\left(\frac{\Delta I}{I_0} \right) \simeq 0.7.$$

It is interesting to note that this diode showed very markedly the familiar "ten-volt slump effect." The electron current measured simultaneously with the above O_2 evolution increments is plotted in Figure 5.

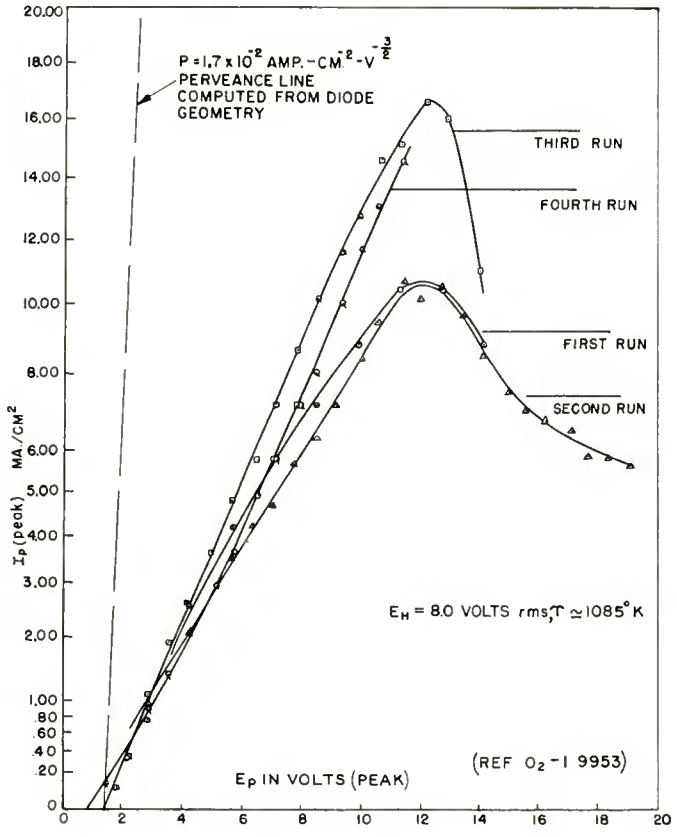

Fig. 5—Electron emission versus anode voltage.

The current is space-charge limited for $E_P < 12$ volts (peak). For $E_P > 12$ volts, the current slumped and the values plotted are time dependent as well as voltage dependent. It is to be noted that the O_2 increment showed saturation in this region rather than a marked increase as one would expect if anode bombardment were dislodging oxygen from the anode and thereby causing poisoning of the cathode

in accordance with a frequently propounded explanation[6-8] of the phenomenon. Examination of the O^+ spectrum peak is complicated by the contribution to this peak produced by H_2O fragmentation during ionization, but there was no indication of a threshold increase in this peak coincident with the slump in emission.

It is to be noted also that the perveance (5×10^{-4} amp cm^{-2} v$^{-3/2}$) computed from the electron current curves in Figure 5 is much smaller than the value (1.7×10^{-2} amp cm^{-2} v$^{-3/2}$) computed from the diode geometry or from handbook characteristics for the 6CB6. This difference is due to the $I_p R_K$ voltage drop across the cathode resistance. The cathode resistance can be calculated (from the geometrical perveance and the current measurements) to range from about 1100 to 850 ohms for the four sets of data plotted in Figure 5. From the cathode coating resistance, the apparent contact potential drop, and the perveance line, it is deduced that for the highest current shown in Figure 5, about 1.1 volt (peak) appeared across the vacuum, and 9.8 volts (peak) appeared across the cathode coating[9] (and/or across an anode film). Because the current did appear to be space-charge limited, it is likely that most of the electrons arrived at the anode with kinetic energies characteristic of the potential drop occurring across the vacuum rather than with energies characteristic of the potential drop between anode and base metal of the cathode. Hence the threshold impact energy of the electrons arriving at the anode at the onset of the slump in current was about 1.1 electron volts. This might be adequate to produce desorption of anode films but not adequate to produce a bona fide dissociation of molecules or ionic crystals.

Typical decay and build-up curves for the oxygen evolution are given in Figure 6. The decay is well represented by two exponential terms, but the build-up requires three. For this figure, the time constant of the amplifier–recorder system was 0.7 second (for 1/e change), hence the curves are little distorted by lag in the recording system after about one second of elapsed time. The shortest measurable time

---

[6] H. Jacobs, "Dissociation Energies of Surface Films of Various Oxides as Determined by Emission Measurements of Oxide Coated Cathodes," *Jour. Appl. Phys.*, Vol. 17, pp. 596-603, July, 1946.

[7] G. H. Metson, "Note on Volt-Dependent Poisoning Effects in Oxide Cathode Valves," *Proc. Phys. Soc.*, Vol. 62, Section B, pp. 589-591, September, 1949.

[8] D. A. Wright, "Some Effects of Slow Electron Bombardment in Thermionic Valves," *Brit. Jour. Appl. Phys.*, Vol. 5, pp. 108-111, March, 1954.

[9] J. R. Young and A. S. Eisenstein, "Oxide Cathode Interface and Coating Voltages," *Phys. Rev.*, Vol. 75, p. 347 (Abstract), January 15, 1949. These authors used a retarding field method for measuring coating conductivity. They also found substantial voltage drops across cathode coatings.

constants in Figure 6 are about 10 seconds, the longest about one minute. With increasing anode voltage and cathode temperature, the initial rise (say during the first 10 seconds of elapsed time) accounted for more and more of the final increment value. Like electron pulse current versus time curves,[3] these O_2 evolution versus time curves can

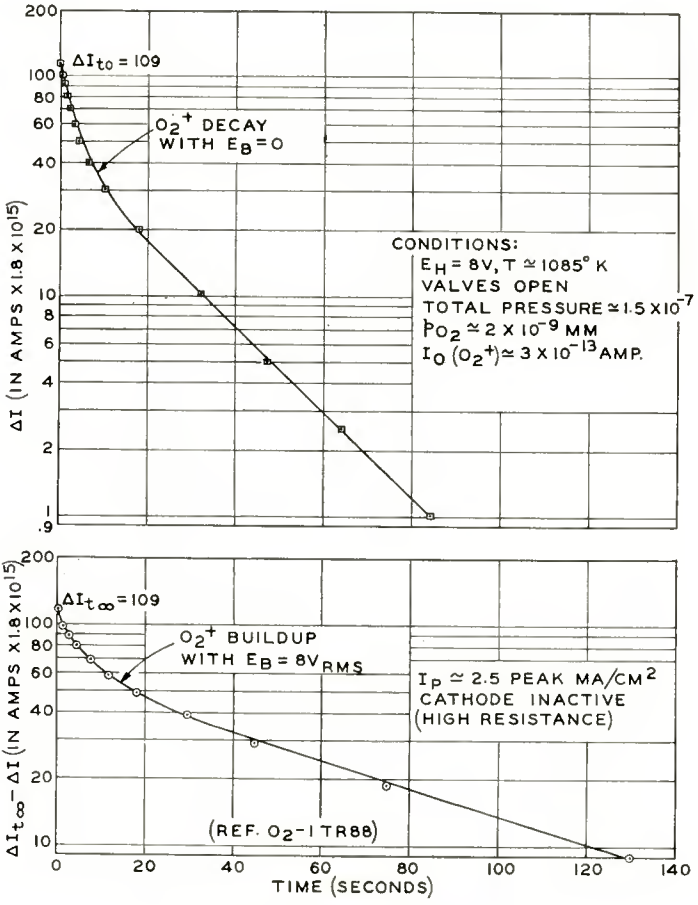

Fig. 6—O_2+ build-up and decay.

be represented by a single exponential if the time variable is replaced by an O_2-evolved variable. It may be noted that the Sproull decay formula for pulse emission as originally stated with the time variable is representable by one exponential term if the decay is slight and by several exponential terms if the decay is large.[3] Facilities were not available for synchronized recording of both the gas evolution and the

electron current, hence we have no plots of O_2 evolution versus electron-current passed or q variable. At the low-temperature limit of detection of the field-produced O_2 increment (about 1000°K), the increment still had an initial rise as fast or faster than the recorder could follow.

The cathode was always more active when the pump lines were shut than when the pump lines were open. The apparent activation energies computed from the temperature dependence of the O_2 increment were 3.4 electron volts when the valves were shut and 2.4 electron volts when the valves were open. This agrees with an observation made earlier regarding the data of Figure 4, namely, that the more active the cathode, the lower the field-dependent rate of O_2 evolution. The difference in electron current produced by closing the pump lines was about a factor of two at a temperature of 1085°K.

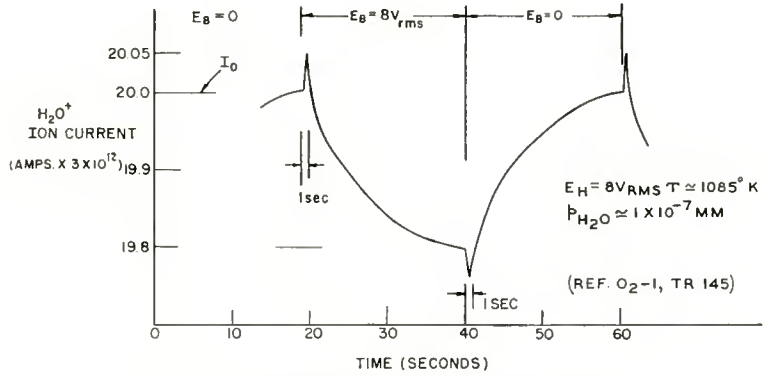

Fig. 7—H_2O evolution from BaO cathode.

The precision of the measurements was inadequate for quantitative comparison of measurements made under one set of conditions with those made under another set of conditions. On a semilogarithmic plot of peak height increment versus time, e.g., Figure 6, at least two decades of amplitude change appeared to be significant. Thus even 1 per cent errors in values of asymptotes distort the curve shapes considerably.

H_2O Evolution

The field-dependent evolution of H_2O from the BaO cathode had an unexpected variation with time. This is illustrated in Figure 7. The brief positive increment after E_B was turned on varied with cathode temperature in both amplitude and time constant (but differently) (see Figure 8 — the dashed lines give the amplitudes corrected for amplifier lag). The amplitudes increased with temperature and the

time constants decreased. In addition, the longer the preceding E_B-off period, the larger the amplitudes of the positive spikes, and the shorter the preceding E_B-on period, the larger the amplitudes of the negative spikes. The amplitude of the slow decrease in H_2O peak height produced after switching E_B on also increased with temperature (Figure 9). The variation of this slow decrease is shown in Figure 10. The amplitudes of all three increments had roughly the same proportionality to the anode voltage. The slow decrement was proportional also to the square of the H_2O partial pressure.

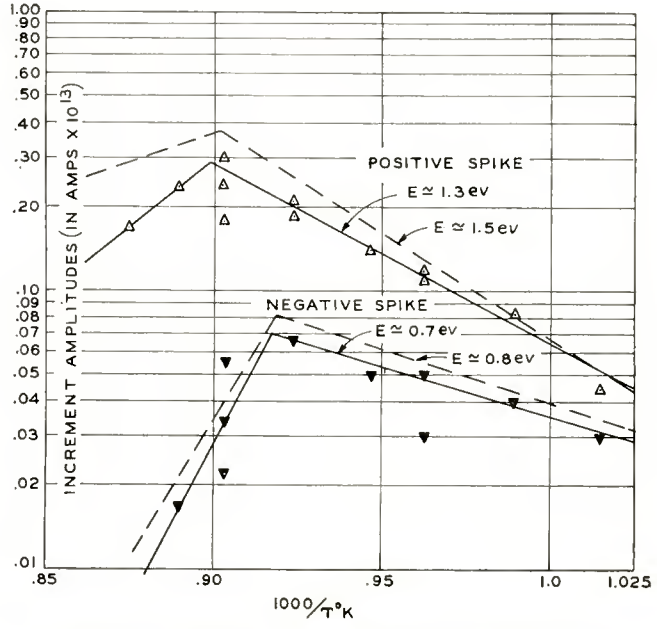

Fig. 8—Temperature dependence of H_2O evolution.

No simple plausible equation for the chemical reaction responsible for square-law dependence of ΔI on I_0 has yet been discovered. If only gaseous reaction species and products are involved, the field-produced increments in the products should bear some approximately integral relationship to the field-produced decrement in H_2O concentration. In Table II only the increments in H_2, CO, and CO_2 are roughly comparable with the H_2O slow decrement. The O_2 increment is very small. Thus reactions of the coating are required by which H_2O is consumed, by which little O_2 is evolved, and by which considerable H_2 is evolved. The over-all process must be second order with respect to H_2O vapor phase concentration. Charge balance must of course be

maintained in the crystal, though the balance in numbers of cation and anion sites may perhaps be allowed to vary some. The second-order requirement, more than any other, would appear to rule out all simple reactions. It is conceivable, however, that this requirement is imposed by a steric factor in the positioning of reacting H_2O molecules on the surface. In this circumstance, reactions describable by simple chemical equations are allowable. Some of these are the following:

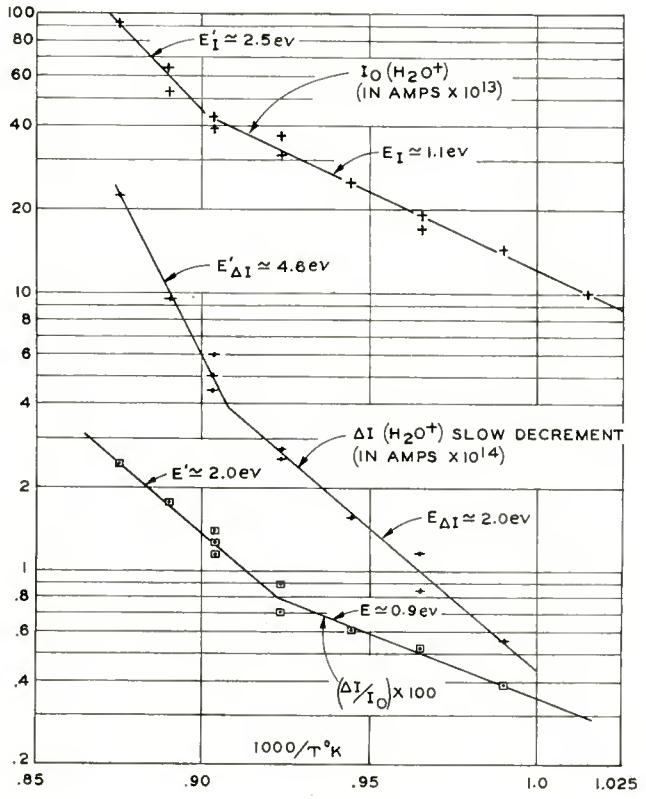

Fig. 9—Temperature dependence of H_2O peak height and of field produced decrement.

$$H_2O(g) + O^{=}(s) \underset{E_B \text{ off}}{\overset{E_B \text{ on}}{\rightleftharpoons}} O_2^{=}(s) + H_2(g)$$

$$H_2O(g) + O^{=}(s) \underset{E_B \text{ off}}{\overset{E_B \text{ on}}{\rightleftharpoons}} 2OH^{-}(s)$$

$$2(OH^- \cdot e)\,(s) \underset{E_B \text{ off}}{\overset{E_B \text{ on}}{\rightleftharpoons}} 2H^-(s) + O_2^=(s)$$

$$H_2O(g) + H^-(s) \underset{E_B \text{ off}}{\overset{E_B \text{ on}}{\rightleftharpoons}} OH^-(s) + H_2(g)$$

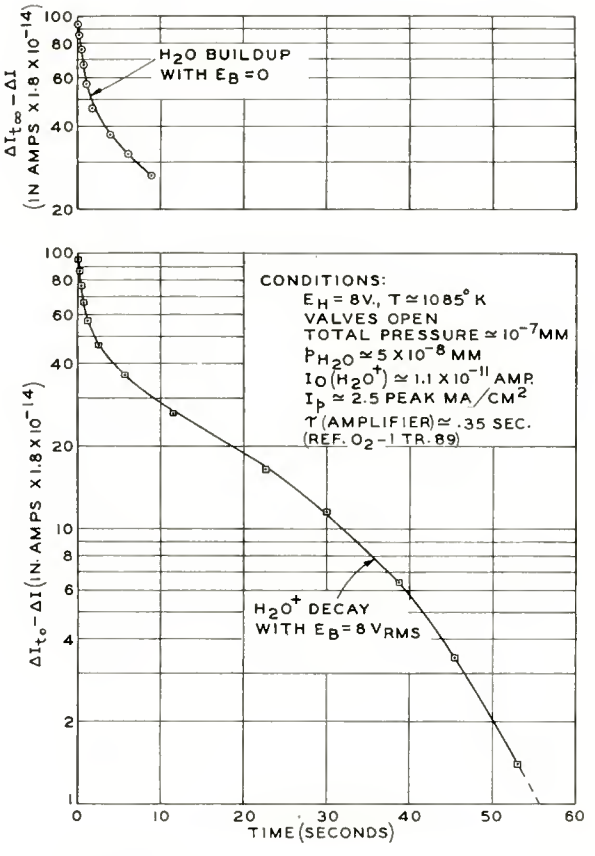

Fig. 10—H_2O^+ slow build-up and decay.

$$HCO_2^-(s) \underset{E_B \text{ off}}{\overset{E_B \text{ on}}{\rightleftharpoons}} OH^-(s) + CO(g).$$

H_2 Evolution

As indicated above, the H_2^+ spectrum peak also showed a depend-

ence on anode voltage. As shown in Table II, the absolute value of this field-produced increment was comparable with the increments in other species. This field dependence is presumed to originate in two ways, (a) by electrolytic discharge of H^- ions from the surface of the coating or, (b) by more obscure reactions with water vapor as suggested above. The chemical literature[10] indicates that hydrogen reduces alkaline earth oxides to form hydrides provided other metals such as aluminum and magnesium are present. Although the cathode nickel is called "pure" nickel, it contains "reducing" materials comprising a total of about 0.1 per cent.

Table II—Spectrum Peak Heights and Increments Produced by Turning on Anode Voltage*

Mass Number	Ionic Species Predominant	I_o Peak Height (Amps. $\times$ 3 $\times 10^{13}$)	ΔI Increment Produced by Turning $E_B = 0$ to $E_B = 8v$	$\frac{\Delta I}{I_o}$
2	H_2+	0.67†	+ 0.07†	+ (1/9.6)
12	$C+$	0.24	+ 0.02	+ (1/12)
14	$CO++$, $N+$	0.38	0.00	
16	$O+$	1.0	+ 0.05	+ (1/20)
17	$OH+$	8.1	— 0.08	— (1/100)
18	H_2O+	30.0	— 0.35	— (1/86)
28	$CO+$, N_2+	4.9	+ 0.15	+ (1/33)
29		0.1	0.00	
32	O_2+	0.31	+ 0.01	+ (1/31)
44	CO_2+	0.94	+ 0.10	+ (1/9.4)

† If these values are multiplied by a factor of 9 to correct for known instrumental discrimination against H_2(g) compared with other common gases, then all current readings have roughly the same proportionality constant relating them to vapor phase concentrations of the un-ionized species.

* Cathode condition: inactive, degassed, $E_H = 8$ volts, $I_p \simeq 5.5$ peak ma/cm^2.

The shape of the plot of increment versus time after E_B has been turned on and off was similar to that shown by O_2 and CO_2 (e.g., Figure 3). Filament failure terminated the experiment before detailed measurements on the field-dependent H_2 evolution were obtained.

CO_2 Evolution

The CO_2 evolved from the BaO cathode was studied more thoroughly than was any other cathode dissociation product. This emphasis

[10] D. T. Hurd, *Chemistry of the Hydrides*, John Wiley and Sons, Inc., New York, N. Y., 1952, p. 41.

occurred largely because, with the range of magnitudes of field-produced and thermal evolutions present, the field effects on CO_2 evolution were more easily measured than were the field effects obtained for any other species. On the basis of chemical evidence there were a priori reasons also for trusting that the measurements on CO_2 were of general significance and not simply freak performances of a specific sample or a specific vacuum system. The existence of remanent carbonate in BaO formed from $BaCO_3$ has long been known to cathode makers and the decomposition of the final few per cent of $BaCO_3$ in BaO is known to proceed slowly.[11]

The variation with time of the field-produced increment in the CO_2^+ spectrum peak is shown in Figure 3. For $E_B > 8$ volts, the increment clearly goes through a maximum and has a slow decay (time constant about 45 minutes) with the field on. The amplitude of the field-produced increment is duty dependent — the longer the previous E_B off-period, the larger the ΔI produced when E_B is turned on. By selecting a fixed time ratio for E_B-on, E_B-off periods, moderately coherent plots of the increment, ΔI, versus anode voltage, temperature, and CO_2 pressure were obtained. However, even at the best, a considerable amount of hysteresis occurred so that some variation with time was always included in measurements of changes produced by other variables. The increment produced by the field appears to be proportional to the field at low field and to saturate when the enhanced rate of loss due to the field becomes comparable with the rate of incidence of CO_2 on the coating from the gas phase. The electron current also showed a hysteresis which may have been related to the CO_2 hysteresis, but the experimental results are inadequate for analyzing the relationship.

The field-produced CO_2 evaporation was also found to be proportional to the partial pressure of CO_2 in the vacuum system. For making these measurements the pump leads from the analyzer tube were closed with the polished glass valves in the pump lines so that CO_2 (and other gases) generated by the vacuum system accumulated in the analyzer. Measurements of the field-produced increments were made both while the valves were shut and after they were opened. Figure 11 shows a plot of the ratio $(\Delta I/I_0)^{2/3}$ versus E_B. The scatter in the points is attributed to the effects of duty dependence and hysteresis which were present in all measurements. The CO_2 partial pressure

[11] J. J. Lander, "Experimental Heat Contents of SrO, BaO, CaO, $BaCO_3$ and $SrCO_3$ at High Temperatures. Dissociation Pressures of $BaCO_3$ and $SrCO_3$," *Jour. Amer. Chem. Soc.*, Vol. 73, pp. 5794-5797, December, 1951.

encompassed in the data has a factor of seven between the highest (when the valves were shut) and the lowest (after the valves had been open long enough to exhaust the accumulated gases). Plots of the data as $\Delta I/I_0$ versus E_B^2 or as $\ln \Delta I/I_0$ versus E_B show saturation for $E_B > 8$ volts. The special significance, if there is any, of the apparently linear variation of the ratio $\Delta I/I_0$ with $E_B^{3/2}$ is not known.

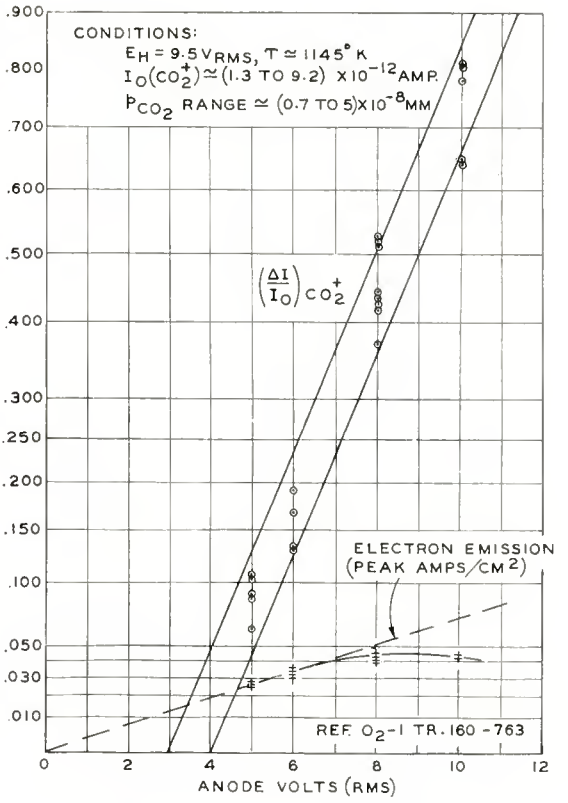

Fig. 11—Voltage dependence of CO_2 evolution.

As in the case of the O_2 evolution, the electron current shows saturation on the $I_p^{2/3}$ versus E_B plot in a region in which the field-produced increment in evaporation is still increasing with its low-field slope.

The proportionality between field-produced CO_2 evaporation and CO_2 background pressure suggests the presence of $CO_3^=$ ions in the BaO structure and indicates that the rate of CO_2 discharge by electrolysis is proportional to $CO_3^=$ concentration.

With the valves open and the system being pumped, the temperature dependence of the CO_2 partial pressure over the BaO cathode was measured and an "activation" energy for the loss of CO_2 was computed from the ln I_{CO_2} versus $1/T$ plot. This agreed quite well with the heat of dissociation computed by Lander[11] from measurements of the dissociation pressure of bulk $BaCO_3$. Assuming an ideal solution of $BaCO_3$ in BaO and applying the rough pressure calibration figure for the mass spectrometer's sensitivity, a mole fraction of 10^{-6} for the concentration of $CO_3^=$ in BaO was estimated.

The ratio $\Delta I/I_0$ was sharply duty dependent over the entire pressure range studied.

Examples of field-produced increment build-up and decay curves for CO_2 are shown in Figures 12 through 18. The data of the initial part of the Figure 12 curve are replotted with an expanded time scale in Figure 13 with $\Delta I_{max} - \Delta I$ rather than ΔI as ordinate. This plot suggests the presence of three exponential terms. The amplifier time constant was about 0.1 second, and the recorder printing frequency was 5 per second, so that the Figure 13 is practically undistorted for elapsed time longer than 0.2 second. Figures 14 and 15 give the decay in the field-produced increment after E_B was turned off following the recording of the data of Figure 12. Figure 15 is the expanded initial segment of this decay.

There was no marking system which precisely defined the time at which anode voltage was applied, and the $t = 0$ point was always selected by following the increment back to zero value on the record. In many of the original records there are indications of the presence of an "induction" period of 0.1 to 0.5 second which occurred after E_B was switched on and before the increment began its chief rise. This is shown in Figure 16. The first three points are 0.2 second apart and form a line discontinuous with the main build-up. The amplifier time constant was again 0.1 second, and the printing frequency of the recorder was five per second. (The recorder prints an instantaneous signal value five times per second, not a value integrated over the previous 0.2 second interval. Printing strokes of the recorder were counted to establish the time base in the early sections of the build-up and decay traces.)

Figures 17 and 18 show what are believed to be more generally significant curve shapes for the build-up and decay of the CO_2 increment than are the previous curves. These semilog plots of amplitude versus time are characterized by a reversal of curvature beginning about 10 seconds after E_B was switched on. Some such plots become

straight lines and the ordinate intercepts of the extrapolated lines are usually nearly the $t = 0$ values of the increments as shown on Figure 18. This characteristic has been found by Nergaard[3] also for semilog

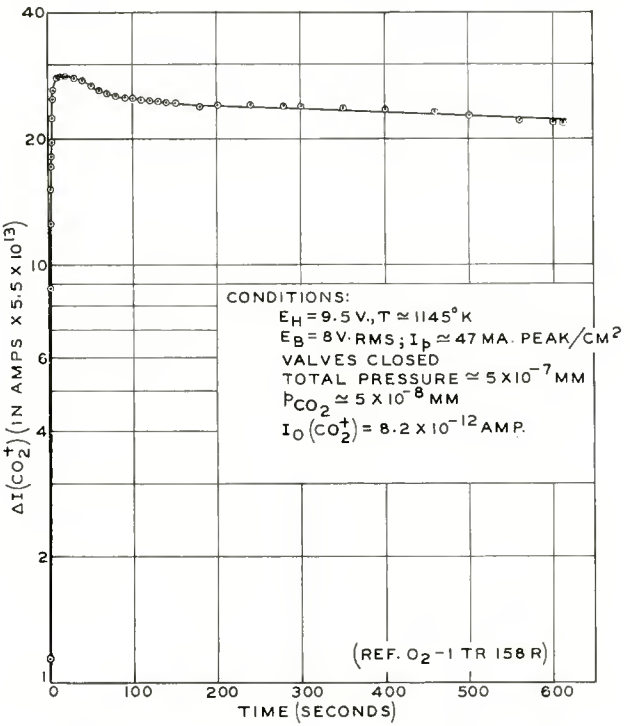

Fig. 12—CO_2+ build-up with $E_B = 8$ volts.

plots of electron emission versus time made from data taken in the course of experiments in which a cathode was activated by deposition of alkaline earth metal ions via the mass spectrometer.[12] He has noted that such plots are consistently representable as sums of two or three exponential terms. When graphically resolved, the terms of many such individual plots are shown to have a common intercept value at $t = 0$; however, in some cases two or three separate intercept values are indicated. Although this representation suggests no unique mechanism, it does indicate the presence of processes which proceed in parallel

[12] R. M. Matheson and R. H. Plumlee, unpublished results. A preliminary description of these results is contained in "Report on Fourteenth Annual Conference on Physical Electronics," Massachusetts Institute of Technology, Cambridge, Mass., March, 1954, pp. 37-41. A more complete account will appear in *RCA Review*.

with different rate constants and an opposing process which regenerates to some extent the condition whose decay is primarily evident.

The behavior of the CO_2 increment is similar to that of the O_2 increment in that plots of ln ΔI values versus $\int_0^t (\Delta I)\,dt$ display one or two straight line segments covering most of the build-up and decay time intervals.

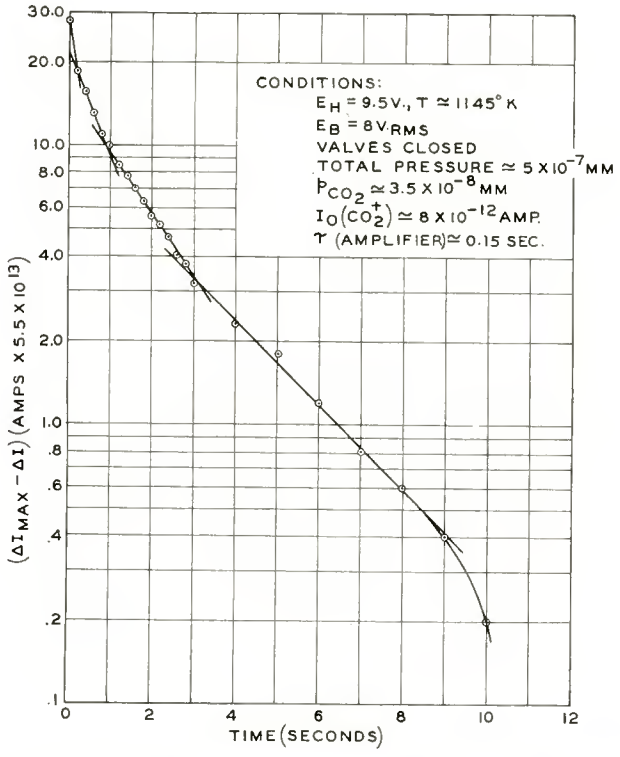

Fig. 13—CO_2^+ build-up with E_B on (initial portion of Figure 12).

Evolution of Barium

Unfortunately, failure of the mass spectrometer filament terminated the experiment before an intensive effort had been made to detect field-dependent barium evolution. Preliminary attempts detected no barium evaporating, either with or without field applied, at temperatures as high as 1085°K. At this temperature, the field-dependent evolution of O_2 and other gases was quite discernible, and many of the

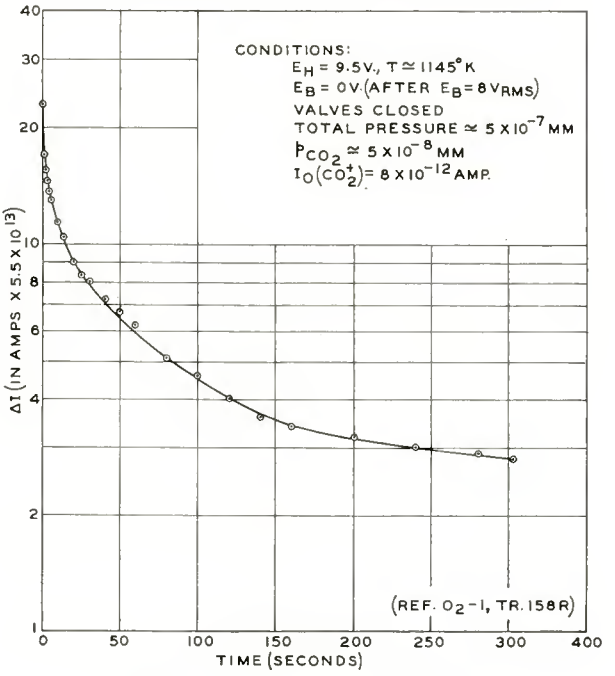

Fig. 14—CO_2^+ decay with E_B off.

measurements on these dissociation products were made at this temperature. The evolution of barium, if it occurred, was fully an order of magnitude less than the evolution of O_2 at 1085°K, and could not

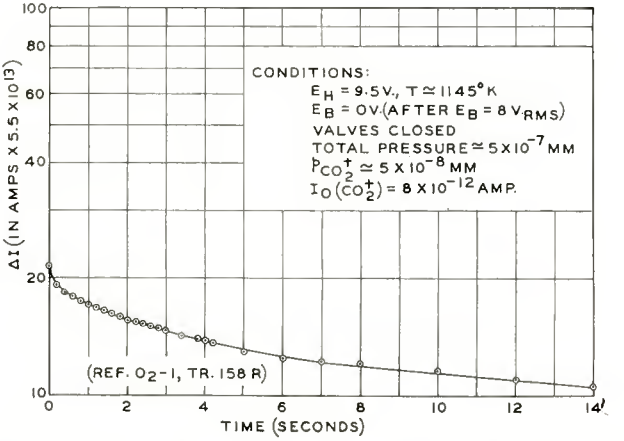

Fig. 15—CO_2^+ decay with E_B off (initial portion of Figure 14).

have been larger than that corresponding to a partial pressure of 10^{-10} millimeter of mercury.

At no time was the field-produced increment in either the O_2 or CO_2 peak larger than the background value of the peak when the anode voltage was zero, though ratio values of $\Delta I/I_0$ ran as high as 0.9. Figures 3 and 6 and others show relaxation times for establishment of steady-state evolution rates of the order of a minute at 1085°K.

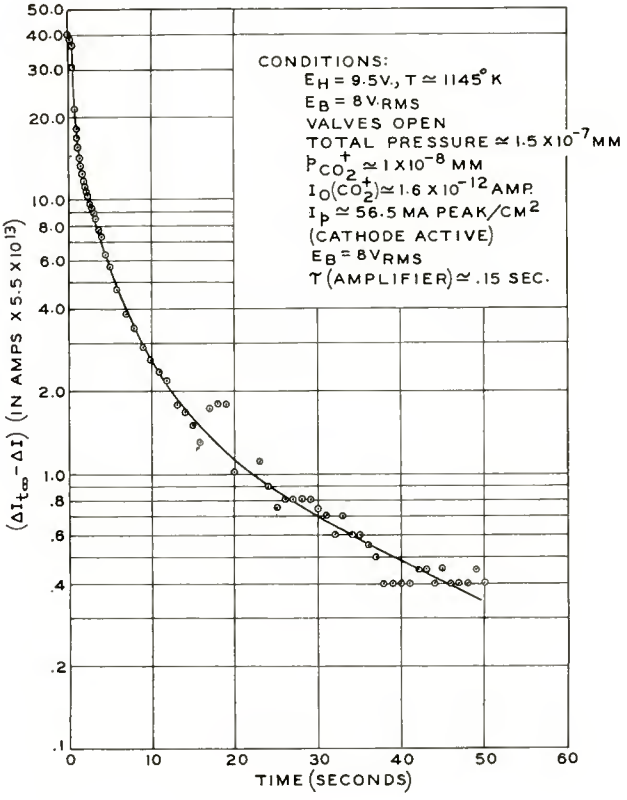

Fig. 16—CO_2^+ build-up with $E_B = 8$ volts.

Thus it seems likely that recombination of the crystals with oxygen (or other anion-forming materials) was adequate to balance the rate of loss of O_2 and that the barium in excess of the stoichiometric value reached an asymptotic level in about one minute. There were indications of processes with much longer time constants, e.g., 45 minutes in the CO_2 hysteresis, but the amplitude changes were smaller for the slow processes than for the fast ones. Therefore, it does not seem

likely that for d-c operation the barium excess continuously increases with time, electron charge passed, and quantity of O_2 electrolyzed in any ordinary vacuum system in which recombination can occur.

This conclusion is in apparent disagreement with Becker's results;[1] however, it is quite likely that the pressures of "residual" gases in Becker's tubes were much lower than those in the present experiment so that the recombination level was much lower. The oxygen evolved from the directly heated filamentary cathodes Becker studied was largely removed from circulation by combination with the *W* filament whose emission decline was used for detecting the oxygen.

The absence of detectable barium vaporization is in agreement, however, with conclusions derived from more recent research reports by investigators[13, 14] using quite different experimental approaches.

Evolution of Other Species

Table II gives a typical set of measurements of field-produced increments in various spectrum peaks and the zero-field background values. Some of these species are of course fragments of the parent molecules. Other species not listed, such as CH_4 and C_2H_2, usually appeared in the spectrum when the cathode was first warmed after having been at room temperature overnight. It is not certain whether these species were affected by the field. Careful examination of the spectrum peaks due to argon and mercury detected no field-produced effects. This satisfactorily demonstrated that not every species in the spectrum showed a behavior dependent on anode voltage applied to the test diode.

For the particular condition of the cathode and the system at the time the values in Table II were taken, the absolute magnitudes of field-dependent components and zero-field background components suggest the conclusion that the field-dependent evolutions of CO_2, O_2, CO, H_2O, and H_2 are mutually independent processes. The ratios of the I_0 values for the different species do not correspond with the ratios of the ΔI values, except for the pairs of values for OH^+ and H_2O^+.

The field-dependence of the mass 28 peak might be attributable to electrolytic discharge of $N^{\equiv}$ as N_2 and/or CO from HCO_2^- (formate) impurity. It is known that CO reacts with hydroxides and hydrides to produce formates.[15] There appear to be no dissociation pressure

[13] L. A. Wooten, A. E. Ruehle, and George E. Moore, "Evaporation of Barium and Strontium from Oxide-Coated Cathodes," *Jour. Appl. Phys.*, Vol. 26, pp. 44-51, January, 1955.

[14] Cornelis Timmer, "The Density of the Color Centers in Barium Oxide as a Function of the Vapor Pressure of Barium." Thesis, Cornell University, Ithaca, N. Y.. February, 1955; *Jour. Appl. Phys.*, in press.

[15] F. Ephraim, *Inorganic Chemistry*, Interscience Publishers, Inc., New York, N. Y., Fourth Edition, 1943, p. 796.

data available on alkaline earth formates from which to estimate the stability of such impurity solutions. It will be shown from thermochemical data that such addition-type anionic impurities are generally more stable under vacuum tube atmospheres than substitutional anionic impurities such as $N\equiv$.

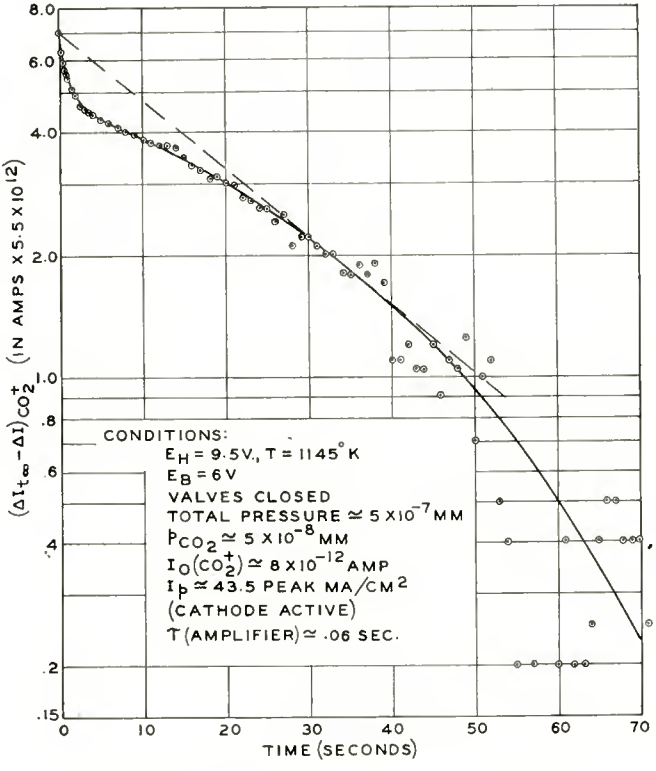

Fig. 17—CO_2+ build-up with $E_B = 6$ volts.

Measurements of Thermal Reactions Associated with a Receiving-Tube Structure

Correlation between Cathode Activity and H_2O Partial Pressure

The discussion of thermal reactions is separated from the discussion of field-dependent reactions described in the preceding section because contributions from thermal reactions of all the parts of the assembly warmed by the cathode heater were necessarily included in the values measured. The parts of the reactions contributed by the oxide coating could not be isolated as were the field-dependent processes.

Substantial evidence was found for the existence of an indirect relationship between electron current and the H_2O partial pressure around the cathode. The measurements are shown in Figure 19. The current promptly reflected changes in H_2O partial pressures of the order of 10^{-9} millimeter of mercury; however, the sign of the correlation depended upon the circumstances producing the pressure change. By contrast there was little semblance of any correlation between

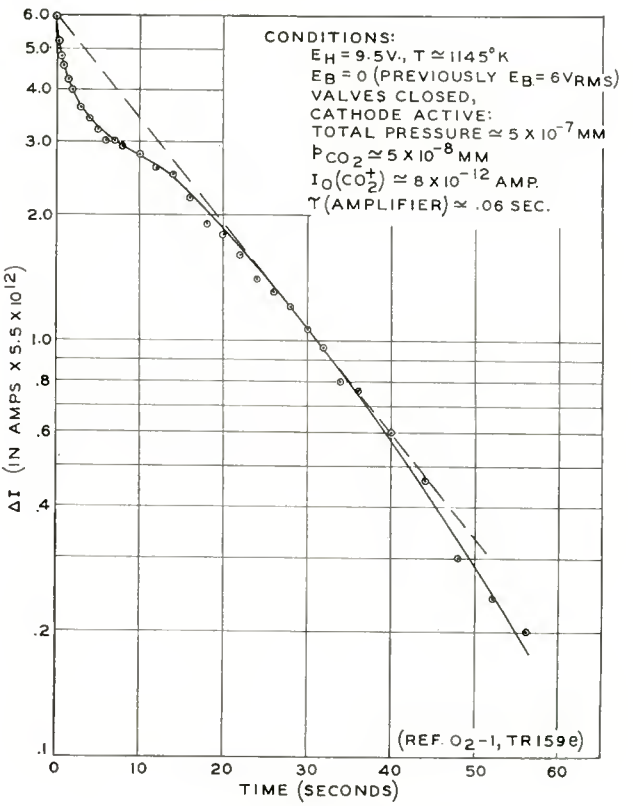

Fig. 18—CO_2^+ decay with E_B off.

electron current and partial pressures of O_2 and CO (Figures 20 and 21). Unfortunately, the experiments were terminated before similar plots could be made of electron current versus CO_2 and H_2 partial pressures. Because of factors to be described, no interpretation was obtained for the specific mechanism through which the H_2O concentration was related to cathode activity. The roughly reciprocal relationship between the CO and H_2O concentrations indicated by Figures 19,

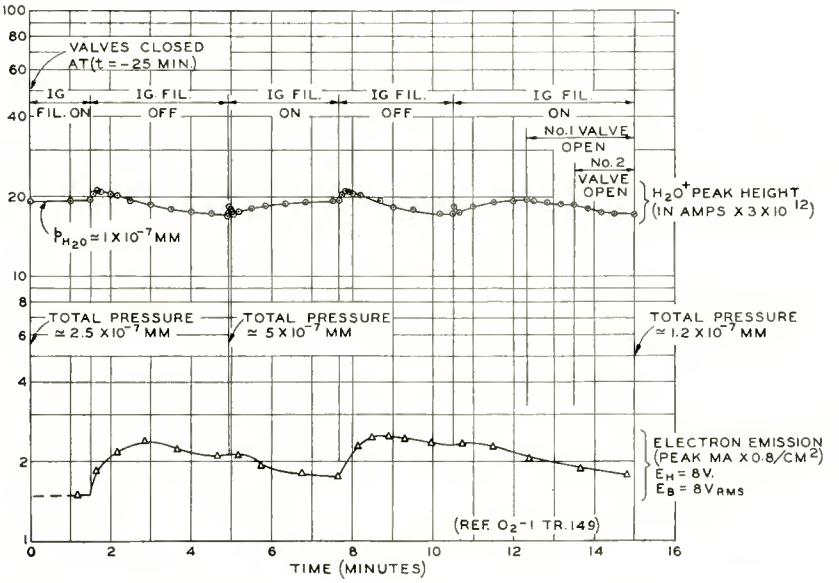

Fig. 19—Concurrent plots of electron emission and H_2O+ peak height.

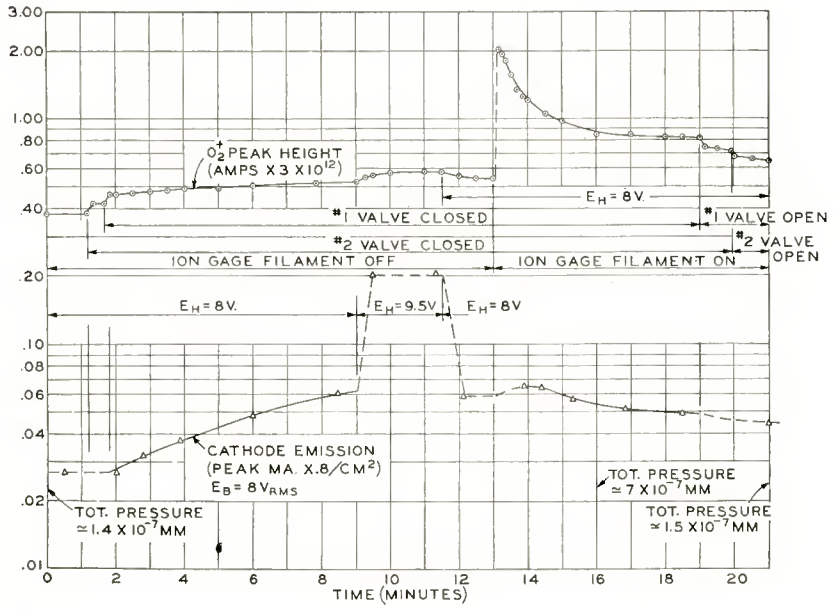

Fig. 20—Concurrent plots of electron emission and O_2+ peak height.

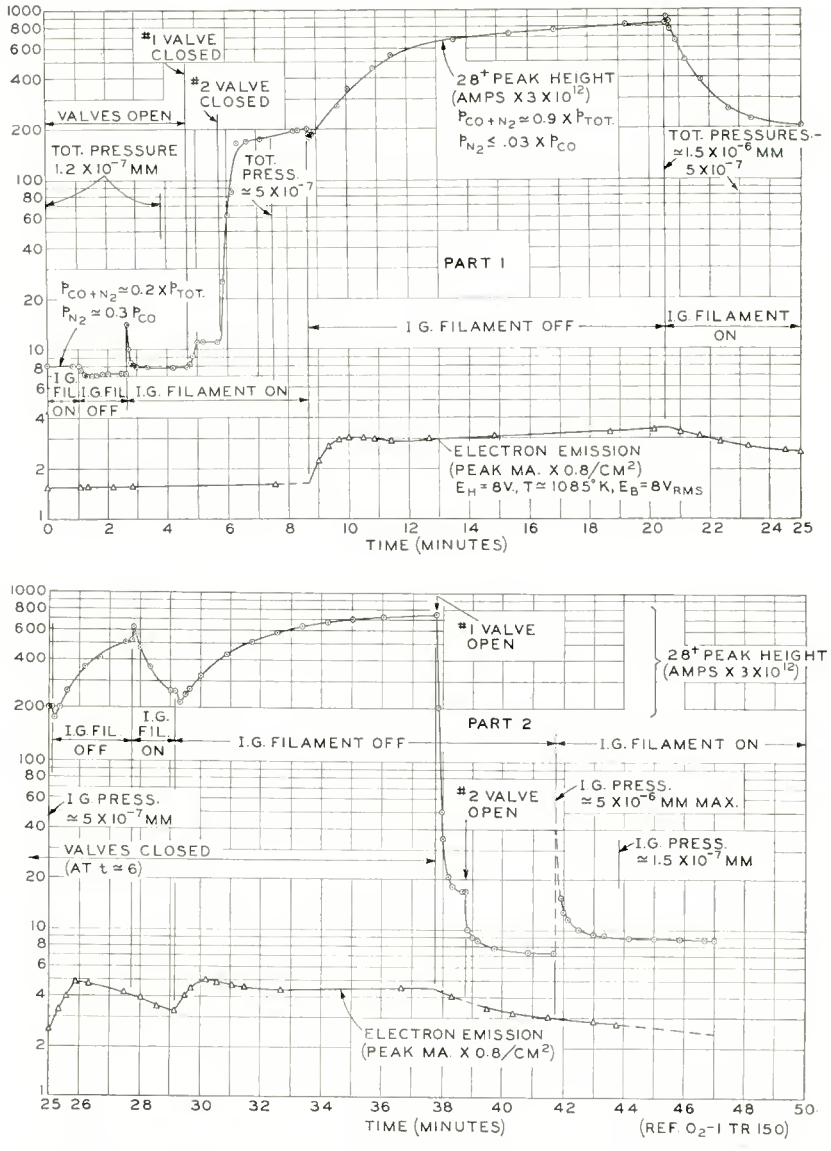

Fig. 21—Concurrent plots of electron emission and CO+ peak height.

20 and 21 suggests that still another constituent, perhaps H_2, was involved in the coating reaction which affected the electron current. The behavior of the H_2O and CO concentrations indicated also that the ionization gauge generated more H_2O than it gettered and gettered more CO than it generated.

These "effects" of "residual" gases were studied only by the expedient of closing the pumping lines for the analyzer tube of the spectrometer and allowing the gases to accumulate. Some additional variation in gas composition was produced by changing the temperature of the ionization gauge filament (tungsten). From the application of these rather limited controls it was found that heating the cathode generated the common gases H_2, H_2O, CO, O_2, and CO_2 at rates which produced, in the vicinity of the cathode, concentrations higher than those maintained there by the remainder of the vacuum system. The cathode, its heater, and mica supports effectively created an environment of gas partial pressures ranging from 10^{-10} up to perhaps 10^{-5} millimeter of mercury, depending on its previous high-temperature history. Any correlation between electron current and partial pressures around the cathode was necessarily a correlation with the steady-state concentration of the species built up by the cathode, its heater, and mica supports, rather than a measure of the effect of an independently controllable foreign species introduced from the outside. The thermal reaction data is perhaps more pertinent to a description of the over-all behavior of a cathode in a standard finished tube structure than to an interpretation of the basic properties of the oxide coating.

Steady-State Conditions inside the Receiving-Tube Envelope

Because of the fact that the sample structure used in the mass spectrometer for studying the cathode was assembled largely from standard components of a 6CB6 receiving tube, the partial pressure data obtained may have some relationship to conditions existing in commercial receiving tubes.

A set of steady-state partial pressure values which fairly represents the range of magnitudes and relative contributions made by the heated "degassed" cathode structure and by the remainder of the vacuum system is given in Table I. The data indicates that, with $E_H = 7$ volts (cathode temperature about 1035°K), the sample structure contributed about three times as much H_2, H_2O, and CO as did the entire system when the heater voltage was zero. The cathode structure also contributed more O_2 and CO_2 than did the remainder of the system. These values were recorded after the cathode had been heated intermittently to electron emitting temperatures for a total of approximately 100 hours. In the 48-hour period just preceding the reading of the values for $E_H = 7$ volts, the cathode had been operated at a temperature of 1035°K or higher continuously (except for an occasional interval of a few minutes at about 500°K for recording the background spectrum). The values for $E_H = 0$ were measured subsequently, about five minutes after the heater voltage had been turned off. At 1035°K, the power

dissipated in the cathode was about 2.4 watts. The power dissipated in the filament of the spectrometer was about 13.5 watts. The cathode and its heater together weighed about 0.1 gram, the two micas weighed 0.3 gram, and the assembly constituted only a minute fraction of the surface area and mass of the ion source of the spectrometer. Yet, having been thus thoroughly heat treated on a continuously pumped system at a total pressure around 10^{-7} millimeter of mercury (maintained largely by gas from the cathode structure, of course), this structure still could maintain steady-state partial pressures about three times those produced by the remainder of the system.

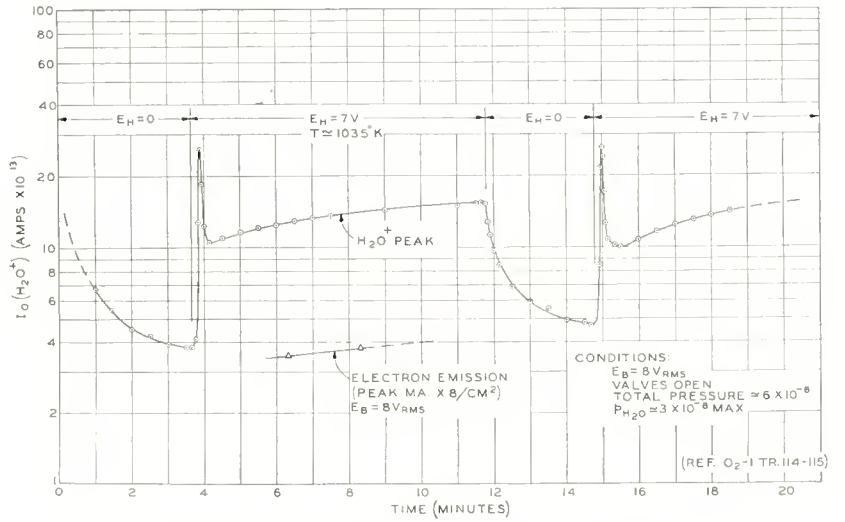

Fig. 22—Cathode temperature cycles and the variation in H_2O equilibrium pressure.

The values plotted in Figure 22 (taken a few hours earlier than those in Table I) further indicates the magnitude of the sample's contribution to the partial pressure of H_2O in the ion-source region. In addition they show a high degree of reproducibility of the amplitudes of the H_2O pressure for repeated cycles of high and low cathode temperature. In Figure 22 for the first high-temperature interval shown, the time-integrated loss of H_2O was roughly three times the amount that could have been recovered during the low-temperature interval following, but the amplitudes in the next high-temperature interval were almost unchanged from those in the first. This, together with the long previous high-temperature history, indicates that the thermally discharged gases H_2O, CO, CO_2, and perhaps H_2 were not

simply stored on the surface of the sample structure by adsorption, but originated, in some way, in the bulk material.

A plot of the envelopes of peak heights generated when the cathode was heated step-wise is shown in Figure 23. Prior to this heating, the cathode had been at room temperature overnight. At the end of the first hour's heating at 1035°K ($E_H = 7$ volts), the partial pressures were down to about three times the terminal values.

Several conclusions may be drawn from the thermal evolution curves shown in Figure 23. One conclusion is that the mechanism producing

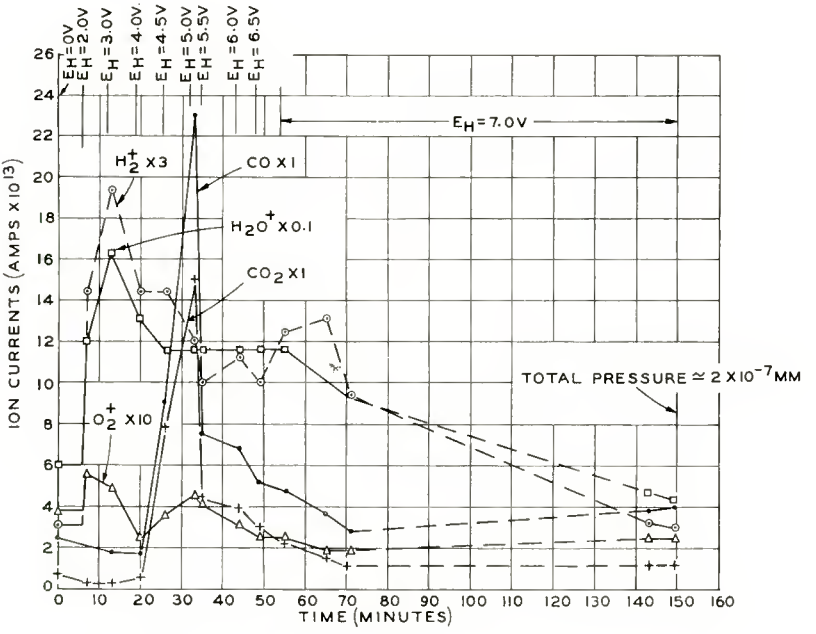

Fig. 23—Cathode degassing during stepwise warmup.

CO seemed to produce CO_2 simultaneously. The curves have the same shape but, because the CO^+ peak was larger at all times than the CO_2^+ peak, the CO^+ could not have been primarily produced by fragmentation of the CO_2 in the ionizing beam. The O_2^+ peak seems only mildly connected with the CO^+ and CO_2^+ peak, and the small hump at $E_H = 4.5$ volts is probably largely due to CO_2 fragmentation. Thus CO and CO_2 were probably just different stages of oxidation of carbon derived from one source.

A second conclusion drawn from curves in Figure 23 is that the H_2 and H_2O were released most abundantly at a very low temperature

($E_H \simeq 2$ volts) but continued to be evolved at temperatures higher than that at which the CO and CO_2 were primarily evolved.

A third conclusion is that the H_2 and H_2O concentrations appeared to be directly connected. One obvious possible means of connection is that the H_2^+ current may have been produced by electron impact fragmentation of the H_2O evolved; however, this does not appear to be true.

That most of the H_2^+ peak actually came from H_2 molecules rather than from electron impact fragmentation of H_2O is shown by the field dependence of the H_2^+ and H_2O^+ spectrum peaks. The data of Table II constitute a typical set of measurements of peak heights and field-produced increments all read within a period of about 35 minutes at the end of a day's operations. If the H_2 were largely produced by H_2O fragmentations in the ionizing beam, the H_2 peak would be expected to have the same sign of field-dependence and show the same value for the $\Delta I/I_0$ ratio. Neither of these conditions was met. It is thus evident that the H_2^+ peak in the spectrum was formed by ionization of H_2 rather than by fragmentation of H_2O.

By similar arguments, the field-dependence of the CO^+ and CO_2^+ spectrum peaks supports the conclusion that most of the mass 28 peak is derived from CO rather than from CO_2 fragmentation. The interpretation of measurements for the mass 28 peak was complicated by the known presence of N_2 introduced by leakage into the system. For the well-degassed condition of the cathode structure, the mass 28 peak probably contained 25 to 50 per cent N_2.

A final conclusion from the Figure 23 curves is that the partial pressures of H_2, H_2O, CO, O_2, and CO_2 over the "room temperature" cathode structure ($E_H = 0$ points) after a few hours' recovery time from previous high temperature operation were the same order of magnitude as the high temperature values for the "well-degassed" condition after many hours of high temperature operation. Because the spent getter surface of a receiving tube is essentially the same material as a cathode coating at envelope temperature, the equilibrium partial pressures of these species over the getter will match fairly closely the partial pressures of the same species maintained by the hot cathode structure in "degassed" condition. In this situation, the getter acts more as a filled sponge than as a pump.

Alternative Mechanisms for Producing the Observed "Field-Enhanced Evaporation"

Before considering the significance of the measurements, it is pertinent to inquire whether spurious properties of the apparatus or of the method could have produced the appearance of field-dependence

in the evolution of various common gas species. As yet we have found no convincing reason for believing that the field enhancement of these evaporation rates is not a real electrolytic reaction of the cathode coating.

One suggested alternative electrolytic source, the support micas, was eliminated experimentally by the test use of negative half-wave anode voltages. With negative anode voltages no enhancement in evaporation of any species was found.

The most obvious alternative interpretation, that anode bombardment desorbs the gases by decomposition of anode contaminants, probably cannot be refuted categorically on the basis of available data; however, the wave form of the increments requires that the bombardment hypothesis incorporate a very complex mechanism to account even for the gross features of the time variation of the increments.

To interpret the anomalous behavior of the H_2O peak, the characteristics of the various increments as functions of cathode temperature, of anode voltage, of anode current, and of duty period as due to erosion of anode films would require a large collection of postulated conditions and restrictions. The coating-electrolysis mechanism is a considerably simpler interpretation. It requires one general postulate, namely that various common gas species in the vacuum system be in labile equilibrium with certain anionic forms or fragments of themselves which readily occupy anion sites in the BaO crystals. The geometrical and thermodynamic feasibility of this postulate will be considered in the following sections.

Crystallographic Aspects of Impurities in Oxide Cathode Coatings

The question to be answered is "Can the addition-type anionic impurities be accommodated in the $O^=$ sites of the BaO crystal?" The answer is yes.

The Ba–O distance in (cubic) barium oxide is about 2.75 angstroms.[16] Using the radii of Ba^{++} and $O^=$, 1.35 and 1.40 angstroms, respectively,[17] and assuming the ions are discretely bounded spheres, one finds the inscribed cube of the void bounded by 4 pairs of Ba^{++} and $O^=$ sites comprising $\frac{1}{8}$ of a unit cell is about 2.0 angstroms on a side and the inscribed square of the void which penetrates the (100)

[16] R. W. G. Wyckoff, *The Structure of Crystals*, The Chemical Catalog Co., Inc., New York, N. Y., 1931, Second Edition, p. 224.

[17] Charles W. Stillwell, *Crystal Chemistry*, McGraw-Hill Book Co., New York, N. Y., 1938, First Edition, pp. 417-424.

faces of this ⅛ unit cell is about 1.15 angstroms on a side. The body diagonals of this ⅛ unit cell are 4.76 angstroms and the (100) face diagonals are 3.89 angstroms. Subtracting the Ba++ radius from the ⅛ cell face diagonal and body diagonal in BaO leaves $R_x = 2.54$ and 3.41 angstroms, respectively, for the radius available to anions to be substituted for $O^=$.

In cubic[18] $BaCO_3$, the Ba–C distance is 3.48 angstroms. The $CO_3^=$ ion is planar and its axis coincides with a body diagonal of the unit cell. Free rotation of the $CO_3^=$ is believed to occur. Below the transformation temperature at which the crystal structure changes to rhombohedral, free rotation does not occur, but an alignment of $CO_3^=$ axis with the short cell diagonal is preserved.

The circumscribing radius of the $CO_3^=$ can be estimated from the following considerations. To quote from Stillwell,[19] "In the $CO_3^=$ group, the radius of oxygen indicated by the C–O distance is less than 0.60 angstrom; whereas its radius in the direction of the cations is approximately the normal ionic radius, 1.40 angstroms." The experimental C–O distance in $CO_3^=$ is about 1.31 angstroms.[19] Adding to this distance these values of the oxygen radius one gets for the possible circumscribing radii of the $CO_3^=$, $R_{CO_3^=} = 1.91$, 2.40, 2.71 angstroms.

Thus if the $CO_3^=$ were oriented in BaO roughly as it is oriented in $BaCO_3$ there should be ample room to accommodate it by making use of the void. Whether free rotation could occur might be open to doubt, but substitution certainly appears possible without excessive distortion of the cell dimensions.

Diffusion of the $CO_3^=$ by transfer of uncharged CO_2 (a linear molecule) through the void from oxygen site to oxygen site would appear to be rather easy. Although CO_2 has no permanent dipole moment, it undoubtedly can have an induced dipole moment. Electrolytic transport of a dipole will obviously not occur in a uniform electric field, but it can occur in a nonuniform field. Thus one can also expect field-dependent motion of uncharged CO_2 through the coating.

If one grants the reasonableness of an orientation of the substituent anion which compromises spatial and electrostatic requirements and which makes use of the void, the substitution of other anionic species, and even molecular species, in the BaO crystal appears to constitute a rather ordinary phenomenon.

It is of particular interest that the H_2O molecule, with a tetrahedral

[18] J. J. Lander, "Polymorphism and Anion Rotational Disorder in the Alkaline Earth Carbonates," *Jour. Chem. Phys.*, Vol. 17, pp. 892-901, October, 1949.

[19] Stillwell, Op. Cit., p. 261.

charge distribution[20] and an apparent radius of 1.38 angstroms, could substitute for $O^=$ if charge balance were maintained in the crystal by electrons. Such an addition of H_2O to a vacant oxygen site would produce a BaO crystal whose chemical composition would be indistinguishable from one having two OH^- sites to each of which is attached an extra electron, i.e., an $OH^- \cdot e$ group.* It has been found that $H_2O(g)$ will react rather completely with the "excess Ba" of an active cathode coating in less than 16 hours[21] even though the coating is kept at room temperature. Presumably diffusion of H_2O or its fragments through the coating proceeds rather readily.

From a purely mechanical viewpoint, a tabulation of ionic radii[17] indicates that substitution of OH^-, $CO_3^=$, $O_2^=$, O_2^-, H^-, $N^\equiv$, CN^-, NO_3^-, ClO_3^-, HCO_3^-, HCO_2^- might be expected in BaO. The postulate derived from the electrolysis experiment—that such substitutions do occur—is still allowable. There are, of course, more subtle considerations which remain unknown.

Finally, it may be noted that the void in BaO is nominally large enough to contain H_2 and N_2 interstitially, or one of several nonmetallic atoms such as H, C, N, F, P, S, Cl, or one of a variety of cations such as Li^+, Be^{++}, Na^+, Mg^{++}, Al^{+++}, Ca^{++}, Ti^{+4}, Mn^{++}, Fe^{++}, and so forth. No anions appear to be allowed as interstitials (cf. Stillwell's tabulation of ionic radii). The continuity of the void in BaO is attained by channels probably large enough to render diffusion of many such likely interstitials rather easy. If cations are contained as interstitials, charge balance must be preserved by incorporating an appropriate number of electrons either as "free" electrons, as trivalent anions substituted for $O^=$, or as anions added, on crystal surfaces, to the stoichiometric number of $O^=$ ions. It is recalled that our early mass spectrometer experiments[4,5] always showed that alkali metal atoms and ions evaporate at low temperatures (500°C and higher) from bare nickel cathode sleeves. By contrast, these experiments detected no evaporation, even at much higher temperatures, of alkali atoms or ions from alkaline earth oxide cathodes supported on sleeves made from the same lots of nickel. Perhaps the alkali ions are contained as void interstitials in the oxide coating.

---

[20] A. F. Wells, *Structural Inorganic Chemistry*, Oxford Univ. Press, London, 1950, Second Edition, p. 428.

* R. H. Plumlee, "The Electron Donor Centers in the Oxide Cathode," *RCA Review*, Vol. XVII, pp. 231-274, June, 1956. Arguments are presented in this paper from which it is concluded that such a group indeed constitutes the most important mobile donor species effective in the oxide cathode rather than the F-center donor species conventionally postulated.

[21] L. A. Wooten, George E. Moore, and W. G. Guldner, "Measurement of Excess Ba in Practical Oxide Coated Cathodes," *Jour. Appl. Phys.*, Vol. 26, pp. 937-942, August, 1955.

THE STABILITY OF SOLUTIONS OF IMPURITY ANIONS IN BaO(*s*)

The thermochemical relationships necessary for considering the behavior of solutions are defined in the following paragraphs.[22]

The standard free energy change, ΔF°, for any reaction process is related to the equilibrium constant K and the activity quotient as

$$\Delta F^\circ = -RT \ln K = -RT \left(\sum_p \ln a_p{}^q - \sum_r \ln a_r{}^s \right).$$

In these equations,

$R = 1.987$ calories/mole-degree, and

$T = {}^\circ$Kelvin temperature of the equilibrium considered.

The $a_p{}^q$ and $a_r{}^s$ values are activities of products and reactants respectively raised to the powers q and s equal to their coefficients in the balanced chemical equation for which the ΔF° value applies. In turn, ΔF°, at any temperature, is the change in free energy associated with a hypothetical process whereby each product is formed in its standard reference state of unit activity ($a_p = 1$) and each reactant is consumed in its standard reference state of unit activity ($a_r = 1$). Each substance is taken as being in its standard reference state when it is in that physical (gaseous, liquid, or solid) form which is stable under one atmosphere of external pressure. The following relationships give with sufficient exactness for present purposes the relationship between the activity a_i of a species in any solution, the partial pressure p_i (or any other colligative property), the vapor pressure $p_i{}^\circ$ which it shows in its pure standard reference state, and its mole fraction N_i in the solution:

$$a_i = \frac{p_i}{p_i{}^\circ} = \gamma_i N_i.$$

The activity coefficient, γ_i, remains as an empirically derived parameter in which is absorbed all deviation from direct equality between a_i and N_i. If γ_i is unity, the component is said to behave ideally; if γ_i is a constant other than unity for some range of N_i values bounded by zero, the component is said to obey Henry's Law for the range. For a component at temperatures above its normal boiling point, the activity, a_i, is numerically equal to its partial pressure expressed in atmospheres

[22] See any textbook on chemical thermodynamics.

It is thus obvious a priori that, with some knowledge of likely gas partial pressures in tube envelopes and with tabulated ΔF° values for reactions in which they participate, one can calculate the activities of some impurity species produced in the cathode coating from reasonable activity values assumed for all other participants of the reaction. In lieu of better information, one may assume ideal solution behavior and tentatively take activities as equal to concentrations. The impurity conditions resulting from a number of such reactions have been computed and the results assembled as Table III.

The emphasis in Table III is on reactions between gases and species present in solution. This representative tabulation largely supplements those given by White[23] and Rittner.[24] One or more of the following categories of conditions is covered by the data for the reactions in Table III:

a. The product of interest generated as a solute at a very low activity value such as 10^{-6} (mole fraction) dissolved in one of the other participants such as $BaO(s)$, the other participants being essentially pure phases having essentially unit activities except the residual gases whose required equilibrium pressures are computed.

b. The product of interest and the alkaline earth metal or reducing agent each dissolved and having a low activity (10^{-6}, 10^{-12}, and so forth) in some other solid participant or even in some other inert solvent such as BaO or the nickel support metal, the required equilibrium pressure of the gas being computed. In some cases, likely solid reactant activities are assumed and product activities are derived.

The activity value of 10^{-6} was selected because roughly this mole fraction of electron donor centers is required to account for the electrical properties of cathode coatings.[25] As a first approximation, activities may often be considered equivalent to mole fractions for solid alloy solutions[26] and salt solutions[27] at mole fractions below .01. The measurements of Timmer[14] on Ba dissolved in BaO indicate that the activity of Ba at a mole fraction of 10^{-6} is essentially equal to its mole fraction.

---

[23] Addison H. White, "Applications of Thermodynamics to Chemical Problems Involving the Oxide Cathode," *Jour. Applied Phys.*, Vol. 20, pp. 856-860, September, 1949.

[24] E. S. Rittner, "A Theoretical Study of the Chemistry of the Oxide Cathode," Philips Res. Reports, Vol. 8, pp. 184-238, June, 1953.

[25] L. S. Nergaard, "Studies of the Oxide Cathode," *RCA Review*, Vol. XIII, pp. 464-545, December, 1952.

[26] Carl Wagner, *Thermodynamics of Alloys*, Addison Wesley Press, Inc., Cambridge, Massachusetts, 1952, p. 22.

[27] L. S. Darken and R. W. Gurry, *Physical Chemistry of Metals*, McGraw-Hill Book Co., Inc., N. Y., 1953, p. 281.

Table III

Reaction	$\Delta F^\circ_{1000°K}$ (Calories/mole)	$\log_{10} K_{1000°K}$	Conditions under which Product Forms (Activities of participants not listed in this column are taken as unity.)	Reference[a]
1. $Ba(l) + \frac{1}{2} O_2(g) = BaO(s)$	— 102,700	22.4	BaO(s); $a_{BaO} = a_{Ba} = 1$; $P_{O_2} \geqq 10^{-45}$ atm.	30
2. $Ba(l) = Ba(g)$	17,700	— 3.9		31
3. $Ba(g) + \frac{1}{2} O_2 = BaO(s)$	— 125,000	27.3	BaO(s); $a_{BaO} = 1$; $P_{O_2} \geqq \frac{1}{2} P_{Ba} \simeq 10^{-18}$ atm.	
4. $\frac{3}{2} Ba(l) + \frac{1}{2} N_2(g) = \frac{1}{2} Ba_3N_2(s)$	— 16,200	3.5	N≡(ss); Ba(ss); $a_{N^{-3}} = a_{Ba} = 10^{-6}$; $P_{N_2} \simeq 10^{-1}$ atm.	32
5. $BaO(s) + \frac{1}{2} N_2(g) = \frac{1}{2} Ba_3N_2(s) + \frac{1}{2} O_2(g)$	86,500	— 18.9	N≡(ss); $a_{N^{-3}} \geqq 10^{-6}$; $\frac{P_{O_2}}{P_{N_2}} \leqq 10^{-26}$	

[a] Where no reference is given, a combination of data for other reactions in the Table has been used to derive the result.

[30] O. Kubaschewski and E. Ll. Evans, *Metallurgical Thermochemistry*, Academic Press, Inc., N. Y., 1951.

[31] K. K. Kelley, *Contributions to the Data on Theoretical Metallurgy III. The Free Energies of Vaporization and Vapor Pressures of Inorganic Substances*, Bulletin 383, U. S. Dept. of the Interior, Bureau of Mines, 1935.

[32] K. K. Kelley, *Contributions to the Data on Theoretical Metallurgy VIII. The Thermodynamic Properties of Metal Carbides and Nitrides*, Bulletin 407, U. S. Department of the Interior, Bureau of Mines, 1937.

Table III—Continued

Reaction	$\Delta F^\circ_{1000^\circ K}$ (Calories/mole)	$\log_{10} K_{1000^\circ K}$	Conditions under which Product Forms (Activities of participants not listed in this column are taken as unity.)	Reference[a]
6. $BaO(s) + \frac{1}{2} O_2(g) = BaO_2(s)$	— 1,900	0.4	$BaO_2(ss)$; $a_{BaO_2} \geq 10^{-6}$; $P_{O_2} \geq 1.6 \times 10^{-13}$ atm.	33
7. $BaO(s) + CO_2(g) = BaCO_3(s)$	— 25,000	5.45	$BaCO_3(ss)$; $a_{BaCO_3} \geq 10^{-6}$; $P_{CO_2} \geq 3.5 \times 10^{-12}$ atm.	11
8. $BaO(s) + H_2O(g) = Ba(OH)_2(s)$	— 6,000	1.3	$OH^-(ss)$; $a_{OH^-} \geq 10^{-6}$; $P_{H_2O} \geq 5 \times 10^{-14}$ atm.	34
9. $Ba(l) + H_2(g) = BaH_2(s)$	— 7,400	1.6	$Ba(ss)$; $H^-(ss)$; $a_{Ba} = a_{H^-} = 10^{-6}$; $P_{H_2} = 2.5 \times 10^{-8}$ atm.	35
10. $BaO(s) + H_2(g) = BaH_2(s) + \frac{1}{2} O_2(g)$	95,300	— 20.8	$H^-(ss)$; $a_{H^-} = 10^{-6}$; $P_{O_2} = 10^{-14}$ atm.; $P_{H_2} = 10^{-2}$ atm.	
11. $BaO(s) + H_2(g) = Ba(l) + H_2O(g)$	56,700	— 12.3	$Ba(ss)$; $a_{Ba} \geq 10^{-12}$; $\frac{P_{H_2O}}{P_{H_2}} \leq 2$	
12. $2BaO(s) + H_2(g) = Ba(l) + Ba(OH)_2(s)$	50,700	— 11.0	$Ba(ss)$; $OH^-(ss)$; $a_{Ba} = 10^{-12}$; $a_{OH^-} \geq 10^{-6}$; $P_{H_2} \geq 10^{-13}$ atm.	

[33] M. de Kay Thompson, *The Total and Free Energies of Formation of the Oxides of Thirty-two Metals*, The Electrochemical Society, Inc., N. Y., 1942.

[34] John Johnston, "Free Energy Changes Attending the Formation of Certain Carbonates and Hydroxides," *Jour. Amer. Chem. Soc.*, Vol. 30, pp. 1357-1365, September, 1908. The present author has been unable to find more recent data than this for $Ba(OH)_2$; however, the data of this reference for $Sr(OH)_2$ agrees moderately well with more recent data for $Sr(OH)_2$.

[35] W. C. Schumb, E. F. Sewell, and A. S. Eisenstein. "Observations on the Stability of the Barium-Hydrogen and Zirconium-Hydrogen Systems," *Jour. Amer. Chem. Soc.*, Vol. 69, pp. 2029-2033, August, 1947. Values used for the ΔF° and K of this reaction are estimated from experimental data listed in journal reference.

Table III—Continued

Reaction	$\Delta F^\circ_{1000^\circ K}$ (Calories/mole)	$\log_{10} K_{1000^\circ K}$	Conditions under which Product Forms (Activities of participants not listed in this column are taken as unity.)	Reference[a]
13. $\frac{1}{2}BaO(s) + \frac{1}{2}BaO_2(s) + H_2O(g) = Ba(OH)_2(s) + \frac{1}{4}O_2(g)$	— 5,150	1.1	OH^- (ss); $O_2^=$ (ss); $a_{OH^-} \geq 10^{-6}$; $a_{O_2^=} = 10^{-6}$; $P_{O_2} = 10^{-12}$ atm; $P_{H_2O} \geq 8 \times 10^{-14}$ atm.	
14. $BaCl_2(s) + H_2O(g) = BaO(s) + 2HCl(g)$	60,900	— 13.3	$a_{Cl^-} = 10^{-6}$; $P_{H_2O} = 10^{-12}$ atm.; $p_{HCl} \simeq 10^{-19}$ atm.	28, 30
15. $Ba(l) + \frac{1}{2}S_2(g) = BaS(s)$	— 95,000	20.8	$BaS(s)$; $a_{BaS} = 1 = a_{Ba}$; $P_{S_2} \geq 10^{-42}$ atm.	36
16. $BaO(s) + \frac{1}{2}S_2(g) = BaS(s) + \frac{1}{2}O_2(g)$	7,700	— 1.7	$BaS(ss)$; $a_{BaS} \geq 10^{-6}$; $\frac{P}{P_{S_2}} \leq 4 \times 10^8$	

[36] F. D. Richardson and J. H. E. Jeffes, "The Thermodynamics of Substances of Interest in Iron and Steel Making III. Sulphides," *Jour. Iron and Steel Institute*, Vol. 171, Part 2, pp. 165-175, June, 1952.

For the moment we shall omit consideration of the halides and sulfides. With these omissions, three general conclusions are apparent from this table of representative reactions:

a. Several substitutional solute anionic species can probably be formed to the extent of mole fractions of 10^{-6} in the cathode coating from reactions between alkaline earth metals or other strong reducing agents and the most abundant residual gas species present at the low partial pressures found in vacuum tubes. These include $C_2^{=}$, $N^{\equiv}$, CN^{-}, and perhaps H^{-}. However, these impurity mole fractions form only if the activities of the metals or reducing agents are within an order of magnitude or so of unity. For the alkaline earth metals, this implies a vapor pressure of the metals in solution in the oxide host near that of the pure metals. For Ba at 1000°K, this would be about 10^{-1} millimeter of mercury. Such conditions probably do not long prevail in vacuum tubes even during cathode activation.

b. The alkaline earth oxides are far more stable than these likely impurity salts. Thus, in the absence of substantial activity values of strong reducing agents in the coating, oxygen (from residual gases O_2, CO_2, CO, H_2O) successfully competes for anion sites and eliminates the substitutional type of impurity practically completely. This is clearly shown by the calculation for reaction No. 5 of Table III which indicates that partial pressure ratios of

$$\frac{P_{O_2}}{P_{N_2}} \geq 10^{-26}$$

would diminish nitride impurity concentration (if previously formed) to values below 10^{-6} mole fraction. The generation of more reactive gas fragments by cracking of gas molecules on the hot cathode does not appreciably alter this situation.

c. In contrast to the substitutional type of impurity anion, oxygen-containing anionic impurities such as $O_2^{=}$, OH^{-}, $CO_3^{=}$ which are formed by *addition* of some atom or groups of atoms to the oxide ion are not subject to displacement by oxygen. The oxide constitutes a suitable sponge for condensation of these species. Under moderate partial pressures of the gaseous dissociation products of these impurity sites, impurity mole fractions of 10^{-6} are easily realizable.

From these conclusions, it is apparent that only the addition-type oxygen-containing impurity anions in cathode coatings need be considered when attempting to explain the action of the most prominent residual gases in vacuum tubes, namely H_2O, CO, H_2, CO_2, N_2, O_2.

Because of considerations now to be stated, little or no significance is attached to the probability that halide and sulfide impurities may also be present in cathode coatings. From thermochemical data, it is apparent that barium fluoride, barium chloride, and barium bromide are about equally resistant to conversion to barium oxide by reaction with H_2O. In a vacuum tube, this is the most likely chemical reaction by which halides can be eliminated from the coating. The elimination of sulfide probably proceeds about equally unfavorably by reaction with O_2. Entry numbers 14 and 16 in Table III give representative thermochemical data pertinent to these reactions. From these entries, it is apparent that small Cl^- and $S^=$ impurity concentrations can exist in BaO under very small partial pressure ratios, p_{HCl}/p_{H_2O} and p_{S_2}/p_{O_2}, respectively.

Experimental evidence bearing on the halide and sulfide situation is the following:

(a) Chloride negative ions were ejected electrolytically from cathodes operated at normal temperatures in the mass spectrometer. The ejection of sulfide negative ions has been found by others.

(b) BaCl (fragment of $BaCl_2$) was detected in the mass spectrum of materials evaporating from cathodes during the early hours of cathode life. $BaCl_2$ is rather volatile, having a vapor pressure[28] in pure condition of about 3×10^{-7} millimeter of mercury at 1000°K.

(c) From the mass spectrometer experiments, we expect that sulfur- and halogen-containing residual gases would be present in normal tubes at partial pressures smaller by several orders of magnitude than those of H_2O, CO, H_2, O_2, and CO_2.

(d) Pulse emission[29] (at 888°K) was reduced by about 60 per cent in normally processed double alkaline earth cathodes by the deliberate addition of any of the four barium halides to the carbonate spray. (The per cent emission decay during 0.3-second pulses was not changed by the addition of halides.) Because this 60 per cent decrease in emission can be attributed to a work function increase of only about 5 per cent, it is concluded that cathodes in normal tubes are not particularly sensitive to the presence of barium halides. Experiments performed by R. M. Matheson in this laboratory indicate that the effects on emission produced by sulfur vapor pressures of the order of 10^{-8} millimeter of mercury are similarly slight, but that the effects

[28] L. L. Quill, *The Chemistry and Metallurgy of Miscellaneous Materials*, McGraw-Hill Book Co., New York, 1950, p. 209.

[29] Unpublished emission tests performed by C. P. Hadley and colleagues of the RCA Tube Division, Lancaster, Pa.

produced by impurities in the sulfur are large and vary from beneficial to deleterious.

Because of these circumstances, we choose to ignore the presence of halide and sulfide impurities in cathode coatings while searching at the present level of confusion for an explanation of cathode performance in the presence of residual gases and an explanation of cathode behavior generally.

Conclusions

1. In BaO maintained at 1000°K, small impurity concentrations of addition-type anions exist in labile equilibrium with molecular species ordinarily present in vacuum systems at partial pressures of 10^{-6} to 10^{-10} millimeter of mercury.

2. Instantaneous partial pressures shown by the dissociation products of these impurities depend on previous history of the oxide including temperature of the oxide, electron emission duty cycle, electric field across the oxide, and exposure to gases in the vacuum system.

3. Time constants measured for changes produced in these partial pressures by changes in field across the oxide ranged from the order of tenths of a second to 45 minutes.

4. Thermochemical considerations dictate that impurity equilibrium concentrations which are large enough to affect electrical properties of the oxide and which are likely to be formed by reactions of the oxide with residual gases consist mainly of addition-type anions containing oxygen rather than substitution-type ions not containing oxygen.

Acknowledgments

The author is happy to acknowledge the very large contributions made by R. M. Matheson and L. S. Nergaard both to the experimental aspects of this research and to the interpretation of the results. The excellent assistance of E. G. Apgar in the early stages of the experimentation is also gratefully acknowledged.

THE ELECTRON DONOR CENTERS IN THE OXIDE CATHODE

By

R. H. Plumlee

RCA Laboratories,
Princeton, N. J.

Summary—*The electronic chemical potential serves as the basis of a new interpretation of the chemistry of the oxide cathode in particular and of electronically active solids in general. Any procedure which raises the Fermi level of a material increases the electronic chemical potential of the material and corresponds chemically to making the material a stronger reducing agent. This principle allows disposal of several fundamental irregularities in earlier interpretations of cathode chemistry through which the F-centers, presumed to be formed from "excess barium" and oxygen vacancies, have been previously identified as the electron donors. On the basis of recent literature it is concluded that the F-center model is not valid. With due regard to thermochemical and other physical properties deduced for the donor centers in the oxide cathode, and with due regard to the electrical properties of the donor centers as prescribed by the mobile donor theory, it is proposed to identify an impurity group, $(OH^- \cdot e)$, as the important electron donor center species in the oxide cathode. A detailed discussion is given of arguments leading to this model.*

The Electronic Chemical Potential

IT IS seldom recalled, in considering the chemistry of the oxide cathode, that the chemical potential of the electrons, $\mu_e(s)$, in any material is determined solely by the Fermi level of the material and is given by the relationship[1]*

$$\mu_e(s) = -\varphi, \tag{1}$$

in which φ is the total work function.[2] The chemical activity, $a_e(s)$, of the electrons in the solid is given by the expressions

$$\mu_e(s) = kT \ln a_e(s) \tag{2}$$

$$a_e(s) = e^{-\varphi/kT}. \tag{2a}$$

At equilibrium, the activity of the electrons in the solid is equal to

* All numbered references are listed at the end of the paper.

the activity of the electrons in the electron gas, $a_e(g)$. The latter is an absolute quantity given by the expression

$$a_e(g) = n_e(g) \frac{h^3}{2(2\pi m_e kT)^{3/2}} = \frac{n_e(g)}{N_c}, \tag{3}$$

in which $n_e(g)$ is the number of electrons per cubic centimeter, N_c is the density of states available to free electrons, and the other symbols have their usual significance.

Conversion of the absolute electronic activity, $a_e(g)$, to the conventionally used thermochemical activity,[3] a_e (thermo.), can be made by the equation

$$a_e \text{ (thermo.)} \simeq a_e(g) \frac{N_C}{N_1}, \tag{3a}$$

in which N_1 is the number of electron gas particles per cubic centimeter at one atmosphere pressure, the conventional thermochemical reference state. For the low pressures under consideration, degeneracy effects and electrostatic field effects will be ignored and partial pressures expressed in atmospheres will be taken as synonomous with activity values. When a dissolved species is in equilibrium with its vapor phase, the activity is the same for the two phases, and the activity of the species in the vapor phase measures directly the activity of the species in the solid phase. For ideal solutions, the activity of the species is also equal to its mole fraction.

It is seen that the absolute concentration of "gas-like" electrons in a solid is diminished from N_C by the factor $e^{-\varphi/kT}$ and that the conventional thermochemical activity of the electrons is given by

$$a_e \text{ (thermo.)} = \frac{N_c}{N_1} e^{-\varphi/kT}. \tag{3b}$$

This thermochemical electronic activity has the same status and significance as the thermochemical activity of any other chemical species and could be used in equilibrium calculations for reactions in which electrons appear as reactants or products, that is, in oxidation–reduction reactions, if appropriate free energy values and work function values were known so that the electronic activities of the materials participating in the reactions could be computed.

Thus, according to statistical thermodynamics, the activity of electrons in ordinary chemical reactions as well as in the thermionic

emission phenomenon is determined solely by the work function of the material. In terms of common chemical procedure, this means that the process of converting an inactive cathode made of any material whatever into a better electron emitter (having a lower work function) makes it into a stronger chemical reducing agent.[4] The cathode "activation" process is necessarily a chemical reduction process. This general approach suggests another obvious fact — that the mechanism by which the electrons are attached to the material is thermodynamically unimportant.

Also, according to statistical thermodynamics, thermionic emission constitutes an absolute measure of the electronic chemical potential. By contrast, in ordinary chemical thermodynamics, the chemical potentials of most other substances are defined on a relative scale, hence only relative values of chemical potentials are determined by observing reactions of one substance with others. Therefore, chemical reduction reactions of thermionic emitters with other arbitrarily selected substances constitute only relative measures of the electronic chemical potential of the thermionic emitters.

In short, a general principle is apparent from statistical thermodynamics — an elevation of the Fermi level is synonymous with an increase in the electronic chemical potential and is always accompanied by an increase in the reducing chemical potential of the material.

Irregularities in Conventional Interpretations of Cathode Chemistry

Upon considering the implications of the general principle evolved in the preceding section, one immediately notes that in the past the low work function phenomenon (in oxide cathodes and other low work function materials) has always (?) been pictured as due to the presence of specific chemical agents, e.g., barium or cesium, rather than due to the presence of a high electronic chemical potential in the coating. Although cathode makers have long been aware of the practical importance of "reducing agents" to good oxide cathode performance, they have usually considered these agents merely as implements which insured an adequate supply of "excess barium" rather than agents which in themselves established a certain level of electronic chemical potential. An unbiased mind, uninformed about the early experiments with films of cesium on tungsten and thorium on tungsten, and about the early F-center model of alkali halides, might have chosen to view the effect of reducing agents as a more general phenomenon than the generation of "excess barium" which lingered on or in the oxide coating.

One notes also that certain chemical properties of "excess barium" have remained constant for some thirty years while the barium was (1) adsorbed on the surface of the oxide, (2) dissolved as atoms in the oxide, (3) colloidally dispersed in the oxide, or (4) distributed in the oxide as bona fide cations with electrons in oxygen vacancies. These chemical properties moreover have been assumed to be essentially those of barium metal. Concomitantly, the vapor pressure of such excess barium has always been several orders of magnitude lower than that which should be predicted from the measured vapor pressure of pure barium for ideal solution behavior of barium in the oxide coating.

It is well known to physical chemists that solute vapor pressure constitutes an appropriate criterion of solute activity in the solution; hence any bonding forces which reduce solute vapor pressure below ideal solution behavior also reduce the chemical activity of the solute; therefore, it is not obvious that the "excess barium" in oxide cathodes which exerts an abnormally low vapor pressure should react chemically as barium atoms. Perhaps it should react more nearly as the Ba^{++} ions of BaO if the electrons it donates to form the postulated F-centers are moderately well fastened to the oxygen vacancies.

Recently a number of research studies have been reported which can be interpreted as showing the following:

1. Solutions of barium in BaO prepared by exposing BaO single crystals[5,6] to barium vapor show roughly ideal solution behavior[7] at a solute barium mole fraction of 10^{-6} and strong positive deviation from ideal behavior at a mole fraction of 10^{-5}. This result is independent of the precise form of the dissolved barium, i.e., whether it is in the form of atoms or excess ions and F-centers.

2. The vapor pressure of barium from active cathodes operated 2,000 to 20,000 hours may be as low as 10^{-12} millimeter of mercury.[8] This vapor pressure corresponds to a mole fraction of solute barium of 10^{-11} or 10^{-12}, if the solution actually shows roughly ideal behavior. Such a barium concentration would be at least five orders of magnitude smaller than the concentration of electron donor centers (10^{-6} mole fraction) required[9] to account for the electrical properties of the coating.

3. The concentration of "excess barium" determined chemically[10-12] in many active oxide cathodes is one or two orders of magnitude larger than the required concentration of electron donors.

4. There is practically no correlation[10-12] between electron emission and measured "excess barium" concentrations in cathodes whose ages

ranged from 0.5 to 56,000 hours. The range of concentrations found was 10^{-6} to about 3×10^{-4} mole fraction. The sensitivity limit of the analytical method prevented measurements of concentrations below 10^{-6}, so it is not known whether a correlation exists at lower concentrations.

One possible interpretation of these apparently incompatible experimental results is that the large "excess barium" content measured in commercial active cathodes made of mixed oxides is indeed real, that it is tightly bound and shows extreme negative deviations from ideal solution behavior as indicated by the low rate of barium vaporization from such cathodes. It might be argued that electron emission may be insensitive to an over-supply of donor centers because of internal space-charge effects or some other condition. In this interpretation, however, it must be postulated that solutions of barium in BaO single crystals are distinctly different from solutions of barium in the oxide cathode, that the solutions of barium in BaO happen to show roughly ideal or positive deviation behavior whereas solutions of barium in the oxide cathode at the same concentrations show extreme negative deviations. This, we think, is rather unlikely.

Another possible interpretation, which will be developed here, fits the above experimental results together as mutually compatible parts of a consistent pattern of rather ordinary chemical behavior. This interpretation assumes that solutions of barium in BaO and of barium in the mixed oxides behave essentially alike and as indicated by the direct equilibrium vapor pressure measurements on barium in single crystals of BaO. If the solute barium behaves roughly ideally in both cases, it can be concluded from vapor pressure data for pure barium and from the BTL[13] measurements that in many practical active cathodes the concentration of solute barium does not exceed 10^{-11} mole fraction. (As mentioned previously, the Cornell[14] data indicate that the solute barium, no matter what its atomic or ionic form in BaO, exerts a vapor pressure roughly that of ideal solutions of barium atoms in BaO at a mole fraction of 10^{-6}.) Therefore, in cathodes we conclude that the mole fraction of solute barium is far too low to be identifiable as the important electron donor center. This conclusion eliminates from consideration F-centers, barium atoms, oxygen vacancies with one electron, colloidal barium, surface monolayer barium, and perhaps other postulated forms of solute or occluded barium. Such species may be present at various times in the life of the cathode, but they can exist only transiently and/or in very low concentrations in the absence of an equilibrium vapor pressure of barium atoms much larger than is commonly sustained in practical vacuum tubes.

When this interpretation is applied, two important questions remain to be answered:

1. How does one account for the chemical analyses made in the past of "excess barium" contents in cathodes as high as 10^{-4} mole fraction if solute barium is actually present to the extent of only 10^{-11} or 10^{-12} mole fraction?

2. If solute barium and/or F-centers cannot be present in adequate concentrations, what constitutes the electron donor species?

The fundamental relationship, stated earlier, between the work function and the electronic chemical potential provides directly a general answer to the first question and suggests clues useful in finding a plausible answer to the second question:

1. This fundamental relationship tells us that it would be a coincidence indeed if the chemical tests of the past for "excess barium" constitute specific tests for the electron donor centers effective in the oxide cathode; any donor species in (almost) any coating compound which happened to have the same low work function would have shown the same positive test reaction (usually the reaction with H_2O to produce H_2). At present, the reducing chemical reactions of activated oxide cathodes are but uncalibrated relative measures of the electronic chemical potential and conceivably indicate the presence of a collection of reducing species dissolved in the cathodes. This collection almost certainly includes reducing impurity elements from the support metal in addition to any solute barium, colloidal barium, F-centers, and other donor species. Of all these reducing constituents, perhaps only one largely controls the *electronic* properties of the coating. A correlation between chemically measured "excess barium" content and electron emission behavior of a cathode should thus be viewed as a coincidence unlikely to occur and should not be viewed as a necessity.

2. Our fundamental relationship, having thus disencumbered us of the "excess barium" hypothesis, encourages us to consider on its own merits any conceivable donor center species. The electronic chemical potential is satisfied with any identification irrespective of the chemical composition of the species.

The Nature of Electron Donor Centers

This analysis is based on the premise that the chemistry of electronically active structures does not differ markedly from ordinary chemistry. This premise may be quite wrong; however, by assuming roughly ideal solution behavior, that the thermochemical activities of metallic and salt-like solute species are approximately equal to concen-

trations in extremely dilute solutions, and that the donor and acceptor species are rather ordinary reduced and oxidized forms of ordinary impurities, an intriguing view of cathode phenomena is obtained. It transfers a surprising variety of experience from the category of "mysterious" into "ordinary." This approach is not exactly novel—it borrows considerably from the ideas of Verwey and his colleagues. So far as is known, it has not previously been applied to the oxide cathode nor has it been so concretely and explicitly stated as it is here.

A. Thermochemical Properties of Donor Centers

1. Affinity for Electrons

Regardless of the chemical identity or composition of the electron donor center, it is apparent that the energy difference between an electron in the conduction band and an electron attached to the impurity center[15] helps determine the vapor pressure of barium from the oxide cathode coating. The greater the binding energy between the electrons and the impurity centers, the lower the vapor pressure of barium becomes from the oxide, approaching in the limit the barium vapor pressure value characteristic of the dissociation of intrinsic BaO. The contribution of this bonding to the free energy of vaporization of barium from the oxide can be described formally by the sum of the following reactions for the filled donor impurity, D_f, forming from Ba^{++} the empty impurity, D_e, and a barium atom in solid solution:

$$2D_f(ss \text{ in BaO}) = 2D_e(ss \text{ in BaO}) + 2e(\text{conduction band}); \quad \Delta F^\circ_4 = \Delta E^\circ_4 - T\Delta S^\circ_4. \tag{4}$$

$$2e(\text{conduction band}) + Ba^{++}(s \text{ in BaO}) = Ba(ss \text{ in BaO}); \quad \Delta F^\circ_5 = \Delta E^\circ_5 - T\Delta S^\circ_5. \tag{5}$$

These when added give[16]

$$2D_f(ss \text{ in BaO}) + Ba^{++}(s, \text{BaO}) = 2D_e(ss, \text{BaO}) + Ba(ss, \text{BaO}); \quad \Delta F^\circ_6 \simeq \Delta E^\circ_4 + \Delta E^\circ_5. \tag{6}$$

Assuming the D_f, D_e, and barium impurities form ideal solutions in BaO, one may write equations[17] for all three similar to the following for barium:

$$Ba(ss, \text{BaO}) = Ba(s); \quad \Delta F^\circ_7 = 0. \tag{7}$$

From thermochemical data,[18]

$$Ba(s) = Ba(g); \quad \Delta F^\circ_{8(1000^\circ\text{K})} \simeq 0.77 \text{ ev}. \tag{8}$$

The sum of Reactions (6), (7), and (8) is

$$2D_f(ss, \mathrm{BaO}) + \mathrm{Ba}^{++}(s, \mathrm{BaO}) = 2D_e(ss, \mathrm{BaO}) + \mathrm{Ba}(g);$$
$$\Delta F^\circ{}_{9(1000^\circ\mathrm{K})} \simeq 0.77 + \Delta E^\circ{}_4 + \Delta E^\circ{}_5 \text{ ev.} \qquad (9)$$

Here $\Delta E^\circ{}_4$ has a positive numerical value essentially equal (for 2 electrons) to twice the activation energy (Fermi level distance below the conduction band) of one electron for the conduction process. For the condition in which practically all the impurity centers are filled, this activation energy is half the energy distance between conduction band and donor level; for the condition in which there are far more empty impurity centers than filled ones, this activation energy is equal to the entire distance between conduction band and donor level. From DeVore's measurements[19] of photoconductivity, taking the highest set of donor levels as 1.4 electron volts below the conduction band gives $\Delta E^\circ{}_4$ (for two electrons)

$$2.8 \geqq \Delta E^\circ{}_4 \geqq 1.4 \text{ ev.}$$

$\Delta E^\circ{}_5$ has a negative numerical value corresponding to the recombination energy of a Ba^{++} ion and 2 electrons dissolved in BaO. For purposes of discussion, $\Delta E^\circ{}_5$ may be taken as

$$\Delta E^\circ{}_5 = -\frac{(I_1 + I_2)}{\epsilon^2} = -1.2 \text{ ev.}$$

by using the two ionization energies[20] of the barium atom I_1, I_2, and by taking $\epsilon = 3.5$ as the effective high-frequency value[9,21] of the dielectric constant of BaO.

It is seen then that the binding energy between the impurity centers and the electrons contributes to the free energy requirement for atomic vaporization of an equivalent concentration of Ba^{++} ions by the amount of 1.4 to 2.8 electron volts. The vapor pressure of this number of Ba^{++} ions (equal to half the number of D_f impurity centers) differs then from that which the same number of dissolved Ba atoms would show (if they were present) because of their additional free energy of vaporization over that of Ba atoms. This additional free energy requirement is superficially estimatable as

$$(\Delta E^\circ{}_4 + \Delta E^\circ{}_5) \simeq 1.6 \text{ to } 0.2 \text{ ev.}$$

Using Reaction (9) itself and the BTL measurements of barium

vaporization from cathodes, one can also estimate $(\Delta E^\circ_4 + \Delta E^\circ_5)$ directly. The vapor pressure, p°_{Ba}, of pure barium at 1000°K is about 10^{-4} atmospheres.[18b] For a 10^{-6} mole fraction, X_{D_f}, of donors exerting no binding toward the electrons, the barium vapor pressure in the cathode would be

$$p_{Ba} = X_{D_f} p^\circ_{Ba} \simeq 10^{-10} \text{ atm., about } 10^{-7} \text{ mm.}$$

To depress this to the BTL measured value of 10^{-15} atmosphere ($\sim 10^{-12}$ mm.) corresponding to a Ba activity, $a_{Ba} \simeq p_{Ba}/p^\circ_{Ba} \simeq 10^{-11}$, the equilibrium constant K_9 for Reaction (9) must be

$$K_9 \simeq 10^{-11} = a_{Ba}$$

for the condition of the cathode in which $a_{D_f} = a_{D_e}$, i.e., roughly half the donor impurities full. From K_9, $\Delta F^\circ_{9(1000°K)}$ is computed and from this,

$$(\Delta E^\circ_4 + \Delta E^\circ_5) \simeq 1.4 \text{ ev.}$$

As discussed later, the 10^{-12} mm. vapor pressure value for barium used above is probably an upper limit for the "donor destroying" barium vaporization so that this value of $(\Delta E^\circ_4 + \Delta E^\circ_5)$ is a minimum value.

2. Relationship to Reducing Agents in the Coating

Disregarding any particular significance of the above numerical values, one sees from this thermochemical treatment that the vapor pressure of barium from the cathode should vary (a) with the donor level position, (b) with the donor center concentration and/or (c) with the extent to which the donor levels are filled with electrons. (Chemically speaking, donor centers have reduced and oxidized forms corresponding to their full and empty conditions, respectively.)

It is also apparent that the activities (effective concentrations) of *all* the reduced forms of *all* the coating constituents rise with the Fermi level and vice versa. At thermal equilibrium, the most easily reduced ion in the coating will appear in highest activity though not necessarily in highest concentration[22] (because of likely deviations from ideal solution behavior). Under applied electric fields, thermal equilibrium relationships are perhaps so thoroughly disturbed that the reduced forms even of the most difficultly reduced constituents may appear at equal activities with those of the most easily reduced species. Under this circumstance, such factors as solubility of the reduced form,

rate of diffusion, and vapor pressure enter also to affect the steady state activity values and concentrations.

For want of a better rule of thumb, it may be said that dissolved atoms of the *least* easily reduced cationic constituent of the cathode constitute the most efficient reducing agent. A continuously supplied small activity of atoms of the *least* easily reduced cation supports at equilibrium a much larger activity of the reduced forms of the more easily reduced constituents. This is illustrated in the following reactions:

$$\mathrm{BaO}(s) + \mathrm{Mg}(l) = \mathrm{Ba}(l) + \mathrm{MgO}(s); \quad \Delta F^{\circ}_{1000^{\circ}\mathrm{K}} = -16{,}450 \text{ calories}. \qquad K_{10} \simeq 10^{3.6}. \qquad (10)^{23}$$

Assuming a reasonable activity of MgO, $a_{\mathrm{MgO}} \simeq 10^{-6}$, (it may conceivably go as high as 10^{-4}) one finds

$$\frac{a_{\mathrm{Ba}}}{a_{\mathrm{Mg}}} \simeq 10^{10}.$$

$$\mathrm{BaO}(s) + \mathrm{Ni}(s) = \mathrm{Ba}(l) + \mathrm{NiO}(s); \quad \Delta F^{\circ}_{1000^{\circ}\mathrm{K}} = +67{,}800 \text{ calories}. \qquad K_{1000^{\circ}\mathrm{K}} \simeq 10^{-15}. \qquad (11)$$

(a) Assuming $a_{\mathrm{NiO}} \simeq 10^{-6}$,

$$\frac{a_{\mathrm{Ba}}}{a_{\mathrm{Ni}}} \simeq 10^{-9}.$$

(b) Assuming $a_{\mathrm{Ba}} \simeq 10^{-11}$, as deduced from the BTL and Cornell data,

$$\frac{a_{\mathrm{NiO}}}{a_{\mathrm{Ni}}} \simeq 10^{-4}.$$

Hence, if here $a_{\mathrm{Ni}} \simeq 10^{-4}$, then $a_{\mathrm{NiO}} \simeq 10^{-8}$. We see that the oxidized form of even a very weak reducing agent such as nickel can be present in the oxide cathode coating if a large activity of the reduced form is present.

Reaction (6) constitutes the critical reaction as far as general performance of the donor centers is concerned. If $\Delta F^{\circ}_{6} = \Delta E^{\circ}_{4} + \Delta E^{\circ}_{5}$ is positive, a substantial portion of the impurity centers is normally filled with electrons (provided enough "reducing agent," Ba, is present) and the number n of electrons per cubic centimeter in the conduction band is given by the equation[24]

$$n \simeq N_{D_f}^{\frac{1}{2}} N_C^{\frac{1}{2}} e^{-\frac{E_d}{2kT}},$$

in which N_{D_f} is the number of filled impurity centers per cubic centimeter, N_C the density of available states, and E_d the energy distance from the conduction band to the donor level. E_d is, of course, also half the maximum value of the $\Delta E^\circ{}_4$ for Reactions (4) and (6). If $\Delta F^\circ{}_6 = \Delta E^\circ{}_4 + \Delta E^\circ{}_5$ is a negative value, most of the donors are empty (although the same barium content assumed above may be present) and

$$n \simeq \frac{N_{D_f}}{N_{D_e}} N_C e^{-\frac{E_d}{kT}}.$$

Then n is small because N_{D_f}/N_{D_e} is small and because of the loss of the factor 1/2 in the exponential term. This condition may correspond to the situation in thermionic emitters for which the "A constant" in the Fowler emission equation is small and should perhaps be expected in materials in which the donor levels are near the conduction band. This will be more easily appreciated after the discussion of variable-charge cationic electron donors.

Because $\Delta E^\circ{}_4$ will always be positive and $\Delta E^\circ{}_5$ will always be negative, it would seem desirable to have as the reducing agent in the coating the most easily ionized (most electropositive) atoms in order to keep a large fraction of high donor levels full.

It is apparent further that the character of the reducing agent does not determine $\Delta E^\circ{}_4$. Upon substituting in Reaction (5) the impurity reactants M^{++} (ss in BaO) and M (ss in BaO) for Ba^{++} and Ba, respectively, M being any other metal used as a reducing agent, and writing $\Delta E^\circ{}_{5M}$ for $\Delta E^\circ{}_5$, it is apparent that the sum $(\Delta E^\circ{}_4 + \Delta E^\circ{}_{5M})$ rather than the sum $(\Delta E^\circ{}_4 + \Delta E^\circ{}_5)$ may determine the degree of fullness of the donor impurity population. The functions of reducing agent and donor impurity are, in principle, clearly separable and hence can be performed by separate species or by the same species. In systems in which both functions are performed by one species, the "reducing agent" becomes the most important donor impurity, either because of its concentration or its small ionization energy. This condition is exemplified in the highly purified covalent Group IV transistor materials, and until the present has also been believed to exist in the oxide cathode.

For the general situation illustrated by the Reactions (4) through (10), the donor impurity alone determines the donor level position (value of $\Delta E^\circ{}_4$). The precedent for considering level positions as

characteristic of particular impurities which are not reducing agents is found in phosphor work. In contrast to cathode work, phosphor work has ignored the intrinsic relationship of "excess metal" and the relationship of the state of reduction or oxidation of the material to its performance.

Because the reducing agent merely keeps the donors filled, and because even the most improbable reaction occurs to some extent, a given activity of any "reducing" agent can produce a certain ratio of filled to unfilled donor impurities (the empty impurity species having already been incorporated). The weaker the reducing agent, the larger the activity required to maintain a given fraction of filled donor impurities.

In some instances it is certain that the incorporation of these impurities or the manufacturing of these impurities in the host crystal may also result from chemical reduction reactions, so that the processes of manufacturing impurities and filling them with electrons may proceed together.

Reaction (6) also shows the usefulness of solubility of the reducing agent in the host crystal. As deduced from the BTL measurements and the ideal solution assumption about Ba in BaO, it is seen that the solubility required of Ba as the reducing agent is rather small—about 10^{-11} mole fraction of barium atoms. However, if one employs some other reducing element, so that the value of $(\Delta E^{\circ}_{4} + \Delta E^{\circ}_{5M})$ becomes negative, then a larger activity of the reducing agent is required to keep the donor levels reasonably filled. In this case, solubility limitations can become critical. It would seem worth-while for the reducing element to have an atomic radius not much larger than that of the cation of the host crystal and an ionic radius not much smaller than that of the host cation.

The mode of solution of base metal constituents such as iron in the AEO[25] cathode might well be considered at this point.

The disproportionation reaction[26] of FeO, and of other similar oxides of variable charge elements,

$$\mathrm{FeO}\,(s) = \frac{1}{3}\,\mathrm{Fe}\,(s) + \frac{1}{3}\,\mathrm{Fe_2O_3}\,(s)\,; \quad \log_{10} K_{1000^{\circ}\mathrm{K}} \simeq -0.6, \qquad (12)$$

neatly satisfies the charge-balance condition when these solute metal atoms are incorporated in the AEO cathode coating. Since charge balance is automatically maintained by the formation of $2\mathrm{Fe}^{++}$ and 3 $\mathrm{O}^{=}$ ions and roughly one FeO molecule for every iron atom incorporated, no vacancies need be formed. It is not known what the solubility

limit of these species is in BaO nor how their presence affects the electronic behavior of the cathode—presumably Fe and Fe^{++} can act as donors. The Fe^{+++} ions, though in principle capable of being ionized further, require a still larger ionization energy and contribute a negligibly small number of conduction electrons. Most base metals contain at least 10^{-4} mole fraction of Fe impurity, hence the Fe activity maintained in or around the cathode by the base metal will usually be of the order of 10^{-4} or larger. Cathode carbonate sprays also contain iron salts approaching 10^{-4} mole fraction.

Figure 1 illustrates a general type of energy level model helpful in considering the behavior of complex impurity systems in ionic solids. (The iron impurity system in BaO is chosen for this rough qualitative treatment because most of the species involved are familiar ones for which thermochemical data are available.) In Figure 1A, the

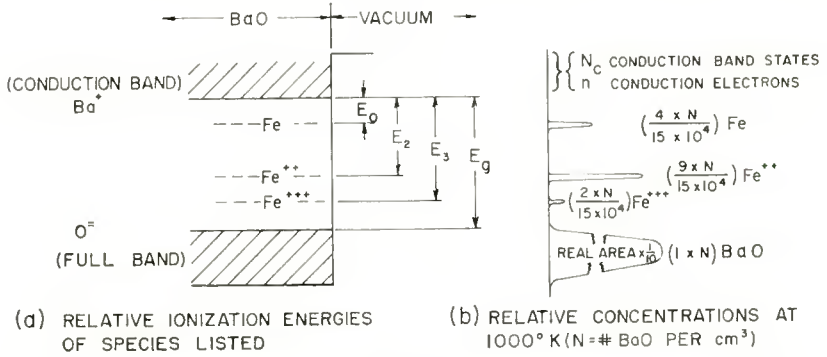

Fig. 1—Relative ionization energies and equilibrium concentrations for a solution of ~ 0.01 mole per cent of iron atoms in BaO.

vertical distances downward from the conduction band represent, very arbitrarily,[27] the energy required to remove one electron each from the species, Ba^+, Fe, Fe^{++}, Fe^{+++}, $O^=$, and to place that electron in the conduction band. The approximate concentrations given in Figure 1B are derived by assuming ideal solution behavior for all species, assuming an Fe activity of 10^{-4} supplied by the base metal, and computing the Fe^{++} and Fe^{+++} concentrations from the equilibrium constant for the disproportionation reaction.[28]

For incorporating other reducing elements which cannot form cations showing more than one appropriate state of oxidation, charge-balance considerations indicate that some sort of pseudo-separation of metal phase, *M*, is required in general. If solute metal atoms such as magnesium are to be dissolved in a BaO crystal whose sites are (almost) all occupied by some ionic species and are to be dissolved

without creating vacant sites containing no ions or atoms, then they must occupy both anionic and cationic sites. It is only a matter of degree as to how many such sites agglomerate to form an incipient metal phase. Since these are moderate or strong reducing elements with which we are concerned, the activity ratio $a_{M^{++}}/a_M$ will ordinarily be considerably larger than unity in the absence of other stronger reducing agents; hence the incipient metal phase (M) will ordinarily be interspersed and bounded with metal oxide (MO) and BaO so that very little bare metal (M) will be exposed to the vacuum.

Such agglomerated impurities may be required to accommodate the high reducing agent contents (even exceeding 10^{-4} mole fraction in some cathodes) measured by the BTL group. The BTL analyses of coatings dropped or scraped from Konal-base cathodes indicate reducing element contents only slightly less than 10^{-4} mole fraction in the detached coatings, so there is little doubt that reducing element contents of the order of 10^{-4} mole fraction exist in or on the oxide coatings themselves.

In principle, the strongly electropositive elements used as reducing agents should place the Fermi level higher than should less electropositive elements; however, in practice a better result is obtained with the less electropositive reducing elements because of solubility and volatility limitations. In addition, if in some way a large activity of very strong reducing element is maintained, it may chew away both the host compound and donor compound at an excessive rate. Thermochemically, a small activity of a strong reducing element may be no more effective in keeping donors filled than a large activity of weaker reducing elements.

The suggestion that metals other than barium may be responsible for the chemically measured electronic activity of the coating may seem absurd until one fully appreciates the fact that reducing agents have always been added to the base metal for the purpose of raising the electronic activity, although the purpose has usually been stated in terms of production of barium.

It is thus to be expected that the chemically measured electronic activity of the coating, i.e., the measured "excess barium" content, should correspond more nearly to the steady-state total concentrations of all the reducing elements present than to the steady-state concentration of barium produced from them. As shown with Reactions (10) and (11), strong reducing elements such as magnesium (and also aluminum, titanium, and silicon) may be present in lower thermal equilibrium concentrations than the barium; however, along with these will be substantial incidental concentrations of weaker reducing

agents (less electropositive atoms) such as iron, manganese, chromium, carbon, cobalt, nickel, and so forth. As pointed out by the BTL group, several of these react slowly in bulk with H_2O at room temperature to produce H_2. In highly dispersed form, iron, manganese, and chromium would react readily with H_2O to form H_2. (C in BaO could give $BaCO_3$ and H_2.) Roughly the same activities (effective concentrations) of elements such as iron, manganese, chromium, and carbon present in the base metal should be maintained in the oxide coating as in the base metal itself by simple vapor phase transport and/or by diffusion; hence these elements very likely constitute practically all the "excess barium" content of cathode coatings.

Being reduced forms themselves, these atoms are overtly identifiable as donor species; however, the (solute) concentrations of strongly electropositive elements such as barium which per se might constitute high donor levels are certainly too small (because of the vapor pressures of these elements) to contribute significantly to the electrical properties of the cathode. On the other hand, those elements present at substantial activities are less easily ionized and perhaps contribute donor levels lying in a useful range below the conduction band.

Whether atoms such as iron, aluminum, magnesium, silicon, etc. are actually soluble enough in the oxide coating to contribute to the important donor population can be surmised only from the prima-facie evidence contained in the BTL measurements of "excess barium" contents of cathodes. Perhaps these elements are actually largely present as a colloidally dispersed metal phase which does not participate directly as donor material but which dissolves gradually to balance the loss of donor cations (e.g., M^+, M^{++}) incurred through coating electrolysis and through oxidation by residual gases.

These elements, if present as a colloidal phase, can certainly exert an electronic chemical potential high enough to register as reducing agents in the H_2O reaction without necessarily being able to act as electron donors. Perhaps, as a colloidal phase, they can also exert an electronic chemical potential high enough to fill the important donor species of the coating with electrons though they are not homogeneously distributed as atoms throughout the oxide. This conceivably occurs by operation of the mass action principle illustrated earlier for the Mg, BaO system.

We have now shown on the basis of fundamental theory and on the basis of common chemical behavior that chemical analyses made in the past of the "excess barium" content of cathodes should not be considered valid indicators of the concentration of the electrically important donor center species. The chemically measured "excess

barium" content of cathode coatings should be comprised of (a) donor-type species some of which are electrically important, some of which are not and (b) solute metal atoms at roughly the same concentrations (within limits allowed by vapor pressures and solubilities) as in the base metal of the cathode.

This interpretation can account quantitatively for the 10^{-6} to 10^{-4} mole fraction "excess barium" contents measured by the BTL group[10, 12] for all their test cathodes *except* those on their purest platinum base metal for which the only impurity detectable was $<$ 0.03 per cent weight of copper. (From their table of analyses we assume they could have detected 0.001 per cent by weight of magnesium, silicon, iron, manganese, and so forth, had such been present in that extremely pure platinum.)

We have not been able to deduce from the BTL papers a thoroughly satisfactory explanation of the "excess barium" contents for the cathodes on that ultra-pure platinum; however, we find room for belief that a simple explanation exists which does not require solute barium per se to be present at mole fractions larger than 10^{-10} in these cathodes either. The most likely cause of the rather uniform median reducing agent contents found in all their different classes of cathodes is that of contamination from the other electrodes. This is discussed in detail in the Appendix.

3. Stability in Vacuum

The impurity constituent which constitutes the donor center, in addition to preventing dissociation of the oxide coating by virtue of its affinity for electrons, must itself be stable at 1000°K under high-vacuum conditions.

Assuming the impurity center is some *cationic* constituent, the stability requirement implies (1) low volatility, (2) resistance against oxidation by residual gases which would create the empty (oxidized) form of the impurity, and (3) resistance to the disproportionation reaction which would also consume the donor form of the impurity. This will subsequently be considered in more detail.

Assuming the impurity center is some *anionic* constituent, the stability requirement implies (1) low volatility and/or low dissociation pressure, (2) resistance against displacement by oxygen from the oxygen-containing residual gases, and (3) stability against disproportionation. This last is relatively unimportant for anionic donors. The second requirement is critical for, as shown in the preceding paper, only halide, sulfide, and addition-type oxygen containing anions such as OH^-, $CO_3^=$, $O_2^=$, HCO_2^-, and so forth, are stable against displacement by oxygen under likely vacuum conditions. Evidence for the

presence of such oxygen-containing impurity anions in BaO was found mass spectrometrically[29] by studying the electrolysis of cathode coatings during the drawing of electron current. The dissociation pressure of the anionic impurity must be low enough that equilibrium partial pressures of its gaseous reaction products may either be tolerated by the vacuum tube or provided by the vacuum tube.

In summary, a thermochemical analysis has shown a previously not generally realized fact — that the donor centers effective in the oxide cathode are required to have a substantial electron affinity. Without such electron affinity they would become empty irreversibly at a rate equal to the vaporization rate of barium from an ideal solution of barium of the same concentration in the oxide.

In addition, the analysis distinguishes two phenomena previously considered as only one:

(a) the presence of impurity centers which, if filled with electrons, define the donor level position;

(b) the presence of reducing chemical potential which determines the degree of fullness of the donor impurity population.

The impurity center is pictured as containing, in general, an ordinary ionic part whose character can be described in ordinary chemical terms and whose reactions can be controlled by ordinary chemical methods. In the empty (oxidized) condition of the center, this ionic part may be practically indistinguishable from an electron trap, recombination center, or from a special type of acceptor center. In the filled (reduced) condition, the impurity center is an electron donor and contains the ionic part described above and a detachable electronic part. The two together also constitute in general a second ordinary ionic species.[30] The chemical characteristics of the impurity center when functioning as a ready electron donor and those which it shows when functioning as a ready electron acceptor or recombination center are presumed to be roughly the same as those which the two same ionic species should show as ideal solutes in an "inert" solvent.

B. The Mobility of Donor Centers

The prime characteristic of the ionic part of the electron donor species in oxide cathodes aside from its thermochemical characteristics is that of moderate mobility. The necessity of this property has been thoroughly analyzed by Nergaard in formulating the mobile donor hypothesis.[9] The high mobility expected of F-centers has been one of their most attractive features. Up to the present, only vacancy and interstitial diffusion mechanisms were considered likely to give the donors sufficient mobility to explain the electrical phenomena of cathodes. As of the present, pulse-emission measurements[31] indicate

that the diffusion constant of the donor centers at 1000°K is about 5.9×10^{-6} cm^2 sec^{-1} and that the activation energy for diffusion is about 0.43 electron volt.

C. Variable-Charge Cationic Electron Donors

In the past 20 years a considerable volume of literature[32-38] has evolved describing the use of "variable-charge cations" as electron donor or acceptor species in materials which, in the absence of such species, would be classed as insulators. We define the term "variable charge" donor to encompass generally the principles and ideas described by Verwey and colleagues as the "controlled valency" method of synthesis and the phenomenon described by Selwood[36, 37] as "valence inductivity."

As shown by Verwey and colleagues, if an impurity cation, $I_C^{(n+1)+}$, having a *more positive charge* than the host cation, $H_C^{(n)+}$, is substituted in a crystal for a host cation under *reducing conditions*, an appropriate number of extra electrons is also added to the crystal to preserve charge balance. (The same principle also presumably applies to impurity anions, $I_a^{(n-1)-}$, substituted for more negative host anions, $H_a^{(n)-}$, and this will be discussed subsequently.)

The site of the more positive substituent ion constitutes a position which has a smaller negative charge density than it should have when compared with the remaining host cation sites and hence constitutes a potential well for one of the charge-balancing electrons added in synthesis. The charge-balancing electron, whether it becomes affixed to the valence shell[39] of the substituent ion or not, spends more time in the vicinity of the substituent than in the vicinity of other ions. If these charge-balancing electrons are attached loosely enough to the substituent so that they can become dissociated occasionally by thermal excitation into the conduction band, the impurity center can act as an electron donor for the n-type conduction process.

If an impurity cation, $I_C^{(n+1)+}$, *of more positive charge* than the host cation, $H_C^{(n)+}$, is substituted for a host cation under oxidizing conditions, too few charge balancing electrons can be captured by the crystal. In this case, an appropriate number of anions is added to the crystal so that cation vacancies are formed to compensate the extra positive charge contributed by the substituent cations.

If an impurity cation, $I_C^{(n-1)+}$, of less positive charge than the host cation, $H_C^{(n)+}$, is substituted for the host cation under *oxidizing* conditions, some $H_C^{(n)+}$ ion may be induced to part with still another electron and, therefore, to act as an $H_C^{(n+1)+}$ ion. Alternatively, an appropriate number of anion vacancies may form to compensate the deficit in cation charge produced by introduction of $I_C^{(n-1)+}$ into

the crystal. In the former case, the $H_C^{(n+1)+}$ ion has an apparent deficit of electrons compared with other host ion sites. This, too, is a potential well for an electron, but the most likely source of an electron is an adjacent host anion, $H_C^{(n)-}$ or nearby host cation $H_C^{(n)+}$; hence the electron must come from the full band of the crystal. This arrangement provides a p-type conduction mechanism.

If, under the appropriate circumstances described, cation or anion vacancies are formed, the crystal may show ionic conductivity because of the easy diffusion mechanism associated with the presence of vacancies. Little or no electronic conductivity may occur in these circumstances unless one of the other charge-compensating mechanisms described is also present.

Verwey and associates have relied somewhat on the premise that solids strenuously try to avoid vacancy formation[32] and that usually the crystal sites are all filled with ions. Our measurements of the electrolysis products of the oxide cathode at high temperature in high vacuum appear to corroborate the opinion that a more stable condition exists if the sites are filled with some convenient ionic species than if they are empty or if filled with electrons only. This is associated somewhat with the fact that at 1000°K, the partial molar free energy of formation of an ideal solution in which the mole fraction is 10^{-6} is equal to $\Delta\bar{F}_i = RT \ln a_i = 4575 \log 10^{-6} \simeq -27{,}000$ calories. Such considerations suggest that crystals exposed to a reducing environment contain metal atoms in the cation vacancies created because of charge compensation requirements of the variable charge cationic impurity systems incorporated.

The general phenomenon of an ion functioning with two or more apparent states of oxidation in the same compound will, for this discussion be referred to as "variable-charge" performance. It connotes the situation in which an ion[40] in the crystal may appear formally to have one, or perhaps several, electrons more or less during part of the time than do similar elements in other equivalent sites in the crystal.

The conductivity of CaO has been shown[41] to be variable from n-type to p-type by such adjustment of substituent content and control of the external atmosphere. Hauffe and Tränckler have suggested[41] the addition of La^{+++} to oxide cathodes to counteract the effect on conductivity of the unavoidable presence of alkali metal ions and to increase the cation vacancy concentration.

The contribution of Selwood's "valence inductivity" concept[36] to the donor incorporation problem is that it presents specific evidence of the importance of the solvent crystal as an environmental factor in

establishing bona fide states of valence[42] or oxidation. Selwood found that γAl_2O_3 impregnated with $Mn(NO_3)_2$ and heated in air yielded over-growths of Mn_2O_3 whereas TiO_2 impregnated with $Mn(NO_3)_2$ and similarly heated yielded MnO_2. If $Mn(NO_3)_2$ is heated alone under the same conditions, MnO_2 is formed. This influence of substrate seems to be generally effective in determining the bona fide state of oxidation and co-ordination of transition elements, and presumably of other elements which can show two or more states of oxidation. These experiments give rise to the expectation that varying degrees of solvent influence on solute valence or ionic charge may be found and that added solute impurities may be "induced" to assume abnormal valence states in which they may function as donors or acceptors according to design.

Do variable-charge elements occur as electron donors in the oxide cathode? This possibility certainly exists because of the traditional presence in cathode support metals of transition elements and others likely to be capable of acting as variable charge electron donors.

One possible reason for not believing that the variable-charge elements constitute the most important electron donors in the oxide cathode is the fact that the ubiquitous nature of the likely metal impurities in tube components makes it improbable that any one of them can be *the* source of such donors and can have escaped accidental discovery as such in the long experimental history of the oxide cathode. Cathode quality, on the whole, seems rather independent of the detailed impurity contents of base metals. One should remember, however, that such contents of elements conceivably capable of showing variable-charge donor performance have ranged from 10^{-5} mole fraction upward. From the results presented by the BTL group, it is very doubtful that any oxide cathode has ever been studied which was not contaminated by a mole fraction of at least 10^{-6} of such elements as iron, manganese, chromium, titanium, or others which might function as variable-charge donors. Because the donor concentration needs to be only of the order of 10^{-6} mole fraction, it is apparent that we do not know how cathodes will perform when the effects of such impurities are certainly negligible.

A second possible reason for excluding the variable-charge elements from consideration as the most important electron donors in the oxide cathode is that the expected mobility of cationic donors in a full crystal would not allow sufficient donor migration to produce polarization effects found in cathodes through studies of their electronic properties. Here again, however, loopholes exist. We know so little about metal solubilities in salts that we cannot be certain that cation

vacancy formation does not accompany cation donor incorporation. Cation vacancies may be necessary in the oxide crystal for charge balance if not enough metal atoms dissolve to fill the vacant cation sites (e.g., one Ba^{++} must be absent for every pair of empty donor impurity ions of the type M^{+++}). Such an adverse atom solubility does not seem likely to this writer's chemical intuition; however, experimental verification of some pertinent metal solubilities in BaO and SrO is needed. Another loophole also exists in the mobility argument; coating polarization can be produced in a system of immobile donors and mobile electron acceptors. At least one species of mobile acceptors is conceivable which might diffuse moderately easily through an exchange reaction. This is the super-oxide ion which would exchange with $O^=$ and which would capture an electron to become the peroxide ion as described by the reactions

$$O^-_2\ (s) + O^=\ (s) = O^=\ (s) + O^-_2\ (s)$$

$$O^-_2\ (s) + e\ (ss) = O^{=}_2\ (s).$$

On the whole, we prefer to suppose that variable-charge elements are important in the cathode but that they do not constitute the mobile donors responsible for pulse-emission decay and for related characteristics. We suppose that they do constitute donors whose ionization energies are substantially larger than that of the principal mobile donor. Such donors can be especially important in interface compounds found near the base metal and, in addition, may constitute a reservoir of chemically less reactive donors which is not so easily destroyed by residual gases as is the principal donor. These immobile donors may even contribute a substantial share of the d-c nonpolarizable part of the conductivity of the coating.

It is apparent that the problem of synthesis of electron-emitting materials by the incorporation of variable-charge cationic electron donors in a host crystal of low electron affinity is twofold:

(a) To find an impurity system which places the levels usefully near the conduction band,

(b) To maintain a durable favorable balance of M, M^{++}, and M^{+++} concentrations without degrading the electron affinity of the host crystal through accumulation of excess impurity content. A mole fraction of 0.01 of any impurity seems likely to affect the electron affinity noticeably.

D. Variable-Charge Anionic Electron Donors

The variable-charge donor concept is presumed to be equally applicable to cations and anions, though in practice its operation with

anions seems somewhat more limited. Verwey and Kröger[33] have shown the occurrence of effects exactly equivalent to variable charge in anions though they explain the effects as due to induced variable charge in the cations. For instance, they say that incorporation of Cl^- in ZnS induces an appropriate number of Zn^{++} ions to act as Zn^+ ions which thereby preserve charge balance. The evidence for this is that the fluorescence is said to be the same[43] with Cl^- in ZnS as with Ga^{+++} substituted for Zn^{++} in which latter case Zn^{++} ions are assumed to be forced into the Zn^+ form.

The interpretation we prefer to use at this time is that alternative explanations compatible with the concept of variable charge "anions" are allowed in the ZnS case because of the possibilities for incorporation of HS and halide impurities, and "interstitial" sulfur via polysulfide linkages, in ways commonly characteristic of covalent sulfur behavior.

We feel free therefore to assume that, in typical more ionic systems such as BaO, substitution of Cl^- for $O^=$ in a reducing atmosphere would form $(Cl^- \cdot e)$ groups which proceed to function as variable charge anionic electron donors.

The F-center with an electron in anion vacancy clearly constitutes the terminal member of the general class of variable charge anionic electron donors. If the host anions are singly charged, only one electron need be present in the anion vacancy for charge balance; however, association of a second electron with the vacancy has been postulated to occur and in the case of the alkali halides is called an F′ center.[44] For divalent anions, the charge analog of the F-center contains two electrons for site electro-neutrality.

These two electrons are bound to a doubly charged "positive" site in the crystal; hence thermal excitation of one electron to the conduction band might require roughly an energy

$$E_f \simeq \frac{I_{He}}{\epsilon^2} \simeq 2 \text{ ev.},$$

I_{He} being the ionization energy of helium and $\epsilon \simeq 3.5$, the dielectric constant of BaO.

In contrast, any singly charged anion with associated charge-balancing electron in BaO would require a thermal excitation energy

$$E_d \simeq \frac{I_H}{\epsilon^2} \simeq 1.1 \text{ ev.},$$

I_H being the ionization energy of a hydrogen atom. In principle, this is the better donor center.

As shown in Reference (29), thermodynamics does not indicate that substitution of any anions other than halide, sulfide, or oxygen-containing addition-type anions in the AEO coatings can be stable against displacement by $O^=$ through reaction with the residual gases of practical vacuum systems. This argument eliminates from consideration as donor centers such exotic species as $N^{\equiv}$ and $P^{\equiv}$ which might conceivably act as variable-charge anions when dissolved in the oxides and contribute electrons for conduction purposes. Similarly, deleterious or beneficial concentrations of species such as $C^{=}_{2}$ and $CN^- \cdot e$ are ruled out. Ionic radii prohibit the use of $P^{\equiv}_{4}$, $SO^{=}_{4} \cdot e$ and the like which might perhaps be postulated to operate as variable charge anions.

It is apparent that any $(X^- \cdot e)$ anionic group which is stable in the oxide coating might be feasible as a variable charge electron donor species. However, the expectation for most of these is that, since no vacancies need be present in the host crystal, diffusion and electrolysis of these centers would be rather small; hence most of these, though they may constitute donor centers if incorporated, cannot be construed as being the donor centers actually important in the conventional oxide cathode.

One outstanding exception in this class of donor species is the one proposed earlier, the $(OH^- \cdot e)$ group for which an easy diffusion mechanism exists.

E. Properties of the $OH^- \cdot e$ Donor Center

By the process of elimination, the field of likely donor center candidates has been narrowed to

(a) A relatively immobile variety, the variable-charge cationic transition element impurities, and

(b) A mobile donor, the $OH^- \cdot e$ species.

Probably the transition element impurities do provide donors which are somewhat functional. There is little or no tangible evidence of their effects. Their apparent lack of mobility necessitates the simultaneous presence of mobile donors to account for the factor of ten or one hundred discrepancy between initial electron pulse-current values and the d-c emission value.

The only tangible experimental evidence we have for the existence of the $(OH^- \cdot e)$ group is derived from the mass spectrometric study[45] of field-dependent gas evolution from a BaO cathode. This consisted of the observation of

(a) Field-dependent H_2 evolution,

(b) A complex field dependence of the H_2O residual pressure,

(c) A complex but direct and immediate response of the electron current from the cathode to small changes in H_2O partial pressure ($\pm 5 \times 10^{-9}$ mm.).

To account for all these phenomena, particularly (b), we are rather driven to postulate that H_2O is consumed by the cathode and that fragments of H_2O are simultaneously ejected from the cathode. We are thus stimulated to consider both the likely chemical properties and the physical properties of the coating which are associated with these reactions.

Most importantly, the $OH^- \cdot e$ center is presumed to participate in rather conventional oxidation–reduction reactions. It is presumed to be formed by any or all of the following illustrative reactions:

$$BaO(s) + \tfrac{1}{2}H_2(g) = Ba^{++}(s) + (OH^- \cdot e) \tag{15}$$

$$BaO(s) + \tfrac{1}{2}H_2O(g) = Ba^{++}(s) + (OH^- \cdot e) + \frac{1}{4}O_2(g) \tag{16}$$

$$2OH^- \text{ (solid solution in BaO)} + \tfrac{1}{2}CO(g) = (OH^- \cdot e) + \tfrac{1}{2}CO_2(g) + \tfrac{1}{2}H_2O(g) \tag{17}$$

$$2OH^- \text{ (solid solution in BaO)} + \tfrac{1}{2}H_2(g) = (OH^- \cdot e) + H_2O(g) \tag{18}$$

$$Ba \text{ (solid solution in BaO)} + H_2O(g) = Ba^{++}(s) + (OH^- \cdot e) + \tfrac{1}{2}H_2. \tag{19}$$

The products of Reaction (19) are the same as might be presumed to form from a *partial* reaction between H_2O and excess barium or between H_2O and an F-center, to wit,

$$2e \text{ (F-center in BaO)} + H_2O(g) = (OH^- \cdot e) + \tfrac{1}{2}H_2(g). \tag{20}$$

Two presumed characteristic reactions of this center are the following:

$$(OH^- \cdot e) \overset{\pm kT}{=\!=\!=} OH^-(s) + e \text{ (in conduction band)} \tag{21}$$

$$O^=(s) + (OH^- \cdot e) = (OH^- \cdot e) + O^=(s), \tag{22}$$

Reaction (22) describes the diffusion mechanism of the donor center which is presumed to occur via proton transfer.

From the above reactions, it is apparent that the presence of water vapor might be beneficial or deleterious, depending upon the amount and upon the presence of certain other species. Too much H_2O would obviously create too many OH^- sites and exceed the number of cation sites. At some point, the crystal structure of BaO would be converted into that of $Ba(OH)_2$.

It is apparent that this method of incorporation of hydroxide ions achieves the equivalent of variable charge in the anion sites of BaO without simultaneously creating lattice (cation) vacancies. The reactions written for the $(OH^- \cdot e)$ centers emphasize the complexity of the behavior to be expected of them because of reactions with components of the water-gas equilibrium. They emphasize also the point that an analysis of cathode behavior in terms of very small partial pressures of any one of these species is likely to be futile. The individual and total reducing potentials of the atmosphere are important. At some point on the scale of donor center concentration, any particular atmosphere maintained by the environment of the cathode might be neutral in its effect on the cathode; for a higher initial center concentration, that atmosphere would produce deactivation; for a lower concentration it would produce activation.

Plausible reactions can be written for the $(OH^- \cdot e)$ centers which are overtly similar to those of free barium or F-centers in BaO (cf. Reaction (20) above with the reverse of Reaction (18)).

The diffusion and mobility of $(OH^- \cdot e)$ centers are expected to be high because the proton may jump to any of six adjacent $O^=$ sites in the crystal and because the activation energy for proton transfer for such jumps is likely to be low. For proton transfer in H_2O, from H_3O^+ molecule to H_2O molecule, the activation energy is less than 0.25 electron volt.[46] A somewhat analogous process may thus be well suited to explain the high rate of diffusion estimated for the (ionized) donor migration in cathodes from pulse-emission decay measurements[31] (activation energy for diffusion, 0.43 electron volt; diffusion constant at 1000°K., $D = 5.9 \times 10^{-6}$ cm^2 sec^{-1}).

Reactions (23), (24), (25), and (26) present some thermochemical relationships concerning the feasibility of the hydroxylated donor center:

$$BaO(s) + H_2O(g) = Ba(OH)_2(s)\ ;\ \Delta F^\circ_{1000^\circ K} = -6{,}000 \text{ calories.} \quad (23)$$

$$\text{For } a_{OH^-} \geqq 10^{-6},\ p_{H_2O} \geqq 5 \times 10^{-14} \text{ atm.}$$

$$Ba(s) + Ba(OH)_2(s) = 2BaO(s) + H_2(g);$$
$$\Delta F^\circ_{1000^\circ K} \simeq -50{,}700 \text{ calories.} \quad (24)$$

For $a_{Ba} = 10^{-12}$ and $a_{OH^-} \geq 10^{-6}$, $p_{H_2} \geq 10^{-13}$ atm.

$$Ba(s) + Ba(OH)_2(s) = 2Ba^{++}(s) + 2(OH^- \cdot e)\ (s);$$
$$\Delta F^\circ_{1000^\circ K} = W \text{ calories.} \quad (25)$$

One can estimate W by assuming a reasonable value for a_{Ba} and necessary values for a_{OH^-} and $a_{OH^- \cdot e}$:

for $a_{Ba} = 10^{-12}$ and $a_{OH^-} = a_{OH^- \cdot e} = 10^{-6}$, $W = -55{,}000$ calories.

$$2BaO(s) + H_2(g) = 2Ba^{++}(s) + 2(OH^- \cdot e)\ (s);$$
$$\Delta F^\circ_{1000^\circ K} = 50{,}700 + W = -4{,}300 \text{ calories.} \quad (26)$$

For $a_{OH^- \cdot e} \geq 10^{-6}$, $p_{H_2} \geq 10^{-13}$ atm.

Reaction (25) is seen to be the (reverse) analog of the general Reaction (6) for which the affinity of donor centers for Ba^{++} was computed. It is recalled that

$$-\Delta F^\circ_6 = -(\Delta E^\circ_4 + \Delta E^\circ_5) \simeq -2.1 \text{ ev} \doteq -48{,}000 \text{ calories.}$$

We are requiring that Reaction (25) form donor centers with practically the same degree of ease as the same reactants produce H_2 in Reaction (24). This amounts to the requirement that the ΔF° for the reaction between BaO and H_2 to form filled donors be roughly zero as found for Reaction (26).

Actually the value of W strictly valid for Reactions (25) and (26) as written cannot be determined in the above fashion without using equilibrium data (which we do not have) for a "pure" system comprised of BaO with only the solutes $OH^- \cdot e$, OH^-, and Ba. Presumably all real cathodes contain relatively large concentrations of numerous solute metals in the range of 10^{-6} to 10^{-4} mole fraction. Charge balance requires that the concentration of OH^- (or D_e) be equal to twice the total concentrations of cation vacancies and metal atoms. The apparent value of W derived in the above fashion (and also the ΔF°_6 value) apply more to the poorly defined real cathode systems than to the "pure" systems described by Reactions (6), (25), and (26). This W is obviously dependent on the assumed OH^- concentration (D_e concentration) which in turn is probably dependent on the total solute metal concentration. In connection with this situation,

one may note also that the ideal solution assumption covers any effect of departure from conservation of site numbers in chemical reactions; however, as mentioned earlier, it is doubtful that significant departures from site balance will be incurred by cathodes in practical environments.

Of concrete practical importance are the results for Reactions (23) and (24) that a 10^{-6} mole fraction of hydroxide ion impurity in BaO is guaranteed in practical vacuum systems in which (a) the partial pressure of H_2O exceeds 10^{-14} atmosphere or (b) a mole fraction of 10^{-12} of Ba in BaO is present along with a partial pressure of H_2 in the vacuum system exceeding 10^{-13} atmosphere. If the value of W derived above is allowed, these same conditions will also provide an equal concentration (10^{-6} mole fraction) of filled ($OH^- \cdot e$) donors.

Chemical intuition leads one to expect that the thermal stability of hydroxide ions dispersed in dilute solution in an oxide would be somewhat greater than that extrapolated from the dissociation pressure of pure $Ba(OH)_2$. One might expect that hydrogen bridge bonding (resonance energies) would make the activity coefficient of OH^- in BaO much smaller than unity. The above thermochemical estimates show specifically only that a reasonably small activity of H_2, a gas which is known to be one of the poorer agents for activating cathodes, will maintain the OH^- and Ba activities at levels compatible with partial pressures of H_2O and Ba observed in vacuum tubes.[47]

There are other similar models which can be conceived for donor centers (e.g., $HCO_2^- \cdot e$, $HCO_3^- \cdot e$, $Cl^- \cdot e$, $H^- \cdot e$, and so forth); however, none of these seems as plausible as the ($OH^- \cdot e$) center.

Conclusions

The *general* aspects of this new viewpoint regarding the donor centers in all electron emitters may be summarized as follows:

1. The chemical property which is characteristic of an active cathode and which distinguishes an active cathode from an inactive cathode is inherently associated with the presence of readily available electrons. The absolute activity, $a_e(s)$, of these electrons is determined by the total work function, φ, as

$$a_e(s) = e^{-\frac{\varphi}{kT}}.$$

2. The chemistry of donor and acceptor species in the oxide cathode (and in ionic compounds generally) is amenable to systematic procedures based on

(a) The principle that an elevation of the Fermi level is synonymous with an increase in the electronic chemical potential and with an increase in the reducing chemical potential of the material,

(b) The assumption that the chemistry of donor and acceptor species is roughly the same as that of ordinary ionic species dispersed in an "inert" solvent.

The *specific* aspects of this new viewpoint regarding the donor centers in the conventional oxide cathode are the following:

1. The usual model of the oxide cathode which postulates that the electron donors are F-centers formed from dissolved "excess barium" and oxygen vacancies is untenable because experimental evidence shows that not enough barium can remain dissolved in cathodes under operating conditions to form the number of F-centers required to account for the electrical properties of oxide cathodes.

2. The large content of reducing agent (e.g., $\geqq 10^{-4}$ mole fraction) measured for typical oxide cathode coatings is naturally and properly assignable to electropositive elements from the base metal such as magnesium, aluminum, iron, manganese, chromium, and so forth, rather than to dissolved "excess barium" or to the electrically important electron donor centers. A mole fraction of reducing element content of 10^{-6} to 10^{-4}, a donor center mole fraction of 10^{-6}, and an apparent Ba mole fraction of 10^{-10} to 10^{-12} are thermochemically reasonable and compatible values.

3. A number of conceptually feasible donor species may be effective in alkaline earth oxide cathodes which do not require the presence of a substantial ($> 10^{-12}$ mole fraction) concentration of dissolved Ba which shows the equivalent vapor pressure behavior of a dilute ideal solution of Ba atoms. Variable-charge transition element impurities constitute one class of donor centers which are probably responsible for part of the electronic behavior of the oxide cathode. Certain variable-charge anionic electron donors are also allowable thermochemically. A member of this class, the $OH^- \cdot e$ center, is proposed as the donor species most likely and able to account for many of the chemical and physical properties of the oxide cathode and for most of its electron emission behavior in practical vacuum systems.

Appendix

A. Vapor Pressure of Ba from Solid Solutions of Ba in BaO—The Cornell Work

Data relating the vapor pressure of Ba dissolved in BaO to the mole fraction of dissolved Ba are derivable from the papers by Schriel,[48]

Sproull, Bever, and Libowitz,[5] and Libowitz.[6] The two latter papers describe measurements made on single crystals of BaO and indicate values around 10^4 for the activity coefficient of Ba dissolved in BaO and a solubility limit of the order of 10^{-4} mole fraction at 1323°K. These results indicate the presence of strong repulsive forces and strong positive deviation from ideal solution behavior. The solution of Ba in BaO produced blue color centers, the concentration of which was found to be essentially equivalent to the total excess Ba content incorporated. More refined experiments on BaO single crystals by Timmer[7] produced measurements leading to the following relationship[49] between the blue-center mole fraction, X_{Ba}, and the Ba equilibrium vapor pressure (expressed in millimeters of mercury), p_{Ba}, for Ba dissolved in BaO:

$$X_{Ba} = 1.4 \times 10^{-4} p_{Ba}^{1/3}.$$

For the limited temperature interval covered by Timmer's experiments, 1423°K to 1473°K, X_{Ba} was independent of BaO temperature within the limits of error of the data when the Ba vapor density was kept constant.

The values derived from Timmer's experiments for the mole fraction X_{Ba}, partial pressure p_{Ba}, and activity coefficient γ_{Ba} are, respectively,

$$X_{Ba} \simeq 5.3 \times 10^{-5} \text{ to } 3.4 \times 10^{-6},$$

$$p_{Ba} \simeq 7.6 \times 10^{-2} \text{ to } 3.4 \times 10^{-5} \text{ mm. Hg.},$$

$$\gamma_{Ba} \simeq 186 \text{ to } 2.1.$$

Thus at a mole fraction of 3.4×10^{-6}, the blue color-center species exerted a higher equilibrium vapor pressure of Ba than should be expected of an ideal solution of barium atoms at the same concentration. The decrease in activity coefficient values with blue color-center concentration from very large values to values near unity at 10^{-6} mole fraction indicate an approach to ideal solution behavior for the Ba dissolved, in whatever form. The larger-than-unity values of the activity coefficients of the blue centers indicate that they were formed endothermically. They bleached in vacuum; hence they were not tightly bound to the BaO. Whether these metastable blue centers were comprised of Ba atoms, BaV_a, $Ba^+V_a^-$, or $Ba^{++}V_a^{=}$ pairs, in which V_a, V_a^-, and $V_a^{=}$ signify anion vacancy sites containing zero, one, and two electrons, respectively, cannot be definitely determined. Other possibilities such as $(Ba^+)_2 V_a$ groups are also allowed.

From Timmer's work, it is clear that the blue solutions of Ba dissolved in whatever form in BaO are created by overcoming considerable repulsive forces and that these solutions approach ideal behavior at solute Ba mole fractions around 10^{-6}. There is no a priori reason for believing that attractive forces develop in the system at lower solute mole fractions, i.e., that γ_{Ba} drops appreciably below unity.

With this evidence that Ba dissolved in BaO behaves nearly as an ideal solute at mole fractions of the order of 10^{-6}, one may proceed with some confidence to estimate the vapor pressure of the dissolved Ba which is usually presumed to contribute the electron donor centers in an active cathode. Taking values for the density of BaO molecular sites N_{BaO} and taking the concentration of dissolved Ba as equal to the concentration of donor centers N_D calculated[9] necessary to account for the electrical properties of BaO one finds from

$$N_{BaO} \simeq 2.2 \times 10^{22}\ \text{cm}^{-3}, \text{ and}$$
$$N_D \simeq 10^{17}\ \text{cm}^{-3}, \text{ that}$$
$$X_{Ba} \simeq 0.4 \times 10^{-5}.$$

Taking $\gamma_{Ba} \simeq 1$, and substituting this value and

$p^\circ_{Ba} \simeq 10^{-2}$ mm. at 1000°K (from Rudberg and Lempert data[49]), or

$p^\circ_{Ba} \simeq 10^{-1}$ mm. at 1000°K (from Hartmann and Schneider data[49])

into the equation given in Footnote (22) relating activity, activity coefficient, and solute mole fraction, one gets

$p_{Ba} \simeq 0.4 \times 10^{-7}$ mm. (from Rudberg and Lempert data), or

$p_{Ba} \simeq 0.4 \times 10^{-6}$ mm. (from Hartmann and Schneider data)

as the equilibrium vapor pressure of Ba expected from an active BaO cathode. Besides the doubt about the vapor pressure of pure Ba, there may be some question about the temperature dependence of γ_{Ba}.

Common behavior of solid solutions indicates that γ varies greatly with composition and little with temperature.[50] Timmer's measurements support the conclusion that this rule is applicable to the Ba–BaO system.

It is worth noting that the F-centers in the alkali halides appear to provide little or no bonding between the excess alkali metal and the salt. The activation energies for formation of the centers from alkali metal vapor are small negative numbers,[51] e.g., -0.25 electron volt in KBr and -0.10 electron volt in KCl. The density of F-centers is

proportional to alkali atom vapor density and the proportionality constant is near unity; hence the solutions are practically ideal. Furthermore, recent microwave measurements on F-centers in KCl are interpreted[44] as indicating that the F-center electron is attached in turn as a 4s (valence) electron to each of the six K^+ ions surrounding the anion vacancy. This model is viewed as consistent with the fact that the F-center absorption energies are of the same general magnitude as the s–p energies observed for optical transitions from the ground states of alkali atoms in free space. This incomplete ionization of potassium adjacent to the center is of course compatible with the ideal solution behavior of the excess potassium.

Thus, by analogy, it is likely that the blue color centers in BaO are very similar species, that they are formally representable as BaV_a pairs, or perhaps $(Ba^+)_2V_a$ complexes, and that they should also behave (at moderate temperatures) as if they were roughly ideal solutions of Ba atoms at low concentrations.

B. "Excess Barium" in Oxide Cathodes—The BTL Work

A series of excellent detailed measurements by the BTL group is primarily responsible for clarification of the fundamental relationship of barium to cathode activity. Only two sets of their experiments will be discussed here.

The Vapor Pressure of Ba from Oxide Cathodes

The measurements of Wooten, Ruehle, and Moore[8] indicate that, from many active cathodes made of standard materials, little vaporization of Ba occurs ($p_{Ba} \leq 3 \times 10^{-11}$ mm) after the first 2,000 hours. From coatings on a passive nickel base (about 0.03 per cent "reducing agent" content), the evaporation of Ba was indetectable ($p_{Ba} \leq 10^{-12}$ mm) after the initial activation. From another series of coatings on "Grade A" nickel alloys (containing about 0.35 per cent of "reducing" agents), the evaporation of Ba proceeded at a constant rate (equivalent to a Ba vapor pressure of 3×10^{-11} mm) after the first 2,000 hours to the end of the tests at 20,000 hours. They concluded that drawing emission at densities as high as 20 ma/cm^2 had no effect on the Ba vaporization rate. They found "no correlation between the rate of Ba evaporation and thermionic emission."

As noted earlier and described in detail below, these measured vapor pressures are probably somewhat exaggerated values because of the continuous arrival at the oxide coating of magnesium evaporated from the anode. This magnesium presumably continuously reduced the oxide and generated barium. For an anode temperature of 520°K attained in these tests when no space current was drawn, a 10^{-4} mole fraction

of magnesium in the anode could supply a partial pressure of magnesium as high as 10^{-10} mm. (The anode composition in these tests is not stated but in the "excess Ba" content tests described later, the anode material was consistently their No. 1 nickel or roughly the equivalent and contained about 2×10^{-3} mole fraction of magnesium —how much of this was present as oxide is not known, however.

These barium vapor pressures from typical cathodes in typical tube structures are therefore very probably substantially higher than the fundamental "donor destruction pressure" characteristic of a certain concentration of the electronically important electron donors. These measurements establish the maximum possible value of this donor-destroying barium vapor pressure as being about 10^{-12} mm for certain typical cathodes having an average state of emission activity, a rather important result. Their second result, that there is no correlation between the barium evaporation rate and thermionic emission, is thus quite consistent with this magnesium transfer interpretation and also understandable in terms of the general thermochemical approach developed in the first section.

In addition, it is of considerable significance that the BTL group demonstrated the existence on or in BaO of two kinds of "excess barium"—one of which (added by an external evaporator) re-evaporated readily as normal barium should, and one of which showed an abnormally low vapor pressure. Moore, Wooten, and Morrison[11] state, ". . . Deposited Ba in excess of .05 layer decreased emission and re-evaporated above 600°K within 5 minutes; production of Ba by exposure to methane usually decreased emission but such Ba was stable even above 1100°K. Median Ba content for demounted filaments prepared commercially was 0.90×10^{17} atoms[52] per cc., equivalent to only .005 monolayer on the true oxide surface but sufficient for emission according to the semiconductor model for oxide cathodes."

The "Excess Barium" Concentration in Oxide Cathodes

The final reports[10,12] on this work by the BTL group indicate the following:

(1) No correlation was found between "excess Ba (or Sr)" content and cathode activity for apparent mole fractions of such excess metal larger than 10^{-6}.

(2) The lower limit of the sensitivity of the analytical method was about 10^{-6} mole fraction of excess metal; hence their measurements do not exclude the possibility that a correlation exists between excess metal mole fractions and emission behavior at lower concentrations.

(3) Apparent mole fractions of "excess barium" as high as 2×10^{-4} were found, with the median value being 6×10^{-5} for indirectly heated cathodes and 2×10^{-5} for filamentary cathodes.

(4) No correlation was found between "excess Ba" content and cathode activity from 0.5 hour to 56,000 hours.

(5) The mean values in "excess Ba" contents differed less than a factor of two for three classes of filamentary cathodes using (a) the No. 1 nickel alloy having about 0.35 per cent weight "reducing agent" content (b) the purer nickel having less than 0.03 per cent weight "reducing agent," and (c) the extraordinarily pure platinum having < 0.03 per cent weight of copper impurity and no other detectable impurities (presumably less than 0.001 per cent of any other element). The mean value of "excess barium" in cathodes on the very pure platinum was actually the highest of these three groups of cathodes.

As stated earlier, our assumption that practically all these "excess barium" contents were actually measures of the total contents of other reducing elements such as magnesium, manganese, iron, and so forth, can readily account quantitatively for the BTL results for all cathodes *except* those on the very pure platinum. For instance, taking the alloys containing 10^{-4} mole fraction of iron, assuming ideal solution behavior and a cathode temperature of 1000°K, a partial pressure of iron equal to 10^{-14} mm is computed. For a base metal sleeve .005 inch thick, the 10^{-4} mole fraction of iron continuously evaporating at this level would last well over 10^6 hours and would provide an activity of iron in the oxide of 10^{-4} for about the same period of time. Thus there is no difficulty in accounting for a 10^{-4} mole fraction of reducing agent being present at any time in the cathode coatings on such alloys.

The problem ultimately in applying this model to the BTL tests for which the ultra-pure platinum was used as base-metal is that of finding some source of such a low vapor pressure element as iron which could contaminate the coating and serve as the reservoir of reducing agent. This we have not found; however, there is conclusive evidence of significant transfer contamination from other electrodes. This obvious transfer is probably not enough to account quantitatively for the reducing element content of cathodes on the purest platinum base metal, but it comes moderately close. The fact that such transfer clearly existed leaves room for expectation that the reducing element contents of all the BTL cathodes were due almost entirely to the presence of elements other than barium.

The BTL comments on their barium vaporization experiments are approximately the following:

(1) More barium evaporated from some of the cathodes than could have been produced from the reducing element content of the cathode base metal.

(2) The rate of barium vaporization was less in tubes with oxidized nickel anodes than with bright nickel anodes until space current was drawn to the oxidized anodes.

(3) Magnesium was found by spectrographic analysis in the outer layers of the aged cathode coatings.

In both studies, the anodes were out-gassed for six minutes at 1125°K. During the final three minutes of this period, the cathodes were broken down by heating to 1300°K.

The composition of their No. 1 nickel alloys used as anodes is listed in weight per cents as magnesium 0.09, silicon 0.02, carbon 0.03, iron 0.24, manganese 0.25, copper 0.14, cobalt 0.05, aluminum 0.001, chromium 0.01, silver 0.001, nickel 99.17.

If one considers the transfer problem as a short term one, he finds that transfer of iron borders on being significant during the six-minute interval of anode outgassing at 1125°K, the last three minutes of which the cathode was heated to 1300°K. The net accumulation of iron in the cathode coating during the breakdown period could amount to about 10^{-6} mole fraction.

Similarly, a very much larger net transfer of magnesium and manganese could have occurred in the same interval. In addition, even assuming an anode temperature of only 350°K during cathode aging and ideal solution behavior of 10^{-4} mole fraction of magnesium in the anode, an equilibrium vapor pressure of magnesium of 10^{-17} mm over the cathode probably existed continuously throughout the aging period. At thermal equilibrium this would correspond to a magnesium activity, a_{Mg}, in the coating of about 10^{-17}. As shown earlier, free-energy data indicate that a small activity of magnesium maintained in a BaO coating containing a small MgO concentration (10^{-6} mole fraction) would generate a 10^{10} times larger Ba activity (and would also convert any moderate content of Fe++, Mn++, and so forth, already present largely to the reduced atomic state). Our own experience is that one seldom obtains alkaline earth carbonates having less than 10^{-4} or 10^{-5} mole fraction of iron salts.

From this interpretation of the significance of the BTL measurements we suspect it is practically impossible to study a "typical" cathode in an inert environment, and that it is also impossible to determine chemically the concentration of the electrically important donor centers.

Though the results of the BTL experiments may not be what the

authors expected they would be when the experiments were begun, they are certainly not less valuable. They provided a large fraction of the experimental foundation for the interpretation presented here of oxide cathode chemistry.

Acknowledgments

The author is happy to acknowledge the many valuable suggestions and constructive criticisms made by R. M. Matheson and L. S. Nergaard. Without their tutelage on the physical theory and practical aspects of cathode behavior, this chemical model could not have evolved. The author is also pleased to acknowledge the helpful conversations with H. B. DeVore, D. O. North, and R. H. Parmenter.

Without the co-operation of Professor R. L. Sproull, Department of Physics, Cornell University, who informed the author about Timmer's work prior to its publication, this paper would not yet be written. His assistance and the kind permission of Mr. Timmer to quote from that work are very much appreciated.

References

1. R. H. Fowler and E. A. Guggenheim, *Statistical Thermodynamics*, Chapter XI, Cambridge University Press, Cambridge, England, 1950.

2. The work function as used here is the minimum energy required to take an electron at the Fermi level in the solid to a point in field-free space.

3. This activity as defined here is the same as the fugacity defined by Lewis and Randall for a perfect gas as equal to the pressure. Since the thermochemical Standard Reference State for gases is one atmosphere, the conventional thermochemical activity of the electron gas is equal to its fugacity, that is,

$$a_e(\text{thermo.}) = \frac{f_e}{f^\circ_e} = \frac{f_e}{1} = f_e.$$

The thermochemical activity is thus dimensionless; however, for an ideal gas at temperatures above its boiling point, the activity is numerically equal to its partial pressure expressed in atmospheres.

4. Because our atmosphere is a strongly oxidizing atmosphere, materials having a low work function cannot be exposed to air without damage. Similarly, it is thermodynamically impossible to maintain a low work function material in a poor vacuum containing high activities of oxidizing gases such as H_2O, O_2, CO_2, Cl_2, etc.

5. R. L. Sproull, R. S. Bever, and G. Libowitz, "Oxygen Vacancies in Barium Oxide," *Phys. Rev.*, Vol. 92, pp. 77-80, October 1, 1953.

6. G. Libowitz, "The Growth and Analysis of Barium Oxide Crystals Containing a Stoichiometric Excess of Barium," *Jour. Amer. Chem. Soc.*, Vol. 75, pp. 1501-1502, March 20, 1953.

7. Cornelis Timmer, Thesis, "The Density of the Color Centers in Barium Oxide as a Function of the Vapor Pressure of Barium," Cornell University, Ithaca, N. Y., February, 1955; *Jour. Appl. Phys.*, in press.

8. L. A. Wooten, A. E. Ruehle, and George E. Moore, "Evaporation of Barium and Strontium from Oxide-Coated Cathodes," *Jour. Appl. Phys.*, Vol. 26, pp. 44-51, January, 1955.

9. L. S. Nergaard, "Studies of the Oxide Cathode," *RCA Review*, Vol. XIII, pp. 464-545, December, 1952.

10. L. A. Wooten, George E. Moore, and W. G. Guldner, "Measurement of Excess Ba in Practical Oxide-Coated Cathodes," *Jour. Appl. Phys.*, Vol. 26, pp. 937-942, August, 1955.

11. George E. Moore, L. A. Wooten, and James Morrison, "Excess Ba Content of Emitting Oxide-Coated Cathodes," *Bulletin of the American Physical Society*, Vol. 29, No. 5, p. 29, June 28, 1954.

12. George E. Moore, L. A. Wooten, and J. Morrison, "Excess Ba Content of Practical Oxide-Coated Cathodes and Thermionic Emission," *Jour. Appl. Phys.*, Vol. 26, pp. 943-948, August, 1955.

13. This abbreviation for "Bell Telephone Laboratories" refers, in this paper, to results described by BTL scientists in journal references (8), (10), (11), and (12).

14. "Cornell" refers to the blue color-center experiments described in References (5), (6), and (7) by Professor Sproull and his students.

15. For use in this paper an impurity center, or center, is defined as a rather ordinary but usually unidentified chemical entity such as an anion or cation which, in its reduced condition, contains an electron that is optically or thermally excitable into the conduction band. Such an excitation leaves the impurity center in an oxidized condition. In its reduced condition, the impurity center is an electron donor center or donor; in its oxidized condition, the impurity center is an acceptor awaiting refilling to become a donor again. If the donor impurity is present in substantial concentration and can lose its electron easily

by thermal excitation, it contributes importantly to the electrical conduction process. Conversely, impurities may be present which have the reduced chemical form of electron donors but which are not easily enough ionized to contribute appreciably to the electrical conduction process at attainable temperatures; nevertheless, they may be important thermodynamically in determining the degree of fullness of other centers which do contribute to the conduction process. The degree of fullness of the centers contributing directly to the conduction process is thus variable (1) with temperature because of thermal excitation, (2) with temperature because of shift in the total chemical potential of the reducing agent content, and (3) with concentration of reducing agent.

16. Since $\Delta F^0 = \Delta H^0 - T\Delta S^0$ and since these processes, Reactions (4) and (5), occur in a solid, then $\Delta H^0 \approx \Delta E^0$, and $\Delta F^0 \approx \Delta E^0 - T\Delta S^0$. Because the main entropy change occurs in Reactions (4) and (5) from distributing and withdrawing the electrons in the available conduction band states, ΔS^0_4 and ΔS^0_5 are essentially equal and opposite in sign so that they cancel in the summation which gives ΔF^0_6 and in other reactions in which the sum $(\Delta E^0_4 + \Delta E^0_5)$ appears.

17. The partial molal free energy change, $\Delta \overline{F}_i$, for putting a substance, i, into any solution is

$$\Delta \overline{F}_i = RT \ln \frac{a_i}{a^0_i}$$

in which a_i is the activity of the component in the solution and the a^0_i is unity for the defined activity of the component in its pure standard state, usually that physical state stable at the same temperature under one atmosphere of external pressure. Although the free energy change in the Ba of Reaction (7), $\Delta \overline{F}_{Ba}$, is given by

$$\Delta \overline{F}_{Ba} = -RT \ln a_{Ba(ss)},$$

the corresponding standard free energy change, ΔF^0_7, to which the equilibrium constant is related is zero because it refers to the free energy change accompanying the consumption and production of reactants and products in their pure standard reference states of unit activity. By deleting the notations (ss in BaO) from the other reactions, Reaction (7) could also be deleted and the description made more accurate; however, the specifications of the state of the reaction would be less apparent.

The ideal solution assumption requires that the partial molal enthalpy change, $\Delta\overline{H}_i$, for dissolving the component be zero (zero heat of solution). In this circumstance, activities of components in the solutions are automatically equal to mole fractions. If gaseous components (at temperatures above their normal boiling points) are also in equilibrium with components of the ideal solutions, the activities of the gaseous components are equal to their partial pressures expressed in atmospheres (if they are ideal gases). The activity of a solute (e.g., Ba) at a temperature below its boiling point is given by the equation,

$$a_i = \frac{p_i}{p^0_i},$$

in which p_i is the partial pressure it shows in the solution and p^0_i the vapor pressure it would show at the same temperature in its pure state.

The activity is an essential quantity in discussing non-ideal solutions and a very convenient quantity for discussing ideal solutions. In the latter, it is convenient because it is dimensionally correct for use in the equilibrium constant and because it also avoids the awkwardness of describing components in terms of two sets of units, mole fractions and atmospheres partial pressure.

18. Thermochemical data will be quoted mainly from the following sources or computed from a combination of data from these sources.

a. *Selected Values of Thermodynamic Properties, Series III,* National Bureau of Standards, Washington, D. C., 1950-1954.

b. K. K. Kelley, *Contributions to the Data on Theoretical Metallurgy III.* "The Free Energies of Vaporization and Vapor Pressures of Inorganic Substances," Bulletin 383, U. S. Department of the Interior, Bureau of Mines, Washington, D. C., 1935.

c. Maurice de Kay Thompson, *The Total and Free Energies of Formation of the Oxides of Thirty-Two Metals,* The Electrochemical Society, Inc., N. Y., 1942.

d. O. Kubaschewski and E. Ll. Evans, *Metallurgical Thermochemistry,* Academic Press, Inc., N. Y., 1951.

e. L. L. Quill, *The Chemistry and Metallurgy of Miscellaneous Materials: Thermodynamics,* National Nuclear Energy Series IV-19B, McGraw-Hill Book Co., Inc., N. Y., 1950.

f. John Johnston, "Free Energy Changes Attending the Formation of Certain Carbonates and Hydroxides," *Jour. Am. Chem. Soc.,* Vol. 30, pp. 1357-1365, September, 1908.

19. H. B. DeVore, "Photoconductivity Study of the Activation of Barium Oxide," *RCA Review*, Vol. XIII, pp. 453-463, December, 1952.

20. Therald Moeller, *Inorganic Chemistry*, p. 158, John Wiley and Sons, N. Y., 1952.

21. This is obviously an approximation for the effective value of the dielectric constant because it ignores local relaxations in the crystal.

22. The thermochemical activity a_i of a solute species defined in Reference (17) is further defined as

$$a_i = \frac{p_i}{p^0{}_i} = \gamma_i X_i ,$$

in which γ_i is the activity coefficient, X_i the mole fraction, p_i the partial pressure of the solute, $p^0{}_i$ the vapor pressure of the pure (solute) component.

23. Reaction (10) could also be written as the sum of the two half reactions,

$$\mathrm{Mg}\,(l) = \mathrm{Mg}^{++}\,(ss, \mathrm{BaO}) + 2e\,(ss, \mathrm{BaO}),$$

$$2e\,(ss, \mathrm{BaO}) + \mathrm{Ba}^{++}\,(s, \mathrm{BaO}) = \mathrm{Ba}\,(l).$$

At equilibrium, the electronic activities produced by the greatly different activities, a_{Ba} and a_{Mg}, are equal. By assuming various values for the ratio, $a_{\mathrm{BaO}}/a_{\mathrm{MgO}}$, one readily sees that the equilibrium values of the ratio, $a_{\mathrm{Ba}}/a_{\mathrm{Mg}}$, depend on the composition assumed. Thus whether a small activity of a "strong" reducing agent can generate the same electronic activity as can a large activity of a "weak" reducing agent depends somewhat on the effect of mass action. Similarly, it is obvious that the state of reduction of the system as measured by the work function (or Fermi level or electronic activity) depends on the activities of all the species present, the oxidized as well as the reduced species.

24. Cf. N. F. Mott and R. W. Gurney, *Electronic Processes in Ionic Crystals*, p. 159, Second Edition, Clarendon Press, Oxford, England, 1948. The derivation of these equations assumes that only one donor species contributes appreciably to the population of conduction electrons and that the energy required to remove a second electron from the donor species is considerably larger than E_d, the energy required to remove the first electron.

25. For brevity, AEO is used to signify the conventional alkaline earth oxide composition containing BaO and SrO, or BaO, SrO, and CaO in optimum ratios.

26. The term "disproportionation" describes a type of reaction shown by many species which react with themselves to form both a more highly oxidized product and a less highly oxidized product than the reacting species.

27. From thermochemical data, it is likely that $(E_2 - E_0) \approx 2(E_3 - E_2)$; no more than this can even be estimated about the absolute or relative values of the ionization energies of the solute iron species. In aqueous solutions, many ionic species exist which cannot ordinarily be isolated in "pure" compounds. Accordingly, the presence of "extraordinary" as well as "ordinary" species should be expected in solid solutions, hence the iron impurity system in BaO may also include Fe^+. Whether the "level" for Fe (and also one for Fe^+) lies in the conduction band of BaO cannot be estimated. Alternatively, the "level" for ionization of solute Fe^{+++} may lie below the full band. Even in this case, an energy $(E_g - E_2)$ must be *supplied* to take an electron from the $O^=$ band and place it on an Fe^{+++} ion thereby converting it into an Fe^{++} ion, hence electrons do not drain off the $O^=$ sites into the Fe^{+++} sites. Neither do electrons drain from Fe and Fe^{++} sites into Fe^{+++} sites—the energy of the system is not lowered by a spatial rearrangement of species unaccompanied by a change in relative numbers of species.

28. The O_2 pressure does not affect this distribution because we have assumed a fixed activity value of Fe supplied by the support metal. A far smaller equilibrium activity of Fe would be produced from the dissociation of FeO under any likely residual O_2 pressure such as 10^{-12} atmosphere.

29. R. H. Plumlee, "Electrolytic Transport Phenomena in the Oxide Cathode," *RCA Review*, Vol. XVII, pp. 190-230, June, 1956.

30. As will be noted later, charge balance considerations and the nature of the species involved do not *require* that the thermally detachable electrons be incorporated in the valence bonds or valence shell of the donor ion. For anionic donors, the detachable electron will seldom be part of the valence shell.

31. H. B. Frost, "Transient Changes in Oxide Cathodes," Report on Fourteenth Annual Conference on Physical Electronics, Massachusetts Institute of Technology, Cambridge, Mass., 1954.

H. B. Frost, Thesis, "Transient Changes in Oxide Cathodes," Massachusetts Institute of Technology, Cambridge, Mass., 1954.

32. E. J. W. Verwey, P. W. Haaijman, F. C. Romeijn, and G. W. van Oosterhout, "Controlled-Valency Semiconductors," *Philips Res. Rep.*, Vol. 5, pp. 173-187, June, 1950.

33. E. J. W. Verwey and F. A. Kroger, "New Views on Oxidic Semiconductors and Zinc-Sulfide Phosphors," *Philips Technical Review*, Vol. 13, pp. 90-95, October, 1951.

34. F. A. Kroger, H. J. Vink, and J. van den Boomgaard, "Controlled Valency in CdS Single Crystals," *Z. für physik. Chem.*, Vol. 203, pp. 1-72, May, 1954.

35. F. A. Kroger and H. J. Vink, "Physico-Chemical Properties of Diatomic Crystals in Relation to the Incorporation of Foreign Atoms with Deviating Valency," *Physica*, Vol. 20, pp. 950-964, November, 1954.

36. P. W. Selwood, "Valence Inductivity," *Jour. Amer. Chem. Soc.*, Vol. 70, p. 883, February, 1948.

37. P. W. Selwood, T. E. Moore, Marylinn Ellis, and Kathryn Wethington, "Supported Oxides of Manganese," *Jour. Amer. Chem. Soc.*, Vol. 71, pp. 693-697, February, 1949.

38. G. H. Johnson, "Influence of Impurities on Electrical Conductivity of Rutile," *Jour. Amer. Cer. Soc.*, Vol. 36, pp. 97-101, March, 1953.

39. In principle, it is useful to distinguish two types of variable-charge behavior: (a) variable-valence performance in which the charge-balancing detachable electron has a bona fide role in the bonding of the ion to the crystal and is part of the "valence shell" of the ion, (b) potential-well trapping, in which the charge-balancing detachable electron is merely held in the electrostatic field due to the charge deficit of the site. In practice, all degrees of shading between the two types should be expected.

40. From previous thermochemical discussions, it is obvious that "cations" of *zero* charge (atoms) must also be included as an important part of any variable charge donor system.

41. Karl Hauffe and Gerhard Tranckler, "Calciumoxyd, ein amphoterer Halbleiter," *Z. für Physik*, Vol. 136, pp. 166-178, November, 1953.

42. In connection with discussion of ionic and co-valent solids and complex compounds, it seems worth while to follow the convention used by Y. K. Syrkin and M. E. Dyatkina, *Structure of Molecules and the Chemical Bond*, p. 108, Interscience Publishers, Inc., N. Y., 1950, and

to reserve the term *valence* to connote only the *number of unpaired electrons* which a species has. This in turn defines the number of co-valent bonds it can form. In co-valent or largely co-valent crystals, the valence is then identifiable with the co-ordination number.

The co-ordination number in an ionic crystal is in general not related to the number of surplus or deficit electronic charges which the ions carry. The ionic *charge* or *state of oxidation* of a species is thus different from its crystalline co-ordination number. Since the bonds in any real crystal are comprised of the whole gamut of conceivable electronic configurations ranging from "normal" fully ionic through fully covalent to those completely reversed from "normal" ionic, it is pertinent to distinguish ionic charge, coordination number, and number of co-valences. Even in the most ionic crystals, the average electronic charge density between ions drops at the nominal ionic radii boundaries only to about 5 per cent or 10 per cent of the maximum between nuclear centers. The variable-charge electron donors may be either co-valently or ionically bonded in the solid. The electron more or less by which the donor's charge varies will probably always be an unpaired electron. The important point is that the concentration of such electrons can be controlled by the degree of reduction of the crystal. At present it seems immaterial whether one describes the variation in electron content of a site in terms of a nominal number of electronic charges or in terms of the numbers of covalent bonds and "surplus" electrons having unpaired spins.

43. This result agrees only approximately with findings in these Laboratories. Here, it has been found that the luminescence spectrum shifts slightly and consistently with the identity of the impurity anion for the entire halide series. See I. J. Hegyi, S. Larach, and R. E. Shrader, "Electroluminescence of Zinc Sulfo-Selenide Phosphors with Copper Activators and Halide Co-activators," Abstract No. 39, Enlarged Abstracts, The Electrochemical Society Inc., Spring Meeting, April 29-May 3, 1956.

44. C. Kittel, *Introduction to Solid State Physics*, pp. 313-315, John Wiley and Sons, Inc., N. Y., 1953.

45. This experiment (Reference (29)) actually provided the clues and inspiration which caused the F-center model to be subjected to scrutiny and which led to the entire development of this chemical model of the donor centers based on the electronic potential concept.

46. S. Glasstone, K. Laidler, and H. Eyring, *The Theory of Rate Processes*, p. 566, McGraw-Hill Book Co., Inc., N. Y., 1941. These authors show that continuous conduction of protons in H_2O requires

rotation of H_2O molecules for which the activation energy (in ice) is 0.375 electron volt. The actual proton transfer step is the rate limiting step (because of the low H_3O^+ concentration) and has an activation energy of 0.213 electron volt. At cathode temperatures, rotation of the OH group probably would not be the slow step in the donor center diffusion process.

47. G. H. Metson, S. Wagener, M. F. Holmes, and M. R. Child, "The Life of Oxide Cathodes in Modern Receiving Valves," *Proc. Inst. Elec. Engrs.* (London), Vol. 99, Part III, pp. 69-87, March, 1952. These authors calibrated a number of tube types so that gas pressures could be read from measurements of ion currents collected during the drawing of electron current. They state "The pressure in modern values is between 1×10^{-9} and 1×10^{-4} mm Hg. . . ." They found the lower limit of apparent residual gas level was set by the photoelectron current level from the ion collecting electrode. This is the same limitation inherent in most ionization gage readings.

48. Maximilian Schriel, "Uber die Einwirkung von Bariummetall auf Bariumoxyd bei hohern Temperaturen," *Z. für Anorg. und Allgem. Chem.*, Vol. 231, Part 4, pp. 313-326, April, 1937.

49. The vapor pressure equation for Ba is not thoroughly established. Recent measurements by P. E. Douglass, "The Vapor Pressure of Calcium I," *Proc. Phys. Soc.* (London), Vol. 67B, pp. 783-786, October, 1954, and D. H. Tomlin, "The Vapor Pressure of Calcium II," *Proc. Phys. Soc.* (London), Vol. 67B, pp. 787-794, October, 1954, indicate that the values of E. Rudberg and J. Lempert, "The Vapor Pressure of Barium," *Jour. Chem. Phys.*, Vol. 3, p. 627, October, 1935 are at least a factor of ten too low, that the values for Ba of H. Hartmann and R. Schneider, "Boiling Temperatures of Magnesium, Calcium, Strontium, Barium, and Lithium," *Z. Anorg. Allgem. Chem.*, Vol. 180, pp. 275-283, March, 1929, are more nearly correct but a factor of 2 or 3 too low, nevertheless. A plot of Timmer's values of color center densities against barium vapor concentrations computed from the Hartmann and Schneider data gave also a cube root relationship with a slightly different value of the proportionality constant. The Hartmann and Schneider data give activity coefficients for Ba in BaO ranging from 277 to 4.4.

50. L. S. Darken and R. W. Gurry, *Physical Chemistry of Metals*, p. 270, McGraw-Hill Book Co., Inc., N. Y., 1953. The excess partial molar free energy, $\overline{F}_i^{xs}$, of a solute in a real solution over that in an ideal solution, $\overline{F}_i^{id}$, is given by

$$\overline{F}_i^{xs} = \overline{F}_i - \overline{F}_i^{id} = RT \ln \gamma_i .$$

The corresponding excess partial molar entropy of the solute in a real solution is

$$\left(\frac{\partial \overline{F}_i^{xs}}{\partial T} \right)_p = - \overline{S}_i^{xs} = R \ln \gamma_i + RT \left(\frac{\partial \ln \gamma_i}{\partial T} \right)_p .$$

The excess entropy over the ideal mixing entropy is a measure of the lack of disorder. Since we are concerned with very high temperatures and very high dilution, there is no reason to expect $\overline{S}_i^{xs}$ to be appreciably different from zero.

51. R. W. Pohl, "Electron Conductivity and Photochemical Processes in Alkali-halides," *Proc. Phys. Soc.*, Vol. 49, Extra Part, pp. 3-31, August, 1937.

52. Equivalent to a mole fraction $X_{Ba} \simeq 0.5 \times 10^{-5}$. Mole fractions as high as $X_{Ba} \simeq 10^{-4}$ were measured by R. O. Jenkins and R. H. C. Newton, "Free Barium and the Oxide Cathode," *Jour. Sci. Instr.*, Vol. 26, pp. 172-173, May, 1949.

KINESCOPE ELECTRON GUNS FOR PRODUCING NONCIRCULAR SPOTS

By

R. C. Knechtli and W. R. Beam

RCA Laboratories,
Princeton, N. J.

Summary—*In some cathode-ray-tube applications, small spot size is a necessity. This paper describes two types of electron guns by means of which particularly small spots can be obtained. One type of gun, using a line crossover rather than the conventional point crossover, is suitable for producing narrow, elongated spots. The other type, employing an electron-illuminated aperture as an electron-optical object, can produce sharply defined spots of any desired size and shape. These guns have been found experimentally to produce spots whose current density equals or exceeds that of the best available guns of conventional design.*

Introduction

In some cathode-ray-tube applications the spot size required is quite small. This limitation in spot size is sometimes found to be more severe along one axis than along the other. An example of this is the line-screen color kinescope described by Bond, Nicoll, and Moore in 1951.[1] In such a kinescope, a spot not wider than approximately 10 mils is required; the length of the spot however, can be as large as 30 mils or even more, without loss of color purity and without too poor resolution. In such applications, an elongated spot appears desirable.

It is the purpose of this paper to describe the development of electron guns which produce on the screen of a kinescope a rectangular or elongated spot of high current density. More generally, spots of any desired shape and high current density can be obtained by means of the guns with aperture limited object to be described further on.

The spot on the screen of a kinescope is the electron-optical image of a cross section of the beam. This cross section is called the "object" of the gun; it is usually quite small and is in the vicinity of the cathode. The part of the gun by means of which this object is formed will be called the "object-forming system"; the part of the gun by means of which its image is reproduced on the screen is the "imaging system."

---

[1] D. S. Bond, F. H. Nicoll, and D. G. Moore, "Development and Operation of a Line-Screen Color Kinescope," *Proc. I.R.E.*, Vol. 39, pp. 1218-1230, October, 1951.

In most conventional electron guns, the object-forming system consists of a cathode, located behind an aperture in the electrically negative grid electrode, and a positive accelerating electrode completing the "triode." The conventional gun has cylindrical symmetry, but in some cases electrode apertures may be of other shapes to attain special effects.

The electron imaging system may use either electric fields or magnetic fields, or a combination of both. The choice of the electron lens system is more often an economic compromise than the result of scientific optimization in production kinescopes.

In one type of gun described here, the object-forming system concentrates the electron beam at the plane of an apertured electrode. Spots of any desired shape can be obtained by using a small aperture of this shape as an object. The part of the cathode current transmitted through it forms the spot on the screen as an image of this aperture. Besides the possibility of producing spots of any desirable shape, a gun with an object-defining aperture has two other important advantages:

(1) The dimensions of the object are independent of current,

(2) The position of the object is independent of current.

Thus, the spot size should be less dependent on current in these guns than in guns of the conventional type. This was indeed found to be true.

Fundamental Limitations

The fundamental limitations on the performance of all types of kinescope guns in general are discussed here in order to show how they influenced the conception of the guns described later.

Because of *spherical aberrations*, the highest spot-current density for fixed spot current is obtained when the product $V_o \sin^2 \theta_o$ is minimized, V_o being herein the object voltage and θ_o the angle of beam spread at the object. In this process, the object size is assumed constant.

Thermal electron velocities at the cathode determine the lowest *theoretically possible* value of the product $V_o \sin^2 \theta_o$. Hence, the purpose in designing an object-forming system intended to produce a high spot-current density is to minimize the product $V_o \sin^2 \theta_o$, to as near the lower limit determined by thermal electron velocities as possible. A more general demonstration of the advantage of making $V_o \sin^2 \theta_o$ small is shown in Appendix I.

Space charge produces a mutual repulsion of the electrons in the beam; the beam always tends to spread. This process, called "space-charge defocusing," is approximately equivalent in effect to the weakening of the lenses of the imaging system. To compensate for it, a

focusing voltage of the imaging system should be readjusted as a function of current.

It can be shown* that space-charge defocusing first occurs in the object space if the object voltage is smaller than the image voltage. As the amount of beam spread is dependent upon the local space-charge density in the beam, space-charge defocusing decreases with increasing beam voltage. Therefore, in order to minimize space-charge defocusing in a kinescope, it is desirable to choose the object voltage, V_o, as high

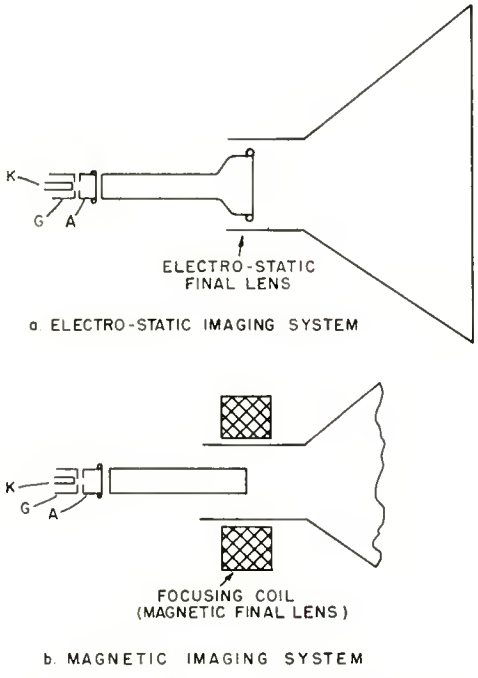

Fig. 1—Conventional kinescope gun.
(a) Electrostatic imaging system; (b) Magnetic imaging system.

as possible.* If the object voltage cannot be chosen high enough to make space-charge effects negligible, these effects can, to some extent, be compensated for by applying a dynamic focussing voltage to a lens electrode of the imaging system.

In a gun with an object-defining aperture or other electron intercepting electrode, the heat developed at this electrode due to the intercepted current may also determine the maximum tolerable value of its voltage.

---

* Appendix II.

Conventional Kinescope Guns

Typical kinescope guns of what will be referred to as the "conventional" type are shown in Figure 1. The cathode, K, grid, G, and accelerating electrode, A, constitute the object-forming system. The imaging system may be electrostatic as in Figure 1(a), or magnetic as in 1(b). The object-forming system, or "triode," of the conventional gun performs two services — it creates a region of high current density upon which the imaging system can be focused, and it controls the amount of current reaching the phosphor screen. The formation of the "crossover," as this high-density region is called, is possible

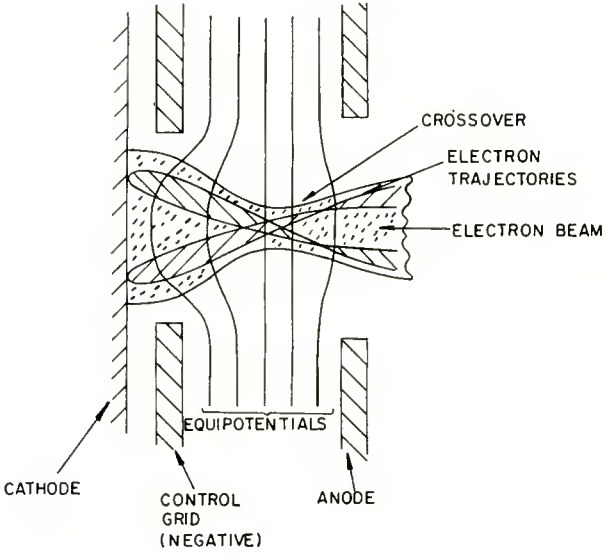

Fig. 2—Triode system of conventional gun.

because of the intense convergent forces produced near the cathode by negative grid potentials. These fields, shown in Figure 2, form a region of very dense, but nonuniform flow in front of the cathode. The dense region is not at all sharply defined but very nonuniform as a result of the absence of perfection in the electron lens and probably to a greater extent the spread in velocities of electron emission.

Despite the fact that at the crossover in a conventional gun, electron flow is highly nonlaminar, this crossover region is small enough to qualify for use as an object in tubes requiring neither an extremely high current density spot, sharpness of the edges of the spot, nor constancy of spot size with current.

The Line-Crossover Gun

The purpose is to produce an elongated spot of high current density. One possibility for this is to alter the object-forming region of a conventional gun to form, instead of a round crossover, a long linear one. This can conveniently be done simply by changing the round grid aperture to a long slit. Pierce[2] has shown that the current density in such a crossover is slightly greater (other things being equal) than in a round crossover.

By changing to a line crossover, and to optics which are infinite in the direction parallel to the line crossover, an infinite line beam would be obtained. While such a situation offers simplicity of description, a beam of a definite (finite) length is desired. This makes it

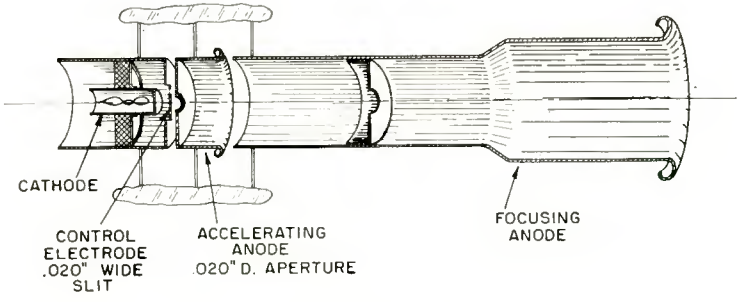

Fig. 3—Line focus gun.

necessary to (1) limit the crossover length, and (2) provide focusing in the direction of the long axis of the crossover. The second objective, it appears, is most practically met by providing an imaging lens with cylindrical symmetry, since lenses with controlled degree of astigmatism are difficult to build. The function of limiting the length of the line crossover, it has been found, can be performed by the apertured diaphragm of the accelerating anode. With this type of gun structure, shown in Figure 3, the line length is implicitly controlled by the electrode dimensions and spacings in the "triode" section. The dimensions shown in the figure are suitable to produce a spot of approximately .010 × .040 inch, with a cathode-to-screen distance of about 21 inches. About 80 per cent of the cathode current is intercepted by the first anode. Maximum spot current is about one milliampere.

---

[2] J. R. Pierce, "Limiting Current Densities in Electron Beams," *Jour. Appl. Phys.*, Vol. 10, pp. 715-724, October, 1939.

The Object-Aperture Gun

An alternate possibility of obtaining an elongated spot is to project a very dense beam onto an aperture shaped in the form of the desired spot. The portion of the beam passing the aperture then forms the object of the imaging lens. By this means, spots of any desired shape and having sharply defined edges can be obtained. Elongated spots in particular are conveniently obtained by means of a rectangular object aperture.

This type of gun has a number of advantages: (1) free choice of spot shape, (2) essentially no change in spot size and shape with current, and (3) ability to utilize a larger cathode area, and thus attain high spot current at reasonable cathode loading. The disadvantages are: (1) the attainment of small spot size requires great gun precision (but perhaps no more than an *equivalent* conventional gun), (2) considerable power may be dissipated by the object electrode, from current which does not pass through the aperture, and (3) more electrodes are generally needed. For applications where spot size, shape and maximum current are of primary importance, this type of gun may be justified.

Since the work of Law,[3] who was the first to our knowledge to investigate guns of this type in 1937, several techniques have come into use in beam type tubes. One of these is the Pierce[4] gun, another the impregnated cathode.[5] Gun construction techniques used for traveling-wave and similar tubes are of importance in achieving the necessary accuracy. It was felt that by putting together some of these advances in gun techniques, an improved object-aperture gun would be possible.

In the following sections, the design considerations and limitations for object-aperture guns are discussed in detail and the construction of some experimental guns explained.

Object-Forming System

The object-forming system consists of the cathode, the object aperture, and the intervening region. As a consequence of spherical aberrations, the essential aim in the design of an object-forming system is to reduce the product $V_o \sin^2 \theta_o$ for given object size and spot current

[3] R. R. Law, "High Current Electron Gun for Projection Kinescopes," *Proc. I.R.E.*, Vol. 25, p. 954, August, 1937.

[4] Described in J. R. Pierce, *Theory and Design of Electron Beams*, D. Van Nostrand Co., Princeton, N. J., 1949.

[5] R. Levi, "New Dispenser Type Thermionic Cathode," *Jour. Appl. Phys.*, Vol. 24, p. 233, February, 1953.

to as near the lower limit determined by thermal electron velocities as possible. How this determines the structure of the object forming systems will be shown in the next section. It is assumed in following sections that cylindrically symmetrical object-forming and imaging systems are to be used; our experience indicates that other types of lenses are almost prohibitively difficult to build. The precise parameters of such an object-forming system are governed to a considerable degree by secondary requirements not apparent in the general relations of Appendix I and Figure 10. Thus,

(1) The *shape of the object-defining aperture* is determined by the required spot shape. In our experiment, elongated spots were desired; therefore, rectangular object defining apertures were used.

(2) The *size of the object-defining aperture* (parameter y_0 in Figure 10) is chosen as small as possible. Small object dimensions are desirable in order to keep the gun short. (This can be deduced from Equations (3) and (5), when y_s, V_s, and V_o are specified.) The minimum practical object dimensions are limited by the mechanical difficulty of making and aligning small apertures. Local bombardment heating must also be taken into consideration.

(3) The *cathode current density*, j_c. Equation (1), indicates it is clearly best to use the maximum cathode current density compatible with good tube life. This is limited by the cathode material, and by the ability of the cathode to replenish its active layer.

(4) The *current I_o transmitted through the object-defining aperture* is approximately equal to the screen current, I_s, when the current lost in the imaging system is kept negligible (as it must be to achieve most efficient operation). The screen current is a quantity which we may choose to attempt to maximize; its minimum usable value is fixed by the minimum picture highlight brightness required in the finished kinescope.

(5) The *object voltage*, V_o, is chosen as high as possible in order to minimize space-charge defocusing (see Appendix II). An upper limit to V_o is usually set by the heat developed at the object-defining aperture due to the intercepted current. Thus the value of V_o is a compromise between the limitations imposed by space-charge defocusing and heat dissipation at the object defining aperture.

(6) The *cathode current*, I_c, is determined by the value of I_o and the transmission ratio I_o/I_c of the object-forming system.

(7) The *transmission ratio I_o/I_c* is made as large as possible in

order to keep the intercepted current, the cathode current and the cathode diameter corresponding to given values of j_c and I_o as small as possible. This is normally achieved by making the (round) beam diameter at the object-defining aperture about equal to the largest dimension of this (rectangular) aperture.*

The last condition is usually rather readily satisfied, the simplest method being to focus the beam to a crossover at the plane of the object defining aperture.

Design of the Object-Forming System

Optimum design, as previously indicated, requires that the value of the product $V_o \sin^2 \theta_o$ be minimized. It was noted that the value of V_o cannot be chosen arbitrarily; its optimum is usually determined

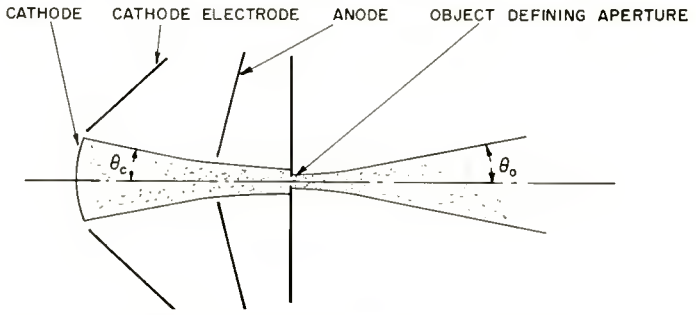

Fig. 4—Convergent Pierce gun with object-defining aperture.

from a balance of power-supply and aperture-heating limitations. Thus, in designing an object-forming system, the direct problem is to minimize the angle of beam spread, θ_o, at the object-defining aperture for given object voltage, V_o, object size, y_o, and transmitted current, I_o. Several electrode configurations were tested.

A simple solution might appear to be a convergent Pierce gun with a small angle of convergence, θ_c (essentially what Law[3] used). In this case, the smallest beam cross section (crossover) would be placed at the object defining aperture itself, as shown in Figure 4. Because the flow is not truly laminar, it was found impossible to make $\theta_o < \theta_c$; in all cases $\theta_o \simeq \theta_c$. Thus, one must minimize the angle of convergence, θ_c, of the Pierce gun (parallel flow was ruled out by the excessive cathode current density implied by the desired values of I_c and y_o). In actual designs, with the relatively high cathode current required (in

* Further improvements might be obtained by means of astigmatic focusing before the object-defining aperture if one of its dimensions appreciably exceeds the other dimension.

this case of the order of 3 milliamperes), small angles of convergence lead to excessively high object voltages. Further, since the "cutoff voltage"* of a Pierce gun increases with decreasing angle of convergence (for given cathode diameter and beam current), too high cutoff voltages are obtained. Hence, in order to keep the cutoff voltage reasonably small and the object voltage at the desired value, a relatively large angle of convergence, θ_c, appears desirable at the cathode.

A preliminary lens combination used to form a dense beam at the object aperture consisted of the convergent-field Pierce gun followed by a decelerating then an accelerating region. The anode voltage of the Pierce gun and the object voltage were almost the same. The intervening lens, of the Einzel** type, served to overcome the space-charge forces, to extend the cathode–object distance and hence slightly reduce

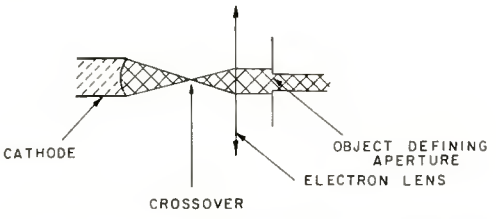

Fig. 5—Principle of object-forming system.

the effective θ_c, and finally to compensate for slight variations in the focusing of the Pierce optics. In this concept, no true crossover was expected within the object-forming optics. The relatively large size of the beam in the Einzel lens region resulted in interception on the low-voltage electrode. Increasing the aperture diameter produced undesirable results as indicated by a less favorable value of the "quality factor," v (defined in Appendix I, Equation (7)). Study of this type of action, limited, as was most of the work, to experiment, was halted when better operation was obtained with a system operating in the mode shown in Figure 5. The elements used in a structure of the type of Figure 5 are physically realizable (convergent lenses only), and successful results have been obtained with guns of that type.

In the object-forming system of Figure 5, a crossover is formed between the cathode and a lens focused on this crossover. The crossover

* With all apologies to Dr. Pierce, the beam *was* modulated by the electrode surrounding the cathode. While this destroys the laminar flow, it also effectively cuts off the beam current. Deep electrodes produce cutoff at less negative control voltage than shallow ones, since the accelerating fields do not penetrate to the cathode so readily.

** An Einzel, or unpotential lens, is one consisting of three electrodes, the outermost pair at the same potential. The inner electrode may have either higher or lower voltage.

is considered, in first approximation, as a point source of electrons; thus, the beam emerging from the lens and passing the object defining aperture is essentially parallel. Actually, the finite size of the crossover and the aberrations of this lens produce some beam spread; the theoretical* minimum angle of beam spread thus obtained is not smaller than the angle obtained with a convergent flow gun converging directly at a small angle on the object aperture. The advantages of the structure of Figure 5 are the lower object and cutoff voltage possible for given cathode current and cathode diameter.

The crossover, in a gun of the type of Figure 5, can be produced either by means of an immersion lens** system similar in principle to

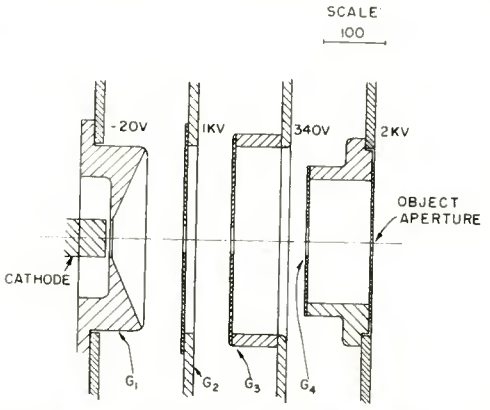

Fig. 6—Object-forming system with immersion lens crossover.

the systems by which the crossover is formed in conventional guns, or by means of a convergent laminar flow produced, for instance, with a Pierce-type gun. Figure 6 shows an object-forming system with an immersion lens crossover. This crossover is formed between the first electrode, G_1 (which is negative) and the second electrode, G_2 (which is highly positive). The three electrodes G_2, G_3, and G_4 constitute a lens focused on the crossover which lies between G_1 and G_2; the lens action is obtained by keeping G_3 at much lower potential than G_2 and G_4. Typical potentials are indicated on Figure 6.

Another method of forming the crossover between cathode and object aperture is to use a convergent Pierce gun. Figure 7 shows a design of this type.

---

* The theoretical minimum angle of beam spread is the angle of beam spread obtained in an ideal system limited only by thermal velocities (Equation 1).

** Defined as a lens in which the object (in this case, the cathode) is immersed in the lens proper.

The Imaging System

Before describing a specific imaging system, let us list the parameters of the imaging systems (left side of Figure 10) and consider how they may best be chosen.

(1) *Lens type* — Preliminary experience showed that the most adequate lenses within practicality were electrostatic cylinder lenses whose cylinders approached in diameter that of the neck of the envelope. Magnetic lenses were abandoned because of the excessively large magnification which they presented; this would have decreased the object size or increased the tube length, neither of which was practical.

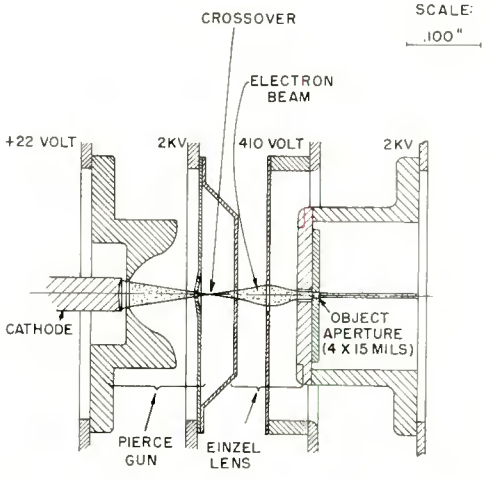

Fig. 7—Laminar-flow object-forming system.

(2) L_s, the *lens-to-screen distance* is determined by deflection requirements and screen size. It is kept as small as possible in order to minimize the tube length, the limitation imposed on the screen current density by thermal velocities (Equation (1)), and space-charge defocusing; indeed, the smaller L_s, the larger the angle of beam convergence at the screen, θ_s.

(3) y_s; the *actual spot dimensions* are determined by picture requirements. (The maximum tolerable spot size can be determined, e.g., by the minimum tolerable resolution.) y_s is a quantity one may choose to minimize.

(4) Δy_s which measures *spherical aberrations* could clearly have

(from Equation (4)) any value from 0 to y_s. Due to the loss of current density in the spot for large Δy_s and the difficulty of attaining small Δy_s, a practical compromise of $\Delta y_s \simeq .2\ y_s$ was chosen.*

(5) M, the *magnification*, is determined once y_o and $y_s' = y_s - \Delta y_s$ have been chosen. However, in order to keep the gun as short as possible, one must avoid too small values of M. This influences to some extent the choice of y_o; further considerations relevant to this choice have already been expressed in the design procedure of the object-forming system.

(6) V_s, the *screen voltage*, should be as high as possible in order to minimize the effect of thermal velocities (Equation (1) applied to the screen) and maximize the highlight brightness. The limit is determined by circuit and safety (including X-ray hazard) requirements.

(7) I_s, the *screen current* is determined by the consideration already expressed in the design procedures of the object forming system in relation with I_o.

(8) V_o, the *object voltage*, is determined in designing the object forming system.

It is seen that the screen (image) voltage, the object voltage, the distance from final lens to screen, L_s, and the magnification, M, usually are determined by the various considerations just expressed.

In a *single-lens* system, once the distance from the lens to the screen, the image voltage, and the object voltage are prescribed, the position of the object plane and the magnification are determined. Usually, the magnification thus obtained does not correspond to the magnification required. In this case, one more degree of freedom is necessary; this is obtained by an additional electron lens.

As an example, a typical electrostatic double-lens imaging system is shown in Figure 8; this system can be used with the object-forming systems of Figures 6 or 7.

Test Procedures

Much effort is saved by testing experimental object-forming systems separately from the imaging system. For this purpose, the following quantities have to be measured at a given object voltage:

(a) The cathode current, I_c,

* An unpublished paper by E. G. Ramberg of these Laboratories shows that, in an elongated spot, the maximum current is obtained when $\Delta y_s \simeq .35\ y_s$. Our choice produces slightly less current, but a sharper edged spot.

(b) The screen current, I_s,

(c) The angle of beam spread, θ_o, at the object.

These quantities are conveniently measured by sealing the object-forming part of the gun into a short bulb, as shown in Figure 9. Care must be taken, by proper electrostatic shielding, to prevent secondary electrons from interfering with the measurement of I_c or I_s. (Such secondaries may be emitted from either the screen or the object aperture.)

In the test of an object-forming system by this method, one measures the transmission efficiency, I_s/I_c, and the angle of beam spread, θ_o, for a given object voltage and screen current as a function of electrode

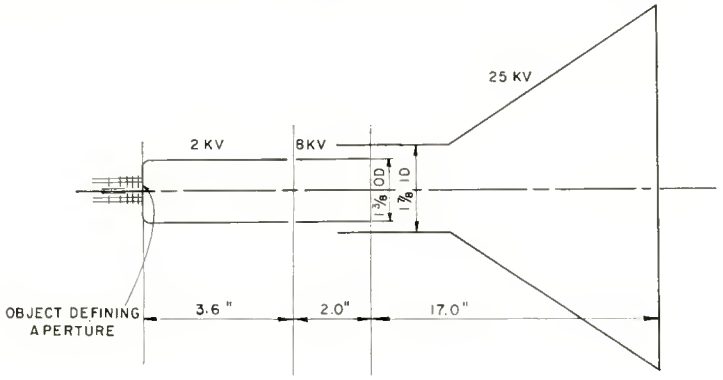

Fig. 8—Image-forming system.

voltage, and calculates the ratio v (Equation (7)), which serves as a "quality factor" for the object-forming structure.

The performance of the imaging system can be tested in a spot magnifier of the type described by Beam.[6] The performance of a complete gun with object forming and imaging system can of course also be conveniently tested by this method.

Experimental Results

As a typical example, results obtained with a complete gun in a 19-inch (screen diameter) kinescope are presented below. This gun consists of an object-forming system of the type shown in Figure 6, and of an imaging system of the type of Figure 8. The object consists of a rectangular aperture of 4×15 mils; the magnification is about two times.

[6] W. R. Beam, "A New Method for Magnifying Electron Beam Images," *RCA Review*, Vol. XVI, pp. 242-250, June, 1955.

Typical performance data of this gun:

Screen voltage	25 kv
Object voltage	2 kv
Maximum screen current I_s	1 ma
Cathode current density for $I_s = 1$ ma	180 ma/cm^2
Cathode current for $I_s = 1$ ma	3.2 ma
Spot size, approximately	10×35 mils
Object size	4×15 mils
Control grid voltage at $I_s = 1$ ma	-40 volts
Control grid voltage at cutoff	-150 volts
Angle of beam spread at the object for $I_s = 1$ ma	$\tan \theta_0 = 0.045$

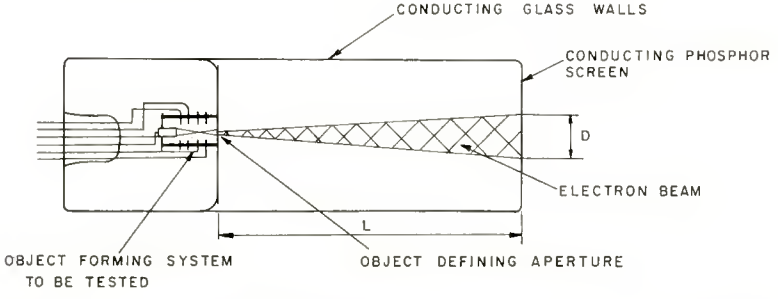

Fig. 9—Test of object-forming systems. Tan $\theta = D/2L$, $\eta = I_{screen}/I_{cathode}$.

It was observed that for screen currents exceeding 0.5 milliampere, space-charge defocusing became apparent, and sharp focus required readjustment of the focusing voltage by 300 volts at 1 milliampere screen current. It should be pointed out that this performance was obtained with the imaging system of Figure 8, which had not been designed for maximum focusing sensitivity.

Life of guns of this type was found to be short because of overheating and out-gassing of the object aperture during operation. This was a consequence of the heavy electron bombardment to which it was subjected. Adequate processing and design should overcome this shortcoming, as similar technological difficulties have been successfully solved in previous tubes with bombarded object aperture, as well as in power traveling-wave tubes.

The performance of the gun described above can be compared with

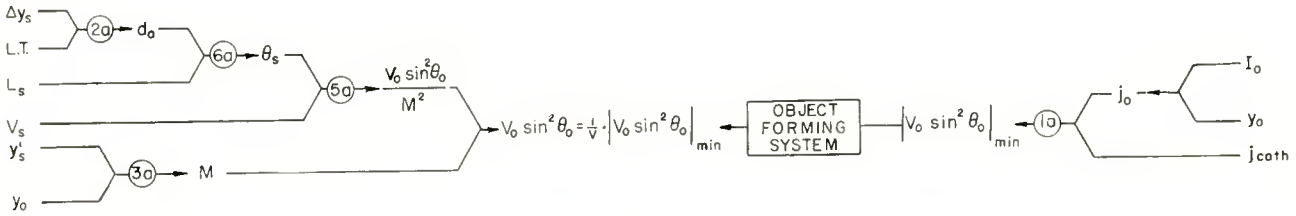

LEGEND

PARAMETERS OF IMAGING SYSTEM

y_s = SPOT SIZE
Δy_s = CONTRIBUTION OF SPHERICAL ABERRATIONS TO SPOT SIZE
y'_s = $y_s - \Delta y_s$ = SPOT SIZE IN THE ABSENCE OF ABERRATIONS
y_o = OBJECT SIZE
L_s = LENS-TO-SCREEN DISTANCE
V_s = SCREEN (IMAGE) VOLTAGE
L.T. = LENS TYPE

PARAMETERS OF THE OBJECT FORMING SYSTEMS

y_o = OBJECT SIZE
I_o = CURRENT TRANSMITTED THROUGH THE OBJECT DEFINING APERTURE
j_{cath} = CATHODE CURRENT DENSITY

SECONDARY PARAMETERS

d_a = APERTURE OF FINAL LENS
M = MAGNIFICATION
θ_o = ANGLE OF BEAM DIVERGENCE AT THE OBJECT
θ_s = ANGLE OF BEAM CONVERGENCE AT THE SCREEN
j_o = OBJECT CURRENT DENSITY

$$v = \frac{|V_o \sin^2\theta_o|_{min}}{V_o \sin^2\theta_o}$$ = PERFORMANCE FACTOR OF OBJECT FORMING SYSTEM ($0 < v < 1$)

Fig. 10—Fundamental relations for the design of a kinescope gun; 1a-6a refer to Equations (1)-(6).

the performance of conventional kinescope guns by defining a gun "quality factor," q:

$$q = [j_{max}/j_{theor.}]^{1/2}$$

where j_{max} = maximum measured screen current density,

$j_{theor.}$ = maximum theoretically possible screen current density for the cathode current density at which j_{max} is measured.*

The value of $j_{theor.}$ can be expressed as a function of the screen voltage, V_{sc} and of the angle of beam convergence, θ_{sc} as follows, assuming thermal velocities to be the factor theoretically limiting j:

$$j_{theor.} \simeq j_{cath} \times 10 V_{sc} \sin^2 \theta_{sc}$$

for a cathode temperature of 1160°K. Hence

$$q = \sqrt{\frac{j_{max}}{j_{cath}}} \times \frac{1}{3.2 \sqrt{V_{sc}} \sin \theta_{sc}}.$$

With the gun described here, a value of $q = 0.5$ has been obtained. (This is at least as good as with the best gun of conventional design available for test.) Further, up to 500 microamperes the spot size remained practically constant.

Conclusions

In this paper the development of guns operating on principles hitherto not fully explored have been described. Their performance has been found comparable with that of some of the best conventional guns except for life. The limitation on life is not inherent and should be straightforward to overcome. The additional advantages of the types of guns described here may bring them into their own in applications where spot size and shape are of primary importance.

Appendix I

In this appendix, justification will be given for the paths taken in the design of a gun of the type described in the text.

Basically, the procedure involves working with certain fundamental and limiting relationships. Within these limitations, it was desired to

* q differs from v (defined in Appendix I) in being a factor for the *entire* gun, whereas v applies only to the object-forming system.

obtain the minimum possible spot-size for a given spot-current, or the maximum possible spot-current in a spot of given size. This objective, while definite enough, does not indicate, per se, the procedure for achieving it. Further, different objectives may also be conceived. Therefore, the general relations between the gun parameters will be established here. The specific applications of these relations to the purpose of minimizing the spot-size for given current is carried out as a particular example.

The fundamental relations to be used are listed below:

(a) *Thermal velocities* of the electrons impose the following limitation for the current density j to a point in the beam at potential V where electrons from the cathode converge with half angle θ:

$$j \leq \left(1 + \frac{eV}{kT}\right) \sin^2 \theta \times j_c,$$

where j_c is the cathode current density, k Boltzmann's constant, and T the cathode temperature in °K. This expression was first derived by D. B. Langmuir.[7] In the usual case where $eV/kT \gg 1$, this reduces to

$$j \leq \frac{eV}{kT} \sin^2 \theta \times j_c. \tag{1}$$

(b) The *spherical aberrations* of an electron lens, which are the only ones of major importance in a well-constructed kinescope gun, result in every point of the object being reproduced as a circle at the image. The result is an increase in the size of the image. Expressing the increase in any dimension of the spot (due to spherical aberrations) as Δy_s, and the lens aperture as d_a,

$$\Delta y_s = C \times d_a^3 \tag{2}$$

C is a constant depending on the lens type and other dimensions. Ramberg[8] has analyzed spherical aberrations in certain types of electron lenses. In general, however, the value of Δy_s is best obtained experimentally.

(c) The *magnification*, M, of an electron lens is defined by

---

[7] D. B. Langmuir, "Theoretical Limitations of Cathode-Ray Tubes," *Proc. I.R.E.*, Vol. 25, p. 977, August, 1937.

[8] E. G. Ramberg, "Variation of Axial Aberrations of Electron Lenses with Lens Strength," *Jour. Appl. Phys.*, Vol. 13, pp. 582-594, September, 1942.

$$M = y_s'/y_o, \tag{3}$$

where y_s' and y_o are equivalent dimensions of the spot and the object in the absence of aberrations. If y_s is the actual spot dimension, one has

$$y_s = y_s' + \Delta y_s. \tag{4}$$

The magnification in a distortionless imaging system can also be expressed by the relation

$$M^2 = \frac{V_o \sin^2 \theta_o}{V_s \sin^2 \theta_s} \tag{5}$$

where V_o and V_s are object and image (screen) voltages, respectively; θ_o and θ_s are the angles that a given ray (electron path) intersecting the axis at the object makes with the lens axis at the object and screen, respectively. When Equation (5) is used, the outermost ray contributing to the formation of the spot will implicitly be considered. Thus θ_o is equal to the angle of beam spread at the object when no current is intercepted on apertures in the imaging system, and θ_s is the angle of beam convergence at the screen.

(d) Let L_s be the distance from the second principal plane of the final lens to the screen. The lens aperture d_a of Equation (2) is equal to the maximum beam diameter at that plane. Thus, *the angle of beam convergence*, θ_s, at the screen is given by

$$\tan \theta_s = \frac{d_a}{2L_s}. \tag{6}$$

The interrelation of the principal parameters of the gun through Equations (1) to (6) and through the design of the object forming system are shown in Figure 10.

On the left side of the figure are parameters of the imaging system, on the right, parameters of the object-forming system. The entire design of the object-forming system is considered in this figure as a single operator determining the ratio

$$v = \frac{(V_o \sin^2 \theta_o)_{\min}}{V_o \sin^2 \theta_o} \tag{7}$$

of the minimum theoretically possible value of $V_o \sin^2 \theta_o$ (fixed from I_o, y_o, j_c by Equation (1)) to the actual value of this product.

When the design of the object-forming system has been chosen (v determined) and all of the parameters on the left side of Figure 10, except one, have been prescribed, this last parameter is determined through the relationship shown on Figure 10. It is seen that *best gun performance is obtained* quite generally *when the object-forming system is designed to make* $v \rightarrow 1$ (its theoretical maximum value).

For example, when all parameters except the spot size y_s' are prescribed, the minimum spot size is obtained when $v = 1$. This is shown as follows:

The value of $V_o \sin^2 \theta_o = (V_o \sin^2 \theta_o)_{\min}/v$ is determined by the parameters on the right of Figure 10 and by the design of the object-forming system. The value of $V_o \sin^2 \theta_o / M^2$ is fixed (call it C) by the parameters on the left of Figure 8 (excluding y_s'). Thus, the magnification, M, is found to be

$$M^2 = \frac{(V_o \sin^2 \theta_o)_{\min}}{Cv},$$

and $y_s' = M\, y_o$. The smallest value of y_s' is obtained when M is minimized; this is done by maximizing v (q.e.d).

One may conclude that for best performance, an object-forming system has to be designed to make $v \rightarrow 1$. Once the principal parameters I_o, j_o, and j_c (right of Figure 10) of the object-forming system have been selected, this amounts to minimizing the actual value of the product $V_o \sin^2 \theta_o$.

Appendix II

The electron trajectories in a converging or diverging beam can be computed, taking space charge into account, under the following assumptions:

(1) Field-free region,

(2) Paraxial rays (small angles between electron trajectories and axis of the beam),

(3) Laminar flow (no crossing of electron paths),

(4) Round beam cross section,

(5) No ion neutralization.

With these assumptions, the equation of the beam envelope is found to be[9]

$$\frac{z}{r_o} = 32.3 \frac{V^{3/4}}{I^{1/2}} \int_1^R \frac{dR}{\sqrt{\ln R}} \tag{8}$$

where r = beam radius at the abscissa z,

r_o = minimum beam radius occurring at the abscissa $z = 0$,

$R = \dfrac{r}{r_o} \geq 1$,

I = beam current in milliamperes,

V = beam voltage in kilovolts.

Space-charge limitation may occur in either the object space or the image space. The object space is the part of the imaging system in which the object is located. Its potential is the object potential, V_o. Let the average angle of beam divergence in the object space be θ_o. One defines similarly the image space with the image potential, V_i, and an average angle of beam convergence, θ_i.

Further, let the imaging system be represented by an equivalent imaging system with a single thin lens, as shown on Figure 11. Let the sum $L_1 + L_2$ be equal to the actual distance L between object and image:

$$L_1 + L_2 = L.$$

The angles θ_o and θ_i being specified together with L, the maximum beam diameter d_a in Figure 11 is also specified.

Let d_o = object diameter (assuming for convenience a round object),

d_i = image diameter.

For $d_i \ll d_a$, the maximum possible current through the object space is obtained when the minimum beam cross section is approximately at the object. Thus, applying Equation (8) to the object space one obtains

[9] B. J. Thompson and L. B. Headrick, "Space Charge Limitations on the Focus of Electron Beams," *Proc. I.R.E.*, Vol. 28, pp. 318-324, July, 1940.

$$\text{Max current which can be passed through } d_a = I_{o\max} = \frac{(32.3)^2 V_o^{3/2}}{\left(\frac{2L_1}{d_o}\right)^2} \left[\int_1^{\frac{d_a}{d_o}} \frac{dR}{\sqrt{\ln R}} \right]^2 \quad (9)$$

Let us express $I_{o\max}$ as a function of the image diameter:

$$d_o^2 = \frac{d_i^2}{M^2},$$

$$\frac{1}{M^2} = \frac{V_i \sin^2 \theta_i}{V_o \sin^2 \theta_o} = \frac{V_i}{V_o} \frac{(L_1)^2}{(L_2)^2}.$$

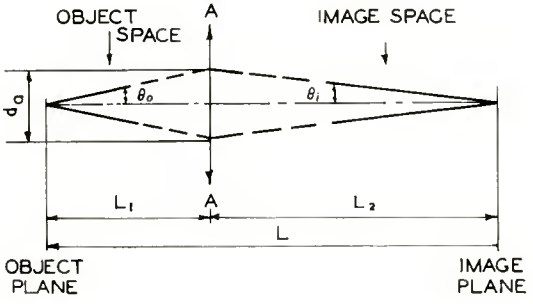

A A = PRINCIPLE PLANE OF EQUIVALENT SINGLE THIN LENS.

Fig. 11—Dimensions of equivalent imaging system.

Introducing these relations into Equation (9) one obtains for, $I_{o\max}$,

$$I_{o\max} = \left(\frac{d_i}{2L_2}\right)^2 \left[32.3 \int_1^{\frac{d_a}{d_o}} \frac{dR}{\sqrt{\ln R}} \right]^2 V_i \sqrt{V_o}. \quad (10)$$

In a kinescope, L_2 is approximately the distance from the screen (image plane) to the final lens. Little freedom usually exists in the choice of this parameter; therefore, we may consider it as prescribed. The image diameter d_i and the image voltage V_i (same as screen voltage) also are prescribed. The maximum beam diameter at the lens,

d_a, is determined by spherical aberrations, as shown in Appendix I. Once the magnification has been chosen, the integral in the bracket of Equation (10) is also determined. Thus, the only parameters left to choice are the object voltage, V_o, and the object distance, L_1, both being related by the condition

$$\frac{V_o}{L_1^2} = \frac{M^2}{L_2^2} V_i. \tag{11}$$

From Equation (10) it appears that the maximum possible current in the object space increases with increasing object voltage:

$$I_{o\max} \propto \sqrt{V_o}.$$

Therefore, in order to reduce space-charge effects in the object space, one has to increase the object voltage (q.e.d.).

Computing the maximum possible current $I_{i\max}$, in the image space, one finds, in a similar fashion,

$$I_{i\max} = \left(\frac{d_i}{2L_2} \right)^2 \left[32.3 \int_1^{\frac{d_a}{d_i}} \frac{dR}{\sqrt{\ln R}} \right]^2 V_i^{3/2}. \tag{12}$$

Numerical evaluation of Equations (10) and (12) shows that for magnification of the order of 2 and $V_o/V_i < 1/2$, $I_{o\max} < I_{i\max}$. Thus, under the usual conditions corresponding to those figures, space-charge effects are more important in the object space than in the image space (q.e.d.).

In the case of object and image shapes other than a circle, the preceding derivations still hold approximately if equivalent object and image diameters are defined, such that the object and image areas of the equivalent round beam are the same ones as in the actual beam. This has been experimentally found to hold for rectangular objects and spots.

In practice, the assumptions of laminar flow and absence of ions appear the least likely to be satisfied, while the other assumptions upon which this analysis relies are usually well satisfied. However, non-laminar flow and ion neutralization have opposite effects. This may explain why the relations indicated in this appendix have been fairly well confirmed by our measurements, at least qualitatively.

PEDESTAL PROCESSING AMPLIFIER FOR TELEVISION STUDIO OPERATION*

By

Ralph C. Kennedy

National Broadcasting Company, Inc.,
New York, N. Y.

Summary—*The pedestal processing amplifier is a device capable of removing the synchronizing pulses from either a color or monochrome television signal so as to permit simultaneous presentation of pictures from separate locations. It utilizes a new type of sync separator which provides a sync signal having constant amplitude for input signal variations of ± 14 decibels.*

Introduction

THE producers of television shows have, quite logically, borrowed many camera techniques from the motion picture industry. A number of the special effects which are called for require the simultaneous presentation of pictures from different locations. These special effects are variously known as split screen, video inset, and lap dissolve, among others.

"Genlocking"

In order to achieve the special effects referred to above, it is necessary that the sync generators involved be locked together. This procedure is known as "genlocking."

Genlock operation in monochrome television depended on the use of stabilizing amplifiers. These amplifiers separated the incoming composite signal into a sync signal and a simple video signal. The sync was used to lock the generators together and the video signal was introduced into the studio switching system in the same manner as a normal camera signal.

Such stabilizing amplifiers, however, are not usable on a color signal. In the signal prescribed by the FCC, and considering the tip of sync to be negative, the blanking level is somewhat below the reference black level. The blanking pulse, upon which the sync signal and the color burst are superimposed is commonly referred to as the pedestal. In recovering the sync signal with a stabilizing amplifier,

* This material was presented at the 1956 National Convention of the Institute of Radio Engineers and will appear in the convention record.

burst and chroma components which are below the pedestal are included; further, the clipping of sync from the signal to produce a simple video waveform results in burst and many chroma components being clipped.

Two-Line Genlock Operation

To circumvent the lack of a suitable stabilizing amplifier, color genlocking has heretofore been accomplished by using two wide-band circuits. One has carried the sync and burst to lock the generators. The simple video signal, free of sync, to be introduced into the switching system has been carried on the other circuit. Clamper amplifiers in the Telephone Company circuits, since they clamp on the tip of sync, have clamped on the blanking signal and operated satisfactorily. This mode of genlock operation has been satisfactory with film camera signals. Pedestal has been easily controlled and no chroma components nor burst have been allowed to extend far enough below blanking to cause confusion in the clamper amplifiers. When live pickups have been attempted, however, the pedestal has not been so easily controlled, and burst and chroma components have extended so far below the blanking level that the clampers have stopped functioning properly.

The Pedestal Processing Amplifier

The pedestal processing amplifier is a device which can separate the video and sync signals from a composite color signal in such a manner as to permit simple genlock operation without the need for an additional line. The saving in line costs is substantial.

The operation of the unit may best be understood by referring to the block diagram, Figure 1. A composite monochrome or color signal is introduced at the input terminals where it branches in two paths. In one the sync is recovered by first amplifying the signal, trapping out the chroma and burst by means of a high Q tuned circuit, and then applying it to a gate tube which opens only during sync. This sync signal is shaped and further amplified to result in a stable sync output. In addition, there are provisions for further sync processing which includes means for manual adjustment of the sync width by changing the timing of the back edge of sync with reference to the leading edge and further clipping and shaping. This signal is used for three purposes. One feed is used to drive the clamp pulse circuits. The other two feeds will be described presently.

The second composite video path is through a cathode follower which acts as a level-adjustment circuit. Following this is an amplifier

feeding an adjustable video delay line. The purpose of this line is to permit time coincidence between the leading edge of the sync in the composite signal and the processed sync mentioned above. This delayed signal is fed to a clamped adder tube which is also fed the sync signal. The sync is added in the same polarity as that in the composite video. Enough is added to cause the sync in the resultant output to extend well below the negative peaks of burst. The sync is clipped so as to produce a clean tip but it is not clipped enough to distort the burst. This signal is fed to another clamped adder tube which is likewise fed the sync signal. The polarity of the sync in the composite signal is opposite to that of the sync being added. This causes the

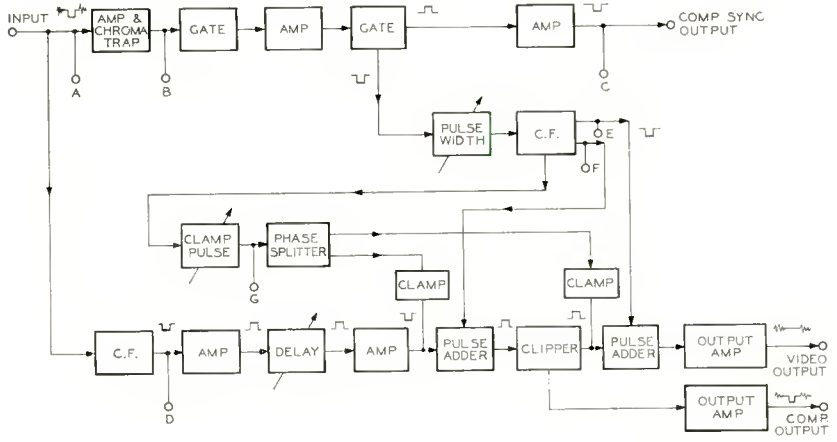

Fig. 1—Block diagram of pedestal processing amplifier for television studio operation.

sync in the output signal to be reduced to zero, i.e., blanking level by proper adjustment of the amount of the sync introduced.

The proper timing of the front edges of the sync in the composite signal and the added sync is realized by adjusting the video delay line. The timing of the back edges of the two syncs is adjusted with the pulse width control.

Three outputs are available from the unit. One is processed sync whose output remains constant for input level variations of ± 14 decibels from a standard one volt peak-to-peak signal. A second output is a composite signal having processed sync. The third output is a simple video signal having a processed pedestal. No effort is made to maintain proper sync-to-video ratio in the composite output since it is intended only for use in a monitor.

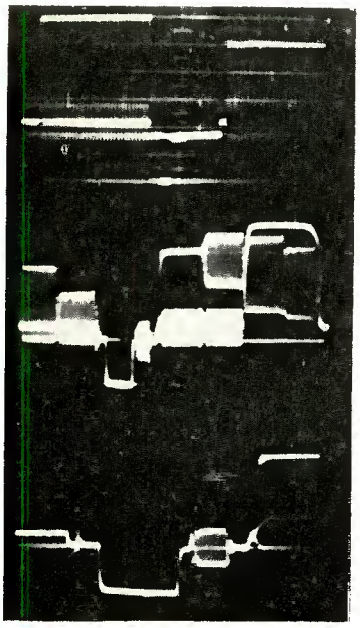

Fig. 2—Waveforms at test point A.

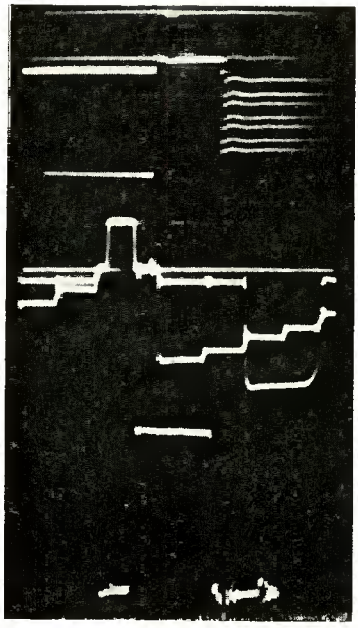

Fig. 3—Waveforms at test point B.

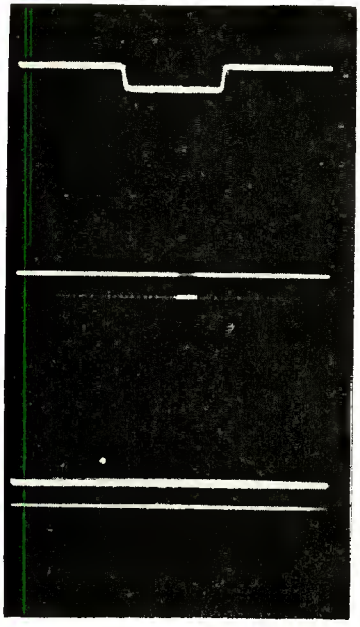

Fig. 4—Waveforms at test point C.

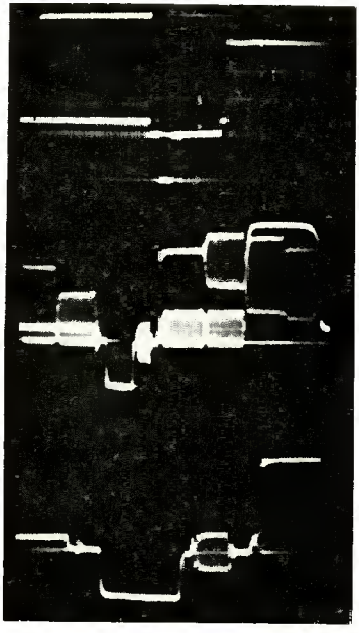

Fig. 5—Waveforms at test point D.

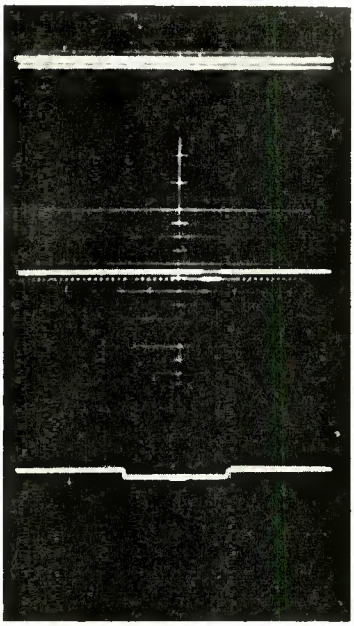

Fig. 6—Waveforms at test point E or F.

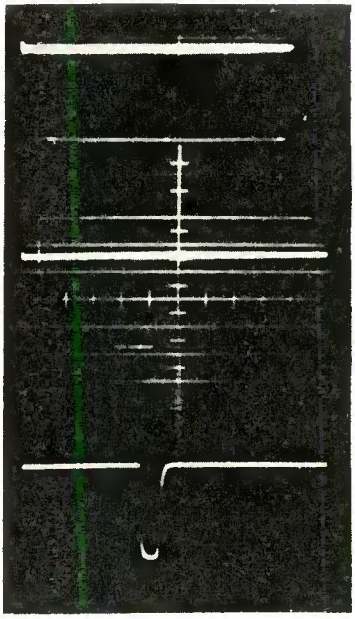

Fig. 7—Waveforms at test point G.

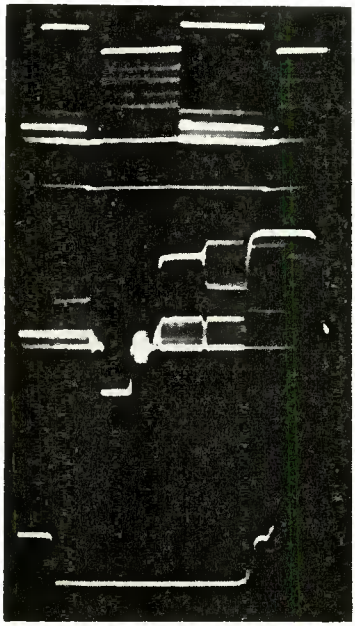

Fig. 8—Waveforms of composite output signal.

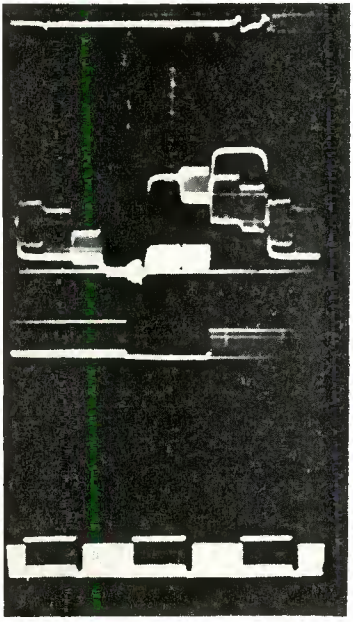

Fig. 9—Waveforms of video output signal.

Figures 2 through 9 inclusive show significant waveforms at various test points throughout the unit when it is properly adjusted. The input color-bar signal may be viewed at test point A and appears as shown in Figure 2.

After the chroma in the signal has been removed, it appears at test point B as shown in Figure 3.

The output sync may be viewed at test point C and is shown in Figure 4.

Figure 5 shows the waveform appearing at test point D. This should be of the same form as Figure 2 except for the level.

Test points E and F show the magnitude and waveforms of the addition and cancellation syncs. Figure 6 shows these waveforms but the two amplitudes manifestly are different.

The clamp pulses are monitored at test point G and should appear as shown in Figure 7.

After sync addition and clipping, the video waveform with processed sync should appear as shown in Figure 8. This waveform appears at the output of the unit. As indicated earlier, the sync-to-video ratio is not standard in this signal. The magnitude of the sync is that which results in minimum transient in the pedestal upon addition of the cancellation sync.

Figure 9 shows the video output when the equipment is properly adjusted.

Test Results

Three of these equipments have been built and used commercially. The first time this method of genlocking was attempted commercially was during the 1955 World's Series where in 6 days a total of 21 hours time genlocking was maintained. The "Great Waltz" and "Producer's Showcase" have also used this method of genlocking. In the latter case the New York facilities were locked to the Burbank, California studio. Split screen and numerous fast switches between the East and West Coast were made with no loss of genlock.

Another test included genlocking a film studio whose output was a continuous loop of film leader which causes extreme signal variations. This signal was fed for half an hour with no interruptions in genlocking.

RCA TECHNICAL PAPERS†

First Quarter, 1956

Any request for copies of papers listed herein should be addressed to the publication to which credited.*

"AFC of Television Receivers Using Junction Diodes," O. Romanis and W. Y. Pan, *RCA Industry Service Laboratory Bulletin LB-1017* (January 23) 1956

"Antennas, Transmission Lines and Distribution Systems for Color TV," J. D. Callaghan, *Service* (March) 1956

"Automatic-Frequency Control of Television Receivers Using Junction Diodes," W. Y. Pan and O. Romanis, *Transistors I*, RCA Laboratories (March) 1956

"Bandwidth Requirements of SW Radio Telegraphy," J. B. Moore, *Tele-Tech* (March) 1956

"Basic Transistor Device Concepts," Harwick Johnson, *RCA Industry Service Laboratory Research Bulletin RB-28* (January 19) ... 1956

"Basic Transistor Device Concepts," H. Johnson, *Transistors I*, RCA Laboratories (March) 1956

"Calculations of Alloying Depth of Indium in Germanium," L. Pensak, *Transistors I*, RCA Laboratories (March) 1956

"Cataphoretic Deposition of Thoria on Tantalum," C. P. Hadley, *Rev. Sci. Instr.* (Laboratory and Shop Notes) (March) 1956

"Color Television Receiver Design—A Review of Current Practice," M. O. Pyle, Co-author, *Proc. I.R.E.* (March) 1956

"Communication by Tropospheric Scatter Propagation," L. E. Thompson, *RCA Engineer* (February-March) 1956

"Comparison of Surface-Excited and Volume-Excited Photoconduction in Cadmium Sulfide Crystals," R. H. Bube, *Phys. Rev.* (March 15) 1956

"Comparison of Surface-Excited and Volume-Excited Photoconduction in Cadmium Sulfide Crystals," R. H. Bube, *RCA Industry Service Laboratory Research Bulletin RB-35* (February 24) .. 1956

"Conversion Factors for Tube Characteristics," *RCA Application Note AN-164* (March) 1956

"Continuous-Process Apparatus for Growing Single-Crystal Germanium," H. Nelson, *Transistors I*, RCA Laboratories (March) 1956

"Coupled Cavity Tunes X-Band Magnetron," W. F. Beltz, *Electronics* (March) 1956

"Cross-Modulation in Transistor R-F Amplifiers," D. D. Holmes, *Transistors I*, RCA Laboratories (March) 1956

"Demagnetizing the RCA-21AXP22 Color Kinescope," *RCA Application Note AN-163*, Tube Division, Radio Corporation of America, Harrison, N. J. (January) 1956

"Design Considerations in Class B Complementary Symmetry Circuits," T. M. Scott and T. O. Stanley, *RCA Industry Service Laboratory Bulletin LB-1021* (February 23) 1956

† Report all corrections or additions to RCA Review, RCA Laboratories, Princeton, N. J.

* *RCA Industry Service Laboratory Bulletins* are not published and are issued only as a service to licensees of the Radio Corporation of America.

‡ *The RCA Engineer* is published exclusively for the use of RCA engineers and is not available for outside distribution.

"Design Considerations in Class-B Complementary Symmetry Circuits," T. O. Stanley and T. M. Scott, *Transistors I*, RCA Laboratories (March) 1956

"A Determination of 1/f Noise Sources in Semiconductor Diodes and Triodes," W. H. Fonger, *RCA Industry Service Laboratory Research Bulletin RB-29* (January 25) 1956

"A Determination of 1/f Noise Sources in Semiconductor Diodes and Triodes," W. H. Fonger, *Transistors I*, RCA Laboratories (March) 1956

"A Developmental Wide-Band, 100-Watt, 20 DB, S-Band Traveling-Wave Amplifier Utilizing Periodic Permanent Magnets," W. W. Siekanowicz and F. Sterzer, *Proc. I.R.E.* (January) .. 1956

"Discharge Mechanism of Mercury Pool Arcs," K. G. Hernqvist, *RCA Industry Service Laboratory Research Bulletin RB-34* (February 23) 1956

"Diversity Reception with Correlated Signals," H. Staras, *Jour. Appl. Phys.* (Letter to the Editor) (January) 1956

"The Drift Transistor," H. Kroemer, *RCA Industry Service Laboratory Bulletin LB-1018* (February 3) 1956

"The Drift Transistor," H. Kroemer, *Transistors I*, RCA Laboratories (March) 1956

"Effect of Magnetic Deflection on Electron Beam Convergence," P. E. Kaus, *RCA Industry Service Laboratory Research Bulletin RB-33* (February 20) 1956

"The Effect of Magnetic Fields on Color Television Receiver Performance," B. R. Clay, *RCA Engineer* (February-March) 1956

"Electromechanical Filters for 100-Kc Carrier and Sideband Selection," R. W. George, *Proc. I.R.E.* (January) 1956

"The Electron Microscope (New Tools for Research)," G. B. Chapman, *Modern Medicine* (January) 1956

"Electron Microscopy of Ultra-Thin Sections of Bacteria II. Sporulation of Bacillus megaterium and Bacillus cereus," G. B. Chapman, *Jour. Bacteriology* (March) 1956

"The Electron-Voltaic Effect in Ge and Si P-N Junctions," E. G. Linder, J. J. Loferski, and P. Rappaport, *RCA Industry Service Laboratory Research Report RB-42* (March 15) 1956

"The Electron-Voltaic Effect in Germanium and Silicon P-N Junctions," P. Rappaport, J. J. Loferski, and E. G. Linder, *RCA Review* (March) 1956

"Equipment for Measuring Junction Temperature of an Operating Transistor," J. Ollendorf and K. E. Loofbourrow, *RCA Industry Service Laboratory Research Bulletin RB-30* (January 27) 1956

"Equipment for Measuring Junction Temperature of an Operating Transistor," J. Ollendorf and K. E. Loofbourrow, *Transistors I*, RCA Laboratories (March) 1956

"Etch Pits and Dislocation Studies in Silicon Crystals," R. V. Jensen and S. M. Christian, *RCA Industry Service Laboratory Bulletin LB-1023* (March 5) 1956

"Evaluation of Transistors for Class-B Power Amplifiers," W. Hasenberg, *Transistors I*, RCA Laboratories (March) 1956

"Exchange Between Adsorbed and Dissolved Sulfate Ions," C. V. King and B. Levy, *Jour. Phys. Chem.* (Notes) (March) 1956

"Frequency Stability of Point-Contact Transistor Oscillators," C. C. Cheng, *Proc. I.R.E.* (February) 1956

"Gas Tubes Protect High-Power Transmitters," W. N. Parker and M. V. Hoover, *Electronics* (January) 1956

"Graphical Solution of Simple Lens Problem," E. Kornstein, *RCA Engineer* (February-March) 1956

"Guided Missiles—Maintenance," S. F. Kennedy, *Rad. and Tele. News* (March) 1956

"Ham-Band Charts—Useful Data on Ham Bands from 1.8 to 148 Mc," *RCA Ham Tips* (March) 1956

"A High-Frequency Measuring Equipment for Transistors," W. F. Sands, *Transistors I*, RCA Laboratories (March) 1956

"How to Make Live Commercials Using RCA 3-V Color Film Chain," S. L. Bendell, H. N. Kozanowski, and T. J. Shipferling, *Broadcast News* (February) 1956

"How RCA Organizes to Meet Changing Needs," J. L. Mastran, *RCA Engineer* (February-March) 1956

"Human Relations and the Manufacturing Engineer," A. Skele, *RCA Engineer* (February-March) 1956

"Hybrid 'Pocket' Radio Receiver," K. E. Loofbourrow and J. E. Stolpman, *RCA Engineer* (February-March) 1956

"A Junction-Transistor Counter with High-Speed Carry," T. P. Bothwell, G. W. Booth, and E. P. English, *Transistors I*, RCA Laboratories (March) 1956

"Junction Transistor Designed for Iterative Operation at Low Frequencies," L. J. Giacoletto, *Transistors I*, RCA Laboratories (March) 1956

"Junction Transistor Switching Characteristics," D. E. Deuitch, *Transistors I*, RCA Laboratories (March) 1956

"Kink-Bands in Germanium," F. D. Rosi, *Acta Metallurgica* (January) 1956

"Luminescence in Electronically Active Solids," H. W. Leverenz, *RCA Industry Service Laboratory Research Bulletin RB-36* (February 24) 1956

"Measurement of Aluminum Film Thickness," C. P. Hadley, *Rev. Sci. Instr.* (Laboratory and Shop Notes) (March) 1956

"Mechanical Engineer's Role in Development of Electronic Equipment," L. Jacobs, *RCA Engineer* (February-March) 1956

"Metal-Based Photoconducting Cells for Controlling High Power," B. Kazan, *RCA Industry Service Laboratory Research Bulletin RB-39* (March 8) 1956

"Microscopic Examination of Germanium Crystals and Transistors," S. G. Ellis, *Transistors I*, RCA Laboratories (March) 1956

"Miniature Loudspeakers for Personal Radio Receivers," J. C. Bleazey, J. Preston, and E. G. May, *RCA Review* (March) ... 1956

"Modulated Transistor Oscillators and Their Applications," H. C. Lin, *Transistors I*, RCA Laboratories (March) 1956

"Molecular Ringing," S. Bloom, *RCA Industry Service Laboratory Research Bulletin RB-40* (March 9) 1956

"Multi-Alkali Photocathodes," A. H. Sommer, *RCA Industry Service Laboratory Research Bulletin RB-44* (March 28) 1956

"Neck-Shadow Problems in Kinescopes," *RCA Application Note AN-162*, Tube Division, Radio Corporation of America, Harrison, N. J. (January) 1956

"New Beam Power Tubes for UHF Service," W. P. Bennett, *IRE Transactions on Electron Devices*, Volume ED-3, Number 1 (January) 1956

"New Expandable Consolette," E. J. Meehan, *Broadcast News* (February) 1956

"New Signal Handling Techniques Simplify Control Operations for Color TV," I. Bosinoff, A. C. Luther, F. W. Millspaugh, and H. M. Potter, *Broadcast News* (February) 1956

"Noise Considerations of P-N-P Junction Transistors," J. W. Englund, *Transistors I*, RCA Laboratories (March) 1956

"The Noise Factor of Junction Transistors," L. J. Giacoletto, *Transistors I*, RCA Laboratories (March) 1956

"Noise Reduction in CW Magnetrons," R. L. Krulee and J. A. Mullen, *Proc. I.R.E.* (January) (Letter to the Editor) 1956

"A Novel Ring Counter Using Junction Transistors," D. E. Deuitch, *Transistors I*, RCA Laboratories (March) 1956

"The Omniguide Antenna; an Omnidirectional Wave Guide Array for UHF-TV Broadcasting," J. Gibson and O. M. Woodward, Jr., *RCA Industry Service Laboratory Bulletin LB-1020* (February 20) 1956

"The Omniguide Antenna—An Omnidirectional Waveguide Array for UHF-Television Broadcasting," O. M. Woodward, Jr. and J. J. Gibson, *RCA Review* (March) 1956

"Optical Multiplexing in Television Film Equipment," A. H. Lind and B. F. Melchionni, *Jour. S.M.P.T.E.* (March) 1956

"Performance of a Radio-Frequency Alloy Junction Transistor in Different Circuits," L. J. Giacoletto, *Transistors I*, RCA Laboratories (March) 1956

"Phase Angle Distortion and Differential Phase Shift in Traveling-Wave Tubes," D. J. Blattner and W. R. Beam, *RCA Industry Service Laboratory Research Bulletin RB-31* (February 3).. 1956

"Phase Angle Distortion in Traveling-Wave Tubes," W. R. Beam and D. J. Blattner, *RCA Review* (March) 1956

"Photoelectromagnetic Effect in Insulating CdS," H. S. Sommers, Jr., R. E. Berry, and I. Sochard, *Phys. Rev.* (February 1) 1956

"Photovoltaic Effect in GaAs p-n Junctions and Solar Energy Conversion," D. A. Jenny, J. J. Loferski, and P. Rappaport, *Phys. Rev.* (Letter to the Editor) (February 1) 1956

"Plasma Oscillations at Extremely High Frequencies," M. A. Lampert, *Jour. Appl. Phys.* (January) 1956

"P-N-P Transistors Using High-Emitter-Efficiency Alloy Materials," L. D. Armstrong, C. L. Carlson, and M. Bentivegna, *RCA Review* (March) 1956

"The Polarguide—A Constant Resistance Waveguide Filter," R. W. Klopfenstein and J. Epstein, *Proc. I.R.E.* (February) 1956

"The Preparation of Single and Multiple P-N Junctions in Single Crystals of Germanium," A. R. Moore, *Transistors I*, RCA Laboratories (March) 1956

"Project Turnkey: A Tropospheric Scatter Circuit," R. W. Allen, W. D. Clement, and H. J. Hamlin, *RCA Engineer* (February-March) 1956

"RCA Electrofax in the Graphic Arts," M. L. Sugarman, Jr., *RCA Engineer* (February-March) 1956

"Recent Advances in Power Junction Transistors," B. N. Slade, *Transistors I*, RCA Laboratories (March) 1956

"Reduction of Power-Line-Conducted Interference Output of Television Receivers," C. G. Seright, *RCA Industry Service Laboratory Bulletin LB-1024* (March 21) 1956

"Remote TV-Control Tuning System Circuitry," S. Wlasuk and J. H. Fisher, *Service* (February) 1956

"Resistivity Studies of Various Leclanche Cathode Materials," R. Glicksman and C. K. Morehouse, *Jour. Electrochem. Soc.* (March) 1956

"Salvaging Valuable Components from Brazed Assemblies," M. B. Lemeshka, *Electrical Manufacturing* (March) 1956

"Semiconductors and Transistors," L. Malter, *RCA Engineer* (February-March) 1956

"A Silicon N-P-N Junction Transistor by the Alloy Process," H. Nelson, *Transistors I*, RCA Laboratories (March) 1956

"Some Aspects of Thermal Conversion in Germanium," H. Kroemer, *Transistors I*, RCA Laboratories (March) 1956

"Spectral Distribution of Photoconductivity," H. B. DeVore, *RCA Industry Service Laboratory Research Bulletin RB-32* (February 8) 1956

"Stability Considerations in Transistor I-F Amplifiers," D. D. Holmes and T. O. Stanley, *Transistors I*, RCA Laboratories (March) 1956

"A Step-Type, Broadband, X-Band Ceramic Waveguide Window," H. K. Jenny and F. E. Vaccaro, *IRE Transactions on Electron Devices*," Volume ED-3, Number 1 (January) 1956

"Stud Welder Used in Assembling Thyratrons," N. R. Goldstein, *Electronics* (Production Techniques) (March) 1956

"Surface Treatment of Silicon for Low Recombination Velocity," H. Nelson and A. R. Moore, *RCA Review* (March) 1956

"A Switched-Zone Furnace for Germanium Purification," P. G. Herkart and S. M. Christian, *Transistors I*, RCA Laboratories (March) 1956

"A Technique for Evaluating Various Cathode Materials," C. K. Morehouse and R. Glicksman, *Jour. Electrochem. Soc.* (February) 1956

"Temperature Effects in Circuits Using Junction Transistors," H. C. Lin and A. A. Barco, *Transistors I*, RCA Laboratories (March) 1956

"A Test Set for Transistor Performance Measurement at 455 Kilocycles," D. D. Holmes, L. A. Freedman, and T. M. Scott, *Transistors I*, RCA Laboratories (March) 1956

"Theoretical and Practical Considerations for Determining the Optimum Semiconductor for Photovoltaic Solar Energy Converters," J. J. Loferski and Paul Rappaport, *RCA Industry Service Laboratory Research Bulletin RB-38* (February 29). 1956

"The Transfluxor," J. A. Rajchman and A. W. Lo, *Proc. I.R.E.* (March) 1956

"Transistor Audio Amplifiers," A. I. Aronson, *Transistors I*, RCA Laboratories (March) 1956

"Transistor Audio Amplifiers," A. I. Aronson, *RCA Industry Service Laboratory Bulletin LB-1022* (March 5) 1956

"Transistor Fabrication by the Melt-Quench Process," J. I. Pankove, *Proc. I.R.E.* (February) 1956

"Transistorized Sync Separator Circuits," H. C. Goodrich, *RCA Engineer* (February-March) 1956

"Transistorized Vertical Deflection for Television Receivers," M. B. Finkelstein, *Transistors I*, RCA Laboratories (March)..... 1956

"A Transmission Line Taper of Improved Design," R. W. Klopfenstein, *Proc. I.R.E.* (January) 1956

"Uniform Planar Alloy Junctions for Germanium Transistors," C. W. Mueller and N. H. Ditrick, *RCA Review* (March).... 1956

"Use of the RCA-2N109 P-N-P Junction Transistor in Class B Audio Applications," *RCA Application Note AN-165*, Semiconductor Division, Radio Corporation of America, Harrison, N. J. (March) 1956

"A Variable-Capacitance Germanium Junction Diode for UHF," J. H. O'Connell and L. J. Giacoletto, *RCA Review* (March) 1956

"Video Transformers," G. W. Gray, *RCA Industry Service Laboratory Research Bulletin RB-37* (February 29) 1956

"The V.T.V.M. How it works. How to use it," Rhys Samuel, Gernsback Library *Book* No. 57 1956

"A 20-Watt Transistor Audio Amplifier," H. C. Lin, *Transistors I*, RCA Laboratories (March) 1956

AUTHORS

WALTER R. BEAM—(See *RCA Review*, Vol. XVII, No. 1, March 1956, p. 135.)

ROBERT B. JANES received the B.S. degree in Physics from Kenyon College in 1928. He did graduate work in physics at Harvard and the University of Wisconsin where he received a Ph.D. in 1935. From 1929 to 1931 he served as instructor in physics at Colgate University and from 1931 to 1935 as research assistant at the University of Wisconsin. From 1935 to 1943, Dr. Janes was an engineer at the Harrison, N. J. plant of RCA where he worked on television camera tubes and phototubes. Since 1943 he has been in the Tube Department of RCA at Lancaster, Pennsylvania. He was in charge of the development and design of television camera tubes until 1950, when he was appointed Manager of the Development Group responsible for camera tubes, storage tubes, and phototubes.

PETER E. KAUS received the B.S. degree from the University of California in 1947, the M.S. degree from U.C.L.A. in 1952 and the Ph.D. degree from the University of California in 1956. From 1951-1953 he was a teaching assistant at U.C.L.A. In 1954 he joined RCA Laboratories in Princeton where he has been working in the field of electron optics. He is a member of the American Physical Society and of the Society of Sigma Xi.

RALPH C. KENNEDY received the B.A. degree from San Jose State College in 1943 and the M.A. and E.E. degrees in Electrical Engineering from Stanford University in 1945 and 1946 respectively. In 1946 he transferred to the Development Group of the National Broadcasting Company. For the past two years he has been engaged in color television transmission studies. Mr. Kennedy is Adjunct Associate Professor of Physics at Hofstra College where he is presenting graduate courses in advanced networks and transients. He is a member of Sigma Pi Sigma.

RONALD C. KNECHTLI received the Diploma in Electrical Engineering from the Swiss Federal Institute of Technology. He spent the academic year 1951-1952 at the Massachusetts Institute of Technology, where he pursued graduate studies while serving as a Research Assistant in the Research Laboratory of Electronics. From 1952 to 1953, he worked in the microwave laboratory of Brown Boveri (Switzerland). He joined the Microwave Tube group at RCA Laboratories in 1953. In 1955 he was awarded the Ph.D. degree from the Swiss Federal Institute of Technology. Since joining RCA, he worked on microwave tubes and electron guns. Dr. Knechtli is a member of the Institute of Radio Engineers and of Sigma Xi.

RALPH H. PLUMLEE received the B.S. degree in Chemistry from the University of Illinois in 1938, and the Ph.D. degree in Physical Chemistry from the Ohio State University in 1951. From 1938-1942 he was a teaching assistant at Ohio State University. In 1942 he joined RCA Laboratories in phosphor research. In 1944 he worked in the Manhattan Project under the auspices of the Ohio State University Research Foundation. In 1945 he returned to the RCA Laboratories in Princeton and has since worked on mass spectrometric and other studies of oxide cathodes. Dr. Plumlee is a member of the American Chemical Society, the American Physical Society, and Sigma Xi.